NTNU

Norwegian University of
Science and Technology

Analysis of IEEE Power System Stabilizer Models

Anders Hammer

Problem Description

In 2005 IEEE (The Institute of Electrical and Electronic Engineers) introduced a new standard model for Power System Stabilizers, the PSS4B. This is an advanced multi-band stabilizer that may give a better performance than the regular PSSs often used today. The new stabilizer has three parallel control blocks, each aiming at damping different oscillatory modes or different frequency bands of the low frequency oscillations in the power system. So far the PSS4B is not very known in the market, but in the future it will probably become a standard requirement for key power plants in the power system. This master thesis is a continuation of a project performed in the autumn 2010, where the power system model and the framework for analysis were established. The power system will during this master thesis be upgraded to contain an additional smaller generator and also two different multiple-input stabilizer models, the PSS2B and the PSS4B. These stabilizer models will be implemented and tuned for the small hydro generator in the network. Comparisons between the different network configurations will be performed where the focus will be at the inter-area and local oscillation modes. This master thesis will seek to find an answer on following questions:

- How should the PSS4B be tuned to give the best damping of the local and inter-area oscillation mode?
- Will an implementation of PSS4B give a better result compared to PSS2B?
- What are the pros and cons of PSS2B and PSS4B?

Assignment given: 10. January 2011
Supervisor: Kjetil Uhlen

Abstract

Student: **Anders Hammer**
Supervisor: **Kjetil Uhlen**
Contact: **Daniel Mota**
Collaboration with: **Voith Hydro**

Problem description

IEEE (Institute of Electrical and Electronics Engineers) presented in 2005 a new PSS structure named IEEE PSS4B (Figure 0-1). Voith Hydro wants to analyse the pros and cons of using this new type compared to older structures. The PSS4B is a multi-band stabilizer that has three separate bands and is specially designed to handle different oscillation frequencies in a wide range. Until now, Voith Hydro has used the common PSS2B in their installations, but in the future they will probably start to implement the new PSS4B. This master thesis will seek to find an answer on following questions:

- How should the PSS4B be tuned to give the best damping of the local and inter-area oscillation mode?

- Will an implementation of PSS4B give a better result compared to PSS2B?

- What are the pros and cons of PSS2B and PSS4B?
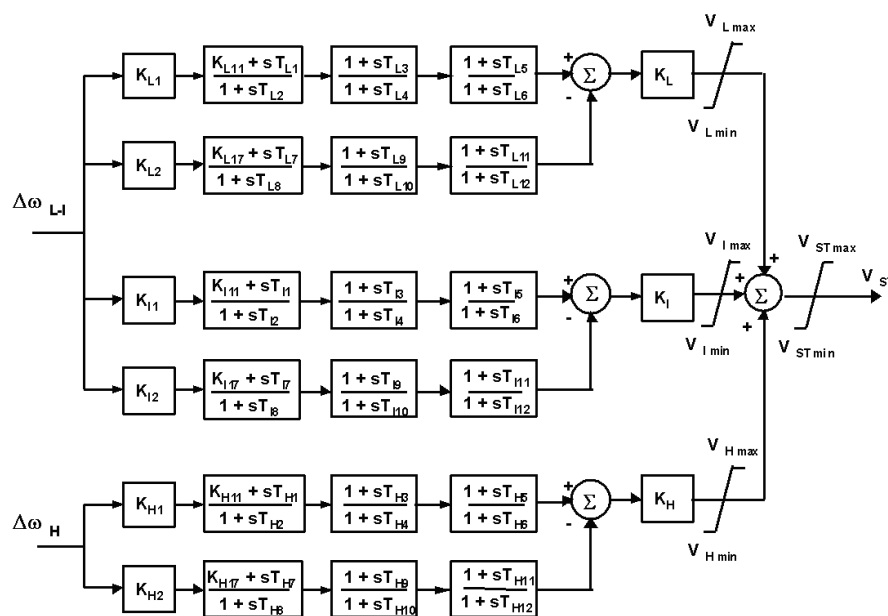
Figure 0-1: The multi-band stabilizer, IEEE PSS4B [1].

Method

In order to test and compare different PSS models, a simple two-area network model is created in a computer simulation programme (SIMPOW). One of the generating units is a

hydro generator, which has a model of a static excitation system made by Voith Hydro. This network is characterised by a poorly damped inter-area oscillation mode, and in addition some local oscillation modes related to each machine. Different PSS structures (PSS2B and PSS4B) are then tuned and installed in the excitation system of the hydro generator, in order to improve the stability of the network. Different tuning methods of the PSS4B are designed, tested and later compared with the more common stabilizer the PSS2B. Simplifications are made where parts of the stabilizer is disconnected in order to adapt the control structure to the applied network and its oscillations. Totally 5 different tuning methods are presented, and all these methods are based on a pole placement approach and tuning of lead/lag-filters.

Results

Initial eigenvalues of the different setups are analysed and several disturbances are studied in time domain analysis, in order to describe the robustness of the system. Figure 2 illustrates the rotor speed of the generator, where the different PSS's are implemented. PSS4B is clearly resulting in increased damping of all speed oscillations in this network. The same results can also be seen in an eigenvalue analysis.
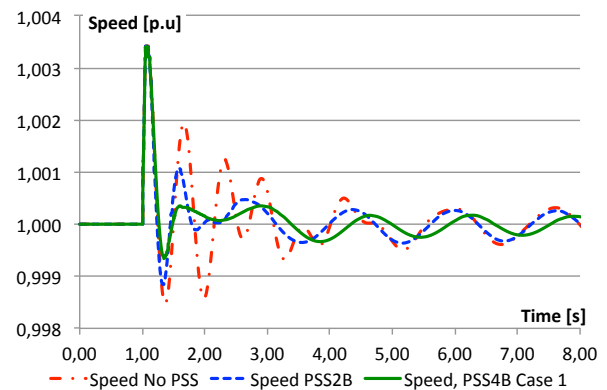

Figure 2: Time domain analysis of rotor speed after a small disturbance in the network.

Conclusion

The best overall damping obtained in this master thesis occurs when the high frequency band of the PSS4B is tuned first, and in order to maximize the damping of the local oscillation mode in the network. The intermediate frequency band is then tuned as a second step, according to the inter-area oscillation mode. Results of this tuning technique show a better performance of the overall damping in the network, compared to PSS2B. The improvement of the damping of the inter-area oscillation mode is not outstanding, and the reason is that the applied machine is relative small compared to the other generating units in the network. The oscillation modes in the network (local and inter-area) have a relative small frequency deviation. A network containing a wider range of oscillation frequencies will probably obtain a greater advantage of implementing a multi-band stabilizer.

Preface

This master thesis presents the results of my master thesis, which is the final course in the Master of Science-degree at the Norwegian University of Science and Technology (NTNU). In front of this master thesis a pre-project is performed, where some of the basics of a simple single-input power system stabilizer (PSS1A) are explained. More advanced PSS structures (PSS2B and PSS4B) are further analysed and compared during this master thesis. Voith Hydro gives this topic, and in addition SINTEF Energy Research has been a major support during the whole period.

A special thank goes to my supervisor, professor Kjetil Uhlen, for support and motivation during my master thesis. I would also like to thank Voith Hydro for giving me this task, and specially Daniel Mota for the introduction of Thyricon® Excitation System and for interesting points of view during the whole work.

<div align="center">

Trondheim 14. June 2011

Anders Hammer

</div>

Table of contents

1 Abbreviations

Table 1-1: Abbreviations used during this master thesis.

Abbreviation	Explanation
PSS	Power System Stabilizer
AVR	Automatic Voltage Regulator
DSL	Dynamic Simulation Language
UEL	Under Excitation Limiter
OEL	Over Excitation Limiter
V/Hz-limiter	Protection form excessive flux due to too high voltage or low freq.
FIKS	Funksjonskrav i kraftsystemet
d-axis	Direct axis in a synchronous machine
q-axis	Quadrature axis in a synchronous machine
IEEE	Institute of Electrical and Electronics Engineers
°	Angular degrees
p.u	Per unit
l-band	Low frequency band of PSS4B
i-band	Intermediate frequency band of PSS4B
h-band	High frequency band of PSS4B
KST	Gain of PSS2B
Tw	Washout-filter time constant
HVDC	High Voltage Direct Current
VAR	Volt Ampere Reactive

2 Introduction

2.1 Background

Electrical power systems are often operated in critical situations that may lead to stability problems in the power grid, and in worst-case blackouts. Large interruptions have historically occurred in many of power systems around the world and this may lead to panic and state of emergency in the society [6]. Because of todays climate change the European Union have decided that at least 20 % of the energy production must come from renewable energy sources by 2020 (Known as one of the 20-20-20 targets) [7]. To reach this goal, an increasing amount of renewable energy sources such as wind farms and smaller hydro plants are implemented in the power grids. The results of this may increase the network stability problems and the grid cannot be loaded close to the limit of maximum transfer capacity. This can in some cases reduce the needs of new power lines and thereby valuable space in the community [8].

The generator control equipment is able to improve the damping of oscillations in an electrical network and thereby prevent instability in the grid. One of the solutions to improve a troublesome grid may be to coordinate and tune this control equipment correctly [9]. In larger key power plants the share of keeping the system stability is high. These plants must be equipped with additional regulator loops, which will increase the damping of the power oscillations. To prevent instability in the Norwegian power grid these Power System Stabilizers (PSSs) are required as a part of the control equipment for generators above 25 MVA [10]. There exist several different types of PSS's in the market. IEEE (The Institute of Electrical and Electronics Engineers) has defined some standards, these are mainly based on different input signals and processing of signals [1].

2.2 Problem description

In 2005 IEEE (The Institute of Electrical and Electronic Engineers) introduced a new standard model for Power System Stabilizers, the PSS4B. This is an advanced multi-band stabilizer that may give a better performance than the regular PSS's often used today. The new stabilizer has three separate control structures, handling different frequency bands of the low frequency oscillations at the power system. So far the PSS4B is not very known in the market, but in the future it will probably become a standard requirement for key power plants in the

power system. This master thesis will be a continuation of a project performed in the autumn 2010, where the power system model and the framework for analysis were established. The power system will during this master thesis be upgraded to contain an additional smaller generator and also two different multiple-input stabilizer models, the PSS2B and the PSS4B. These stabilizer models will be implemented and tuned in the small generator and the different configurations will be compared. The focus during the simulation work will be at the inter-area and local oscillation modes.

2.3 Approach

A pre-project of this master thesis was performed during the autumn of 2010, where a basic single-input PSS (PSS1A) was introduced in a two-area network with four equal rated machines. The goal of the project was to uncover the basics of implementing and tuning a PSS, and thereby improve the stability of the heavy loaded network. To visualize some stability problems of an electrical network a classical two-area network was used as a base. This network model was copied from the book named "Power System Stability and Control" written by P. Kundur [11].

During this master thesis several changes of the classical two-area network are performed in order to better fulfil Voith Hydro's subject: planning and commissioning of hydropower plants. The original network consists of four equal rated synchronous machines with round rotors, and now a new synchronous machine is installed in parallel with one of the existing machines. This new machine is a typical hydro generator with salient poles and the rating is much smaller compared to the other generating units. Additionally a more advanced excitation system is implemented, tuned and tested. This excitation system is a simplified version of the Thyricon® Static Excitation System, developed by Voith Hydro. Next two different PSS models are implemented and tuned in the hydro generator of the five-generator network. First a dual-input stabilizer (PSS2B) is implemented and then a multi-band stabilizer (PSS4B). The goal is to tune these PSS's to maximize the damping of both local and inter-area oscillation modes, and also verify robustness in the system. At the end of the simulation work pros and cons of these two different stabilizer models are discussed.

The applied simulation computer programme in this master thesis is SIMPOW, developed by the Swedish company Stri AB, and MatLab is used in order to create frequency response plots and generally as a mathematical tool.

3 Theory

3.1 Power System Stability

Power system stability is the ability to maintain a stationary state in an electrical system after a disturbance has occurred. This disturbance can for instance be loss of generation, change in power demand or faults on the line. The system's ability to return to a steady state condition depends on the initial loading of the system and type of disturbance. Power system stability can be divided into four different phenomena's: wave, electromagnetic, electromechanical and thermodynamic (listed in ascending order of time response). This master thesis is only focusing at the electromechanical phenomenon, which takes place in the windings of a synchronous machine. A disturbance in the electrical network will create power fluctuations between the generating units and the electrical network. In addition the electromechanical phenomenon will also disturb the stability of the rotating parts in the power system [6].

The stability of a power system can further be divided, according to Figure 3-1, into different categories, based on which part of the system that is affected.
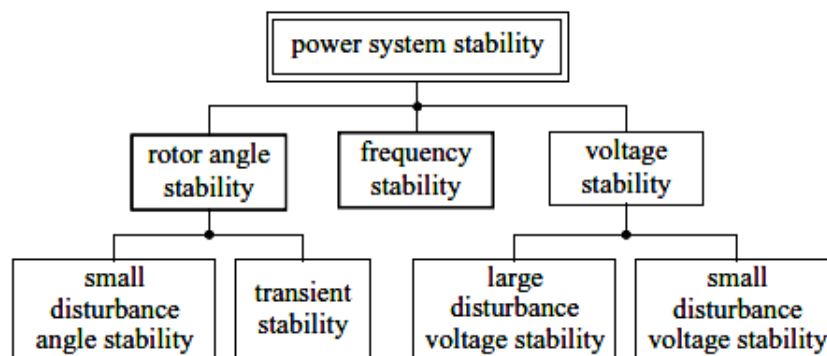
Figure 3-1: Classification of power system stability (based on CIGRE Report No. 325) [6].

Frequency stability and voltage stability are related to the relation between the generated power and consumed power in the system. A change in the reactive power flow will cause a change in the system voltage, and similar a change in the active power flow will lead to a change in the system frequency. The frequency stability enhancement is less significant in a stiff network and this is not further analysed during this master thesis [6].

Rotor angle stability describes the ability for the synchronous machines to stay synchronised after a disturbance has occurred. This criterion can be uncovered by study of the oscillation in

the power system. The rotor angle category can be further divided into small disturbance stability and transient stability. See the following chapter 3.1.1 and 3.1.2 for discussion of these two different stability behaviours.

In order to explain the rotor oscillation in a synchronous machine the swing equation is developed. This equation is presented in equation 3.1 and describes the relation between the mechanical parts in the machine and the accelerating torque.

$$J \cdot \frac{d\omega_m}{dt} + D_d \cdot \omega_m = \tau_t - \tau_e = \tau_{acc}$$ (Equation 3.1)

Where J = Total moment of inertia, ω_m = Rotational speed (mechanical), D_d = Damping coefficient, τ_t = Turbine torque, τ_e = Electrical torque and τ_{acc} = accelerating torque.

The damping coefficient is a result from friction and the effect of electrical damping in the machine. In steady state condition the rotor speed deviation (acceleration) is zero, and the turbine torque is equal to the electrical torque multiplied by the damping torque ($D_d \cdot \omega_m$). A disturbance in the electrical system will cause an approximate instantaneous change in the electromagnetic torque of the generator. The turbine applies the mechanical torque and this can initially be considered as constant. A result of this is a change in the rotor speed followed by an accelerating or decelerating rotor torque [6]. The rotational speed of the rotor (ωm) can be written as:

$$\omega_m = \omega_{sm} + \frac{d\delta_m}{dt}$$ (Equation 3.2)

Where δ_m = mechanical rotor angle and ω_{sm} = synchronous speed of the machine.

The swing equation can be rewritten, to contain rotor angle and power by using the relation $T=P/\omega$, and inserting equation 3.2 into 3.1 and multiply by ω_{sm}.

$$J\omega_{sm} \frac{d^2\delta_m}{dt^2} = P_m - P_e - D_m \frac{d\delta_m}{dt}$$ (Equation 3.3)

Where $D_m = \omega_{sm}D_d$, $J\omega_{sm} = M_m$ = angular moment, P_m = Mechanical power and P_e = Electrical power.

The inertia is often normalized in order to be able to compare different machines in a network. The total amount of inertia (J) is therefore replaced with a normalized H, which is:

$$H = \frac{J\omega_{sm}^2}{2S_n}$$
(Equation 3.4)

Where S_n = installed power.

To describe the oscillation phenomenon in an electrical system the swing equation is often applied. This is derived from the above-explained equations and by applying the relations $M_m = 2 \cdot H \cdot S_n / \omega_{sm}$ and $P_d = D_m \cdot d\delta_m / dt$ the swing equation will be:

$$M_m \frac{d^2\delta_m}{dt^2} = P_m - P_e - P_D = P_{acc}$$
(Equation 3.5)

This equation is often rewritten into two first order differential equations, which is used to describe oscillations in an electrical system [6]:

$$M_m \frac{d\Delta\omega}{dt} = P_m - P_e - P_D = P_{acc}$$
(Equation 3.6)

$$\Delta\omega = \frac{d\delta}{dt}$$
(Equation 3.7)

Rotor speed is clearly dependent on the accelerating power in the machine. In order to enhance the rotor angle stability and improve the dynamic response of a power system, several different methods can be applied. Some of them are listed below:

- Use of fast working circuit breakers
- Use of single pole circuit breakers in the main grid that only disconnect the faulted phase.
- Avoiding weak grids that are operated at low frequency and/or voltage.

The final solution of each power system must be a compromise between a socially useful system, that is more or less exaggerated. An already weak and unstable network can improve its stability performance by implementing additional control equipment, such as a power system stabilizer. This device is the most common and the cheapest way to improve an already unstable network [6].

3.1.1   Small signal stability

Small disturbance stability is explained as the electromechanical oscillations, which is created by disturbances small enough to affect the movement of the rotor. The disturbance must be so small, that the equations that are describing the stability can be linearized around a stable

operation point. Such disturbances are change in load or change in generation and the turbine- and generator- control equipment will then have the time to contribute to the dynamic behaviour of the system.

The values of the parameters in the swing equation, equation 3.5, can be found by linearizing the system around a given operation point. By finding the roots of this equation, the eigenvalues and the system stability characteristic is uncovered. From this characteristic it is possible to tell if the system is either an oscillatory or an aperiodic system. The eigenvalues can be a real or a complex conjugate eigenvalue, where the real ones do not create any oscillations. The notation of the complex conjugate eigenvalues has an absolute damping and a frequency.

When connecting more generators together (consisting of generator-models at higher orders) the total mathematical description of the system will consist of a high number of nonlinear differential equations. These are not easy to solve by hand and in a multi-machine system it is convenient to use a computer programme and eigenvalue analysis to find the steady state stability. Solving the characteristic equation, equation 3.8, will generate all the eigenvalues for an electric system.

$$\det(A - \lambda \cdot I) = 0 \qquad \text{(Equation 3.8)}$$

Where A is the system matrix, λ is the eigenvalues and I is the identity matrix.

An unsymmetrical system matrix gives eigenvalues that is a complex number and is often expressed as:

$$\lambda = \alpha \pm j\beta \qquad \text{(Equation 3.9)}$$

Where α is the absolute damping factor in 1/s and β is the oscillation frequency in rad/s.

A negative real part (α) of a complex conjugate eigenvalue indicates that the system is asymptotically stable and has a decaying contribution. In a damped system, the dominating eigenvalues is the ones that are oriented near to the imaginary axis in the complex plane[6, 12].

The relative damping ratio (ζ) tells how much a complex conjugate eigenvalue is damped where also the oscillation is taken into account. This ratio can be calculated as following:

$$\zeta = \frac{-\alpha}{\sqrt{\alpha^2 + \beta^2}}$$

(Equation 3.10)

The most interesting pair of eigenvalues is the one with the lowest relative damping ratio. These are the ones that give most oscillations in the system. A negative relative damping ratio will create an increase of the oscillation, rather than a damping. Such eigenvalues can not occur in order to have a stable system [6, 12]. Many utility companies require a minimum relative damping ratio of 0.05. For low frequency modes, such as the inter-area mode, the requirement could be set even higher and often greater than 0.1. This limit is then set to secure a safer damping of the oscillations in the network [4].

The oscillations around the stable operation point are divided in several different groups. The American association IEEE has standardized the different oscillation modes that take place when synchronous machines are connected to a power system. By standardizing these modes there are easier for network operators to communicate and cooperate when handling stability problems [13]. The different oscillation modes, described in the literature, are listed below:

Torsional/lateral mode: Torsional mode will act on the generator-turbine shaft and create twisting oscillations in a frequency above 4 Hz and is most distinctive in turbo machines with long shafts. These oscillations are usually difficult to detect with the generator models used to detect oscillations with lower frequencies. If the excitation system is powerful enough the torsional oscillation may add up to such a level that the turbine shaft may be damaged [13]. Lateral modes are related to horizontal mounted rotors that may slightly move from side to side during operation. These oscillations have the same characteristic as the torsional modes [14].

Inter-unit mode: Inter-unit mode will act between different generators in the same power plant or between plants that are located near each other. This oscillation mode occurs in a frequency range from 1.5 to 3 Hz, and by implementing a power system stabilizer when having an inter-unit mode the oscillation may become unstable. This is because the PSS is often tuned at a lower frequency than the inter-unit mode, and the PSS settings are therefore critical. A complete eigenvalue analysis must be executed in order to ensure that the damping of a potential inter-unit mode not becomes troublesome [13].

Control/exciter modes: The control/exciter mode is directly related to the control equipment of the generator and is a version of the local oscillation mode. These oscillations could be a result of poorly coordinated regulators in the system such as excitation systems, HVDC converters, and static VAR compensators. As a result of these oscillations the generator shaft may be affected and the torsional mode will then be more noticeable [11].

Local machine modes: In this mode of oscillation typically one or more generators swing against the rest of the power system in a frequency range from 0.7 Hz to 2 Hz. This oscillation may occur and become a problem if the generator is highly loaded and connected to a weak grid. In an excitation system containing a high transient gain and no PSS, these local machine oscillations may increase. A correctly tuned PSS in such a system may decrease the local machine oscillations [13].

Inter-area modes: The inter-area oscillation mode can be seen in a large part of a network where one part of the system oscillates against other parts at a frequency below 0.5 Hz. Since there is a large amount of generating units involved in these oscillations, the network operators must cooperate, tune and implement applications that will damp this mode of oscillations. A PSS is often a good application to provide positive damping of the inter-area modes [13]. Also a higher frequency inter-area oscillation can appear (from 0.4 to 0.7 Hz) when side groups of generating units oscillate against each other [11].

Global modes: This mode of oscillations is caused by a large amount of generating units in one area that is oscillating against a large group in another area. The oscillating frequency is typically in the range from 0.1 to 0.3 Hz and the mode is closely related to the inter-area mode [11].

Small signal stability means that the above-mentioned modes are dampened within a reasonable level.

3.1.2 Transient stability

Transient stability occurs in the rotor angle stability category when a large disturbance is introduced in the network. This large disturbance may be a three-phase fault over a longer time period, or a disconnection of a line, and such a disturbance gives a new state of

operation. This will result in a change of the system matrix and a linear analysis is no longer adequate. Under this new state of operation the rotor angle tries to find a new point of steady state position [6].

In this project the disturbance in the network will be considered as a small signal disturbance and the transient stability of the network will not be studied.

3.2 Excitation system of a synchronous machine

The main type of generator in the world is a synchronous machine. This is because of its good controlling capabilities, high ratings and a low inrush current. In order to produce electrical power at the stator, the rotor of the machine has to be fed with direct current. This can be executed in several different ways and examples are for instance from cascaded DC generators, rotating rectifiers without slip rings, or from a controlled rectifier made of power electronics. This appliance is named exciter, and the exciter used in this master thesis is a controlled rectifier. Other mentioned systems are not further explained here.
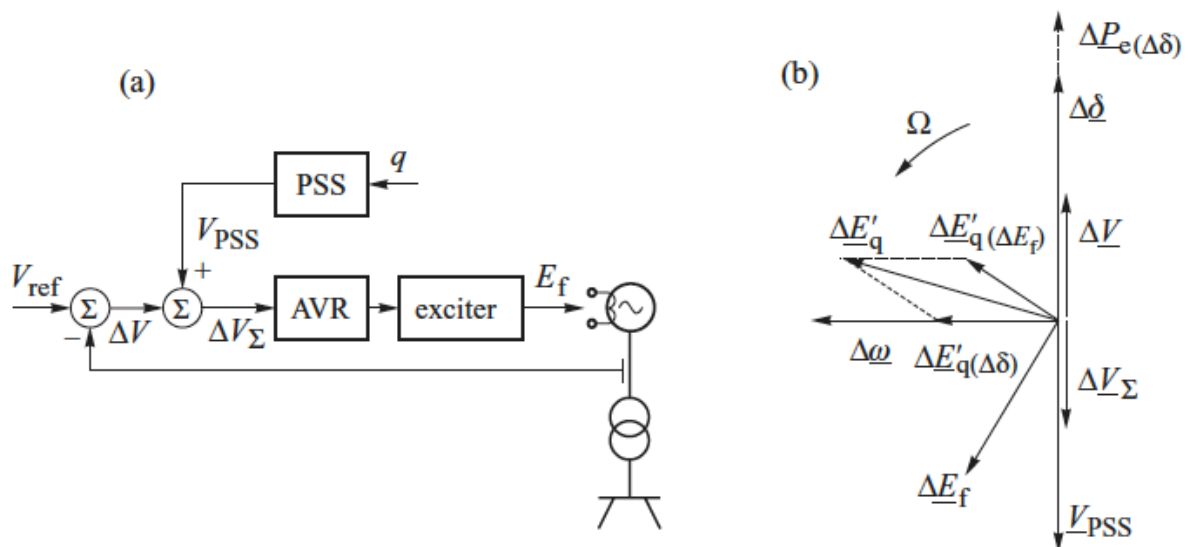
Figure 3-2: (a): Block diagram of the excitation system of one generator connected to the grid. (b): Phasor diagram of the signals in the excitation system [6].

To control the performance of the synchronous machine, the DC rotor current has to be controlled. This is done by an automatic voltage regulator (AVR), which controls the gate opening of the thyristors in the controlled rectifier. The whole system that is controlling and producing the excitation voltage is called excitation system and a typical excitation system block diagram is illustrated in Figure 3-2. This illustrates that the generator voltage is

measured and compared with a reference voltage, in order to calculate a voltage error signal, ΔV. This signal is then regulated to give the wanted DC output voltage of the exciter (E_f), which gives the correct AC generator terminal voltage [6].

The excitation system is capable to make an influence on the oscillations in the connected network. These excitation systems are acting fast and maximize the synchronous torque of the generating unit. This leads to a rotor movement that becomes stable, and goes back to its steady state position after a transient fault has occurred. A fast excitation system can also contribute to a high terminal voltage that leads to a high current during a fault. It is favourable to maintain a high current in order to improve the tripping ability of protective relays. The fast response of the voltage regulator may create an unstable situation if the machine is connected to a weak transmission system. Such problems can be solved by implementation of a power system stabilizer (PSS) in the excitation system, which is introducing an additional voltage control signal (V_{PSS} in Figure 3-2) [15].

3.3 Power System Stabilizer

The main reason for implementing a power system stabilizer (PSS) in the voltage regulator is to improve the small signal stability properties of the system. Back in the 1940 and 50s the generators were produced with a large steady state synchronous reactance. This led to reduction in field flux and to a droop in synchronising torque. The result was a machine with poor transient stability, especially when it was connected to a weak grid. To solve this transient stability problem, a fast thyristor controlled static excitation system was later introduced. This installation eliminated the effect of the high armature reaction, but it also created another problem. When the generator was operated at a high load and connected to a weak external grid, the voltage regulator created a negative damping torque and gave rise to oscillations and instability. An external stabilizing signal was therefore introduced as an input to the voltage regulator. This signal improved the damping of the rotor oscillations and the device was called power system stabilizer (PSS). The PSS introduces a signal that optimally results in a damping electrical torque at the rotor. This torque acts opposite of the rotor speed fluctuations [4].

Other solutions on the oscillation problem exist, but these are not covered in this master thesis. It is the introduction of a PSS that is the easiest and most economical solution in most cases. A single machine connected to an external grid is often used to explain the dynamics of

an electrical network. In 1952 Heffron and Phillips developed a model for this setup, and this model contained an electromechanical model of a synchronous generator with an excitation system. De Mello and Concordia (1969) picked up the Heffron & Phillips model, and developed an understanding of electrical oscillations and damping torque in an electrical system. These understandings can also be transferred to a larger system with several generation units and more complex grids. The Heffron & Phillips model is illustrated in Figure 3-3, where GEP(s) is the transfer function of electric torque and reference voltage input. An additional stabilizing signal should optimally correct the phase
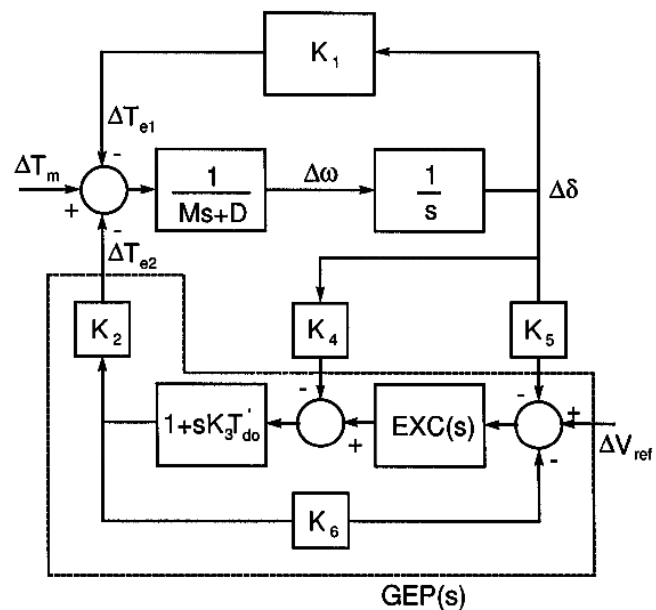
Figure 3-3: Heffron & Phillip's single-machine infinite-bus model [4, 5].

shift of this transfer function. Assuming that the single machine is connected to an infinite bus the GEP(s) transfer function can be uncovered by performing a field test of the generator. When the electrical system obtain a new operation condition, the GEP(s) transfer function changes, and the PSS transfer function must optimally follow this deviation. This is practically impossible and the solution is to provide a phase lead/lag structure that acts in a wide range of frequencies [4].

The excitation system can, with an external damping signal, produce a repressive rotor torque in phase with the rotor speed deviation. Since the generator and the exciter produce a small phase shift, the damping signal from a PSS has to contain a phase angle correction, in addition to the gain. The phase angle correction is realized by adding a phase-lead/lag-filter in the PSS structure, and it is important that the phase-lead generated by the PSS compensates for the lag between the exciter input and the generator air gap torque. Without any phase shift in the system, the phase-angle between the PSS output signal and the electrical torque is directly 180 degrees [4, 6, 11].

3.3.1   Tuning approaches of PSS structures

Basically the tuning of a PSS structure can be performed in three different approaches. These are a damping torque approach (based on Heffron & Phillips model), a frequency response approach and an eigenvalue/state-space approach [4]. When increasing the gain of a well-tuned PSS, the eigenvalues should move exactly horizontally and to the left in the complex plane. Theoretically it is around 180 degrees between the machine rotor speed and the electrical torque variations, and the PSS should contribute with a pure negative signal. The PSS structure contains a negative multiplication that will provide a 180-degree phase shift. In practise the straight horizontal movement of eigenvalues may not happen because of the electrical phase shift in the system. Implementing and correct tuning of lead-lag filters (block 5 in Figure 3-4) can correct the phase shift in the system [6]. Figure 3-4 illustrates the implementation of a simple PSS structure in an excitation system.
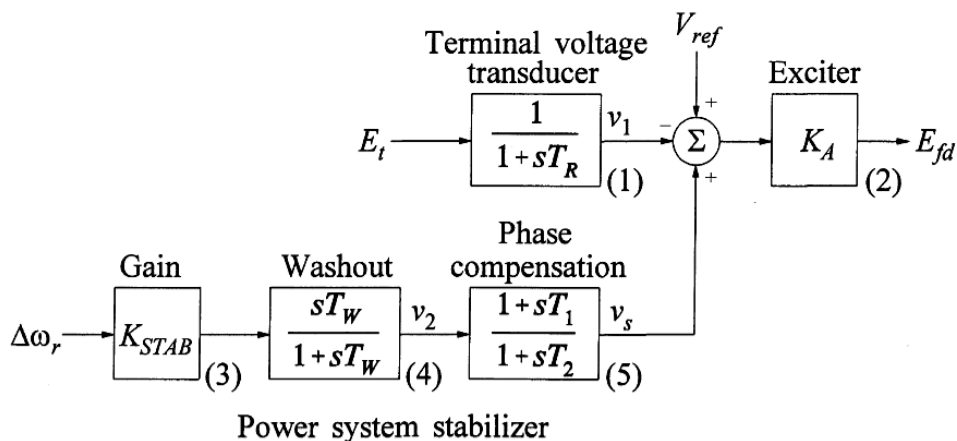
Figure 3-4: Excitation system including a simple PSS structure [11].

If the generator is connected to an infinite bus, it is easy to find a linearized transfer function for a given operation point (GEP from Figure 3-3). With this function it is possible to make a bodé diagram, which describes the phase shift and gain between the rotor speed and electrical torque. The damping torque approach and the frequency response approach are using this relation to tune the PSS. If a generator is connected to a larger network with different operation conditions it is difficult to find this transfer function, and to locate the accurate phase shift. The linearized transfer function depends on synchronous machine parameters, variation in loading condition and system parameters [4, 16].

An opportunity to find the phase shift is to implement the PSS and disconnect the lead/lag-filter and make steps in the PSS-gain. The slope of the eigenvalues can now be uncovered by plotting these eigenvalues in the same diagram. This plot is commonly mentioned as a root

locus plot. Angle between the horizontal real axis in the complex plane and the root locus plot will be the phase angle for that specific eigenvalue. This tuning method is the eigenvalue approach based on pole placement [4].

Another method to locate the total phase angle between the rotor speed and the electrical torque is to plot these two variables in a time domain analysis and thereby find the phase shift.

The preferred method, which is utilized in this master thesis, is the eigenvalue approach where the base is analysis of pole placement and root locus plots. This method is preferred since the computer simulation tool used in this master thesis can easily compute eigenvalues of the whole system, while it cannot create transfer functions and nice frequency responses of the multi machine network.

3.4 Overview of different PSS structures

In order to provide a damping torque signal, the PSS could use the rotor speed deviation from the actual rotor speed from the synchronous speed ($\Delta\omega_r$) as an input. Other parameters, which are easily available and measurable, could also be used to provide the damping torque. These signals could be electrical frequency, electrical power or the synthesized integral of electrical power signal. In the measurements of input signals, different types of signal noise could be present. The stabilizer has to filter out this noise in order to feed the AVR with a steady signal, which could damp the actual rotor oscillation [6]. An explanation of different PSS's is given in the following sub chapters.

3.4.1   Speed-based stabilizer

The simplest method to provide a damping torque in the synchronous machine is to measure the rotor speed and use it directly as an input signal in the stabilizer structure. This method is illustrated in Figure 3-4, where block number 4 is a washout filter and will only pass through the transient variations in the speed input signal. Ordinary variations in speed, frequency and power must not generally enter the PSS structure and thereby affect the field voltage [4]. The washout constant should be chosen according to these criteria [13]: "

1. *It should be long enough so that its phase shift does not interfere significantly with the signal conditioning at the desired frequencies of stabilization.*

> 2. *It should be short enough that the terminal voltage will not be affected by regular system speed variations, considering system-islanding conditions, where applicable."*

Operating a network containing really low frequency inter-area modes, the washout time constant (Tw) has to be set as high as 10 or 20 second. The reason is that the washout-filter has to cover these low frequency oscillation modes. If not having this low inter-area oscillation mode, the Tw could be set to a lower value [4].

After finding the angle of the selected eigenvalue, in the eigenvalue approach, a lead/lag-filter must be implemented in order to correct the angle of the specific eigenvalue. This filter can be a filter of n'th order, similar to the transfer function in Equation 3.11.

$$Lead / lag - filter = \left(\frac{1 + T_1 \cdot s}{1 + T_2 \cdot s} \right)^n \qquad \text{Equation 3.11}$$

n is the order of the filter, s is the Laplace operator and T_1 & T_2 is the time constants.

Tuning of the time constants in this filter can be performed based on the phase shift (φ_l) and the frequency (ω_l) of the selected eigenvalue, according to Equation 3.12 and 3.13 [17].

$$T_1 = \frac{1}{\omega_1} \cdot \tan\left(45° + \frac{\varphi_1}{2n} \right) \qquad \text{Equation 3.12}$$

$$T_2 = \frac{1}{\omega_1} \cdot \frac{1}{\tan\left(45° + \frac{\varphi_1}{2n} \right)} \qquad \text{Equation 3.13}$$

ω_l is the frequency of the eigenvalue in rad/s, φ_l is the phase shift in degrees and n is the order of the filter.

As an example a first order filter and a second order filter should correct an eigenvalue at 1 rad/sec and with a phase shift of 30 degrees.

First order filter:

$$T_1 = \frac{1}{1 rad / \sec} \cdot \tan\left(45° + \frac{30°}{2 \cdot 1} \right) = 1.7321$$

$$T_2 = \frac{1}{1rad / \sec} \cdot \frac{1}{\tan\left(45° + \dfrac{30°}{2 \cdot 1}\right)} = 0.5774$$

$$Lead / lag - filter = \left(\frac{1 + 1.7321 \cdot s}{1 + 0.5774 \cdot s}\right)^{1}$$

Second order filter:

Figure 3-5: Bode plot of a first order filter.

$$T_1 = \frac{1}{1rad / \sec} \cdot \tan\left(45° + \frac{30°}{2 \cdot 2}\right) = 1.3032$$

$$T_2 = \frac{1}{1rad / \sec} \cdot \frac{1}{\tan\left(45° + \dfrac{30°}{2 \cdot 2}\right)} = 0.7673$$

$$Lead / lag - filter = \left(\frac{1 + 1.3032 \cdot s}{1 + 0.7673 \cdot s}\right)^{2}$$
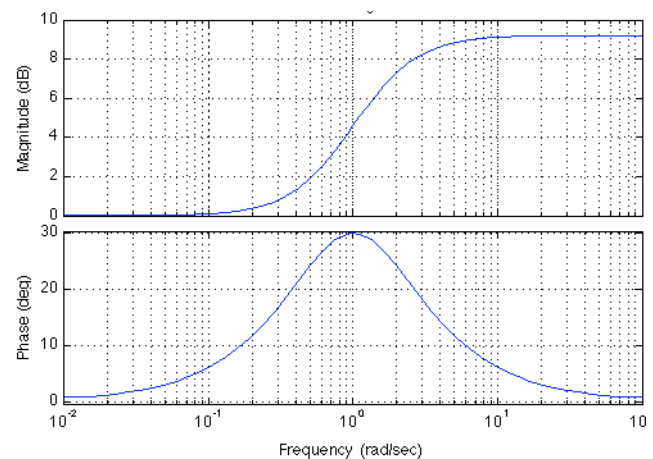
Figure 3-6:Bodé plot of a second order filter.

As seen from the bodé plots (Figure 3-5 and Figure 3-6), both filters will compensate with 30 degrees at the frequency of 1 rad/sec. The second order filter will be more accurate and give a narrower bandwidth in the phase response.

The Norwegian national grid operator, Statnett, have a requirement in the relative damping ratio to be more than 5 % [10]. This will give a safe damping of the rotor oscillations. Practically the PSS gain must be tuned in such a fashion that the critical eigenvalues are moved to the left of the 5 % border to fulfil this requirement. Other demands for the PSS are that it should not disturb the voltage regulation under normal state. If for instance a capacitor bank is shut down, the voltage regulator has to operate unrestrained and maintain a steady voltage level.

The main disadvantage of using the rotor speed deviation as an input signal is that this signal can contain a relatively large amount of disturbance. Rotor speed is directly measured by use of sensors mounted on the rotating shaft. During a disturbance the rotor could create lateral movement in a vertical mounted machine. For large horizontally mounted turbo generators (1800 or 3000 rpm) the rotor shaft can twist and create torsional oscillations. Turbo generators have a long rotor shaft and a short diameter to limit the centripetal force that is created at these rotational speeds. To limit these interactions, several speed sensors could be mounted along the rotor shaft. A disadvantage of doing this is increased costs and maintenance. In addition a special electrical filter can be installed to filter out unwanted signal noise. The disadvantage of this *torsional filter* is that it would also introduce a phase lag at lower frequencies, and it can create a destabilizing effect at the exciter oscillation mode as the gain of the stabilizer is increased. The maximum gain from the PSS is then limited and the system oscillations could then not be as damped as wanted. This torsional filter must also be custom designed in order to fit the generating unit. To get rid of these limitations a new PSS structure was created, the PSS2b, which is an integral of accelerating power-based stabilizer [4, 14]. This type is further described later in this chapter.

3.4.2 Frequency-based stabilizer

This type of stabilizer has the same structure as used in the speed-based stabilizer mentioned above. By using the system frequency as an input signal the low frequency inter-area oscillations are better captured. These oscillations are thereby better damped in a frequency-based stabilizer, compared to the speed-based stabilizer. Oscillations between machines close to each other are not well captured by the frequency-based stabilizer, and the damping of the local oscillations is then not highly improved. The frequency signal may also vary with the network loading and operation. An arc furnace nearby could for instance create large unwanted transients in the measurement signal, and the PSS might produce a unwanted behaviour of the generator [14].

3.4.3 Power-based stabilizer

Power and speed of the rotor are in a direct correlation, according to the swing equation described below:

$$\frac{2 \cdot H \cdot S_n}{\omega_{sm}} \cdot \frac{d\Delta\omega}{dt} = P_m - P_e \rightarrow \frac{d\Delta\omega}{dt} = \frac{1}{2 \cdot H}\left(P_m - P_e\right)$$

Equation 3.14

Where the damping coefficient is set to zero.

The electrical power is easy to measure and also use as an input signal. Mechanical power is a more problematic value to measure. In most power-based stabilizers this mechanical power is threated as a constant value and the rotor speed variations are then proportional with electrical power. Change in the mechanical loading will then be registered by the PSS and it will create an unwanted output signal. A strict PSS output limiter must in those cases be established to prevent the PSS to contribute under a change in generator loading. This will reduce the overall PSS performance and the power system oscillations will not get as damped as wanted. Electrical power as an input signal will only improve the damping of one oscillation mode. Several oscillating frequencies in the network require a compromise solution of the lead/lag-filter [14].

3.4.4 Integral of accelerating power-based stabilizer

As mentioned as a drawback of the speed-based stabilizer, a filter has to be implemented in the main stabilizing path to reduce the contribution of lateral and torsional movements. This filter must also be applied in the pure frequency- and power-based single input stabilizers. The Integral of accelerating power-based stabilizer was developed to solve the filtering problem and also take mechanical power variations into account [4, 14]. Figure 3-7 illustrates the block diagram of the stabilizer based of integral of accelerating power, currently named PSS2B.
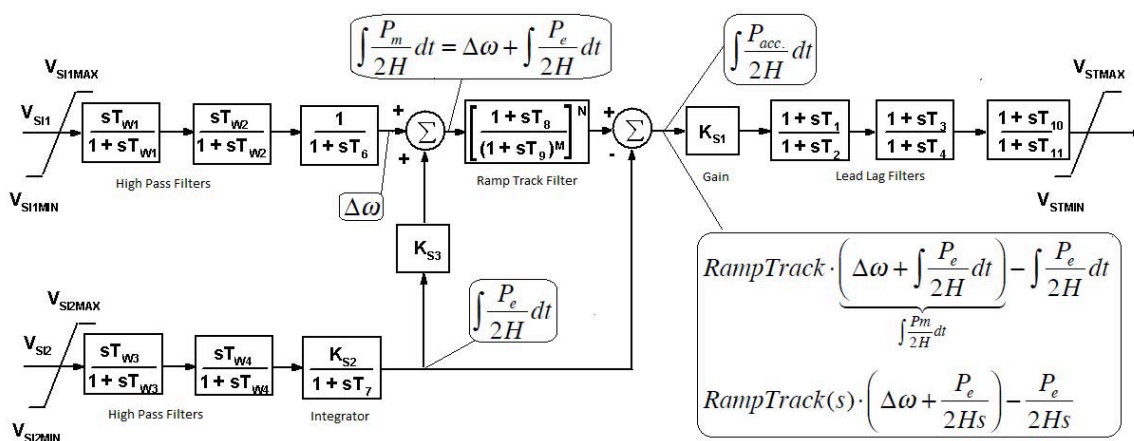
Figure 3-7: IEEE PSS2B, the dual-input stabilizer [1], with explanations.

The two input signals, named V_{si1} and V_{si2}, are treated different in order to synthesize the integral of accelerating power signal. This signal is injected into the gain block (K_{S1}) and can be derived as follows by the swing equation (Equation 3.15):

$$\Delta\omega = \frac{1}{2H}\int(P_m - P_e)dt \rightarrow \frac{1}{2H}\int P_{acc.}\,dt \qquad\qquad \text{Equation 3.15}$$

Change of speed is clearly dependent on power and the integral of mechanical power can now be expressed by change in rotor speed and integral of electrical power:

$$\int\frac{P_m}{2H}dt = \Delta\omega + \int\frac{P_e}{2H}dt \qquad\qquad \text{Equation 3.16}$$

V_{si1} input signal is a speed- or frequency signal and V_{si2} is a power signal. V_{si1} can be used directly and the time constant T_6 is then set to zero. V_{si2}, the power signal, must pass an integral block and also be divided by $2H$, which is performed by the gain constant K_{S2}. Equation 3.15 indicates that the derived integral of accelerating power can represent the speed change in the machine.

The torsional filter is commonly mentioned as a ramp-track filter, and by introducing this filter the torsional and lateral oscillations will be reduced in the integral of mechanical power branch. The electrical power signal does not usually contain any amount of torsional modes, and the torsional filter can be skipped in the integral of electrical power branch. An advantage of doing this is that the exciter oscillation mode will not become destabilized [4, 14]. At the end of the transducer block the electrical signal is subtracted from the mechanical signal, and the integral of accelerating power signal is then synthesized. This can be explained by combining equation 3.15 and 3.16 in such a fashion that only electrical power and speed remains as an input parameter, seen in equation 3.17. By doing this signal processing it becomes unnecessarily to measure the tricky mechanical power in the machine.

$$\int\frac{P_{acc.}}{2H}dt \rightarrow RampTrack\cdot\underbrace{\left(\Delta\omega + \int\frac{P_e}{2H}dt\right)}_{\int\frac{Pm}{2H}dt} - \int\frac{P_e}{2H}dt \qquad\qquad \text{Equation 3.17}$$

Taking the Laplace transformation of equation 3.17 gives equation 3.18, which is the base for the block diagram in Figure 3-7.

$$\int\frac{P_{acc.}}{2H}dt \rightarrow RampTrack(s)\cdot\left(\Delta\omega + \frac{P_e}{2Hs}\right) - \frac{P_e}{2Hs} \qquad\qquad \text{Equation 3.18}$$

The final integral of accelerating power signal should exactly follow the rotor speed variations, and the rest of the PSS2B can then be tuned as a common single-input PSS with a gain and a lead/lag-filter [4].

PSS2B stabilizer uses, as mentioned, to different signals as input parameters: speed/frequency and active electric power of the machine. In order to create a theoretical frequency response (bodé plot) of the whole PSS2B it is possible to synthesize the electric power signal (used as input V_{si2}) from the speed signal. Thereby a transfer function with one input- and one output-parameter can be created and also a frequency response. The method for synthesising the power input signal could be derived from the
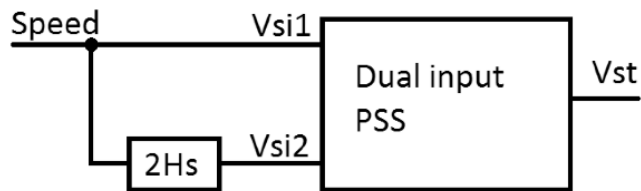
Figure 3-8: Principal model to find the frequency response of a dual input stabilizer [3].

swing equation that explains the relationship between change in speed and change in power. Figure 3-8 is a conceptual drawing of the method of finding the complete transfer function of a dual-input stabilizer [3].

Voith Hydro has given an example of typical transducer parameters presented in Table 3-1. These parameters, except form K_{S2}, are not normally changed in a regular tuning procedure.

Table 3-1: PSS2B transducer parameters, given by Voith Hydro [2].

TF	TP	Tw_{1-4}	T6	T7	KS2=T7/2H	KS3	T8	M	N	T9
0.02	0.02	3	0	3	0.5137*	1	0.4	4	1	0.1

* 100 MVA generator with inertia (*H*) equal to 2.92.

The two parameters *TF* and *TP*, from Table 3-1, are related to measurement equipment and is a fixed value. These parameters explain the time constants of the frequency- and power transducers. First order filters are therefore implemented in the front of the PSS2B, and these represents each input transducer. *Tw* parameters are washout-time constants and acts like high pass filters. Only oscillations above a certain frequency pass these filters. The power-branch needs an integrator block in order to produce the wanted stabilizer signal. *T7* will define this function, and the bodé plot of the integrator block is presented in Figure 3-9.
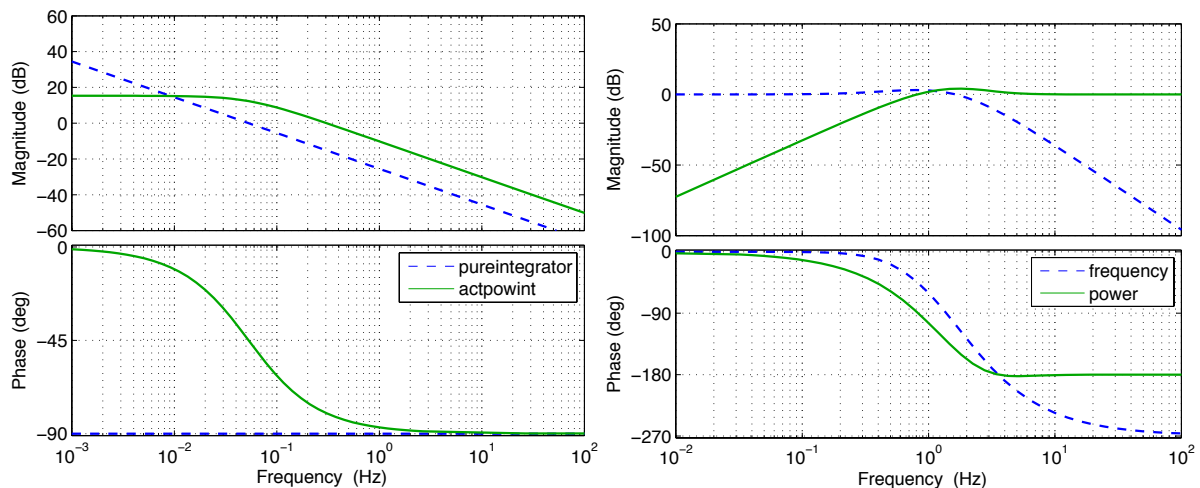
Figure 3-9: Left: Bode plot of PSS2B-integrator block and a pure integrator block. Right: Bode plot of ramp-track filter, where a contribution from frequency and power branch is present.

Time constant $T7$ states that frequencies above 0.053 Hz will be affected by the integrator block ($1/T7$=0.33rad/s → 0.053Hz), this is also illustrated in the left bodé plot of Figure 3-9. The bodé plot oriented to the right in Figure 3-9 illustrates the ramp-track filter performance, where the frequency branch of PSS2B handles the frequencies below approximately 1 Hz and the power branch handles frequencies above approximately 1 Hz. Parameters presented in Table 3-1 gives the frequency response of the whole transducer-part of PSS2B, illustrated in Figure 3-10. The plot indicates that the -3 db cut-off frequency is oriented at 0.08 Hz and 8.5

Hz. This is the boundary where the signals are starting to reduce rather than increase after passing the transducer blocks [12]. In the frequency range of 0.08 ~ 8.5 Hz, the phase response varies of approximately 315 degrees. To achieve a good signal quality, which acts in the direct opposite direction (-180 degrees) of speed variations, the filtering process may get troublesome, especially if the network struggles with several oscillations modes in a wide frequency range.
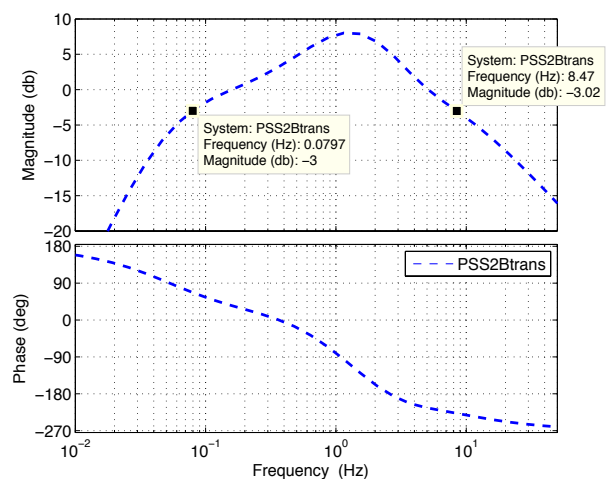
Figure 3-10: Bodé-plot of the transducer-part of PSS2B.

3.4.5   Multi-band stabilizer

The motivation for developing a new type of stabilizer was that the lead/lag compensating filters in the older structures could not give an accurate compensation over a wide range of

oscillation frequencies. If the network suffers from low- and high frequency oscillations, the tuning procedure of the single-band stabilizers have to compromise and will not achieve optimal damping in any of the oscillations. The multi-band stabilizer has three separate signal bands, which can be tuned individually to handle different oscillation frequencies. This stabilizer is presented in Figure 3-11 and this structure has a relative large amount of tuning flexibility.
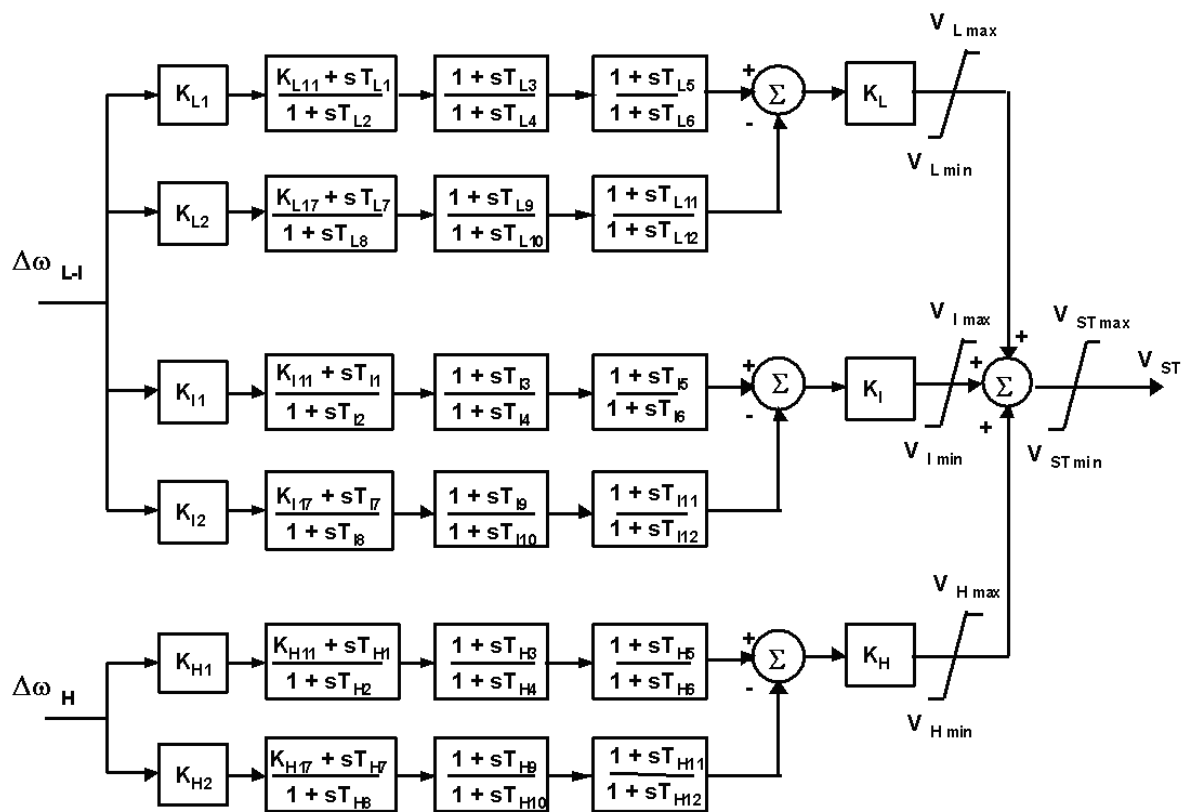
Figure 3-11: Multi-band stabilizer, IEEE PSS4B [1].

At first glance this stabilizer structure seems that it would require a tedious tuning procedure. An IEEE report [1] presents a simple tuning procedure where a selection of three centre frequencies and associated gains are used as base of the parameter settings. One frequency for the low frequent oscillations, one for the intermediate and one for the highest oscillation frequency that occurs at the stator terminals. Totally four equations is used to calculate the time constants for each band. The equations for the intermediate frequency band are presented, as an example, in equation 3.19 – 3.22. R is a constant set equal to 1.2 and Fi is the centre frequency of the intermediate band [1]:

$$Ti2 = Ti7 = \frac{1}{2 \cdot \pi \cdot Fi \cdot \sqrt{R}}$$
<div align="right">Equation 3.19</div>

$$Ti1 = \frac{Ti2}{R}$$

Equation 3.20

$$Ti8 = Ti7 \cdot R$$

Equation 3.21

$$Ki1 = Ki2 = \left(R^2 + R\right)/\left(R^2 - 2R + 1\right) \rightarrow 66, \text{ when R=1.2}$$

Equation 3.22

The associated gains (*Ki, Kl* and *Kh*) are set to a value that gives a reasonable contribution of the amplitude in each band. All other parameters not mentioned here are set to a value that cancels the respective blocks.

By choosing the IEEE tuning method for all the three bands, the frequency response of the total PSS will give a more accurate compensation and in a wider frequency range than for a typical lead/lag-filter structure. As seen in the structure of the PSS4B (Figure 3-11), different input parameters are used in this model ($\Delta\omega_H$ and $\Delta\omega_{L-I}$). This is similar to the dual-input stabilizer, presented in the previous subchapter, which is also using two input signals. The two upper bands of PSS4B (Figure 3-11) are designed to handle low- and intermediate oscillation frequencies, while the high frequency oscillations only enters the lower band. To create these different input signals two different input transducers are used. These are presented in Figure 3-12, where rotor speed ($\Delta\omega$) is used directly as an input signal to the upper transducer. The low and intermediate part of the oscillations is passing this transducer block, and the signal is later injected as an input to the low and intermediate part of the PSS4B. To create a signal that represents the high frequent oscillations, the electrical power (*Pe*) is used as an input to an own transducer and the lower blocks in Figure 3-12 explain this transducer. As explained in the subchapter of the dual-input stabilizer, the electrical power signal must pass an integral-block in order to be considered as a speed signal. Both transducer models can be equipped with a notch filter. These filters are typically used when the PSS is connected to a large nuclear generator that struggles with low frequency torsional oscillations [9]. In this master thesis these notch filters is not further commented. In Figure 3-13 the frequency response is plotted, where the rotor inertia to the generator is chosen equal to four, as an example. The solid curve represents the electrical power-transducer and it clearly works as a band-pass filter, where oscillations in a range from
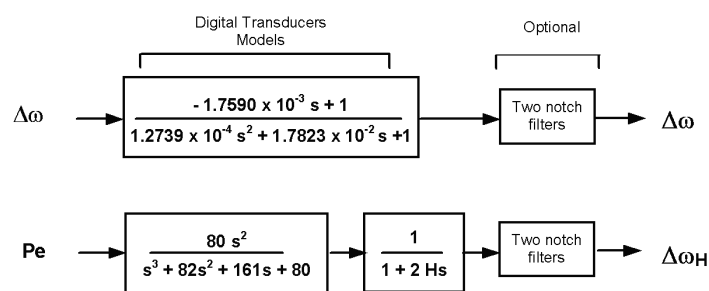
Figure 3-12: PSS4B, input transducer models [1].

0.25 ~ 12.7 Hz is passing. The oscillations at a lower frequency are then taken care of by the bands connected to the speed-transducer. This has only one -3db cut-off frequency and this is located at approximately 12.7 Hz. Oscillations above 12.7 Hz will then not enter the low and intermediate part of the stabilizer structure.
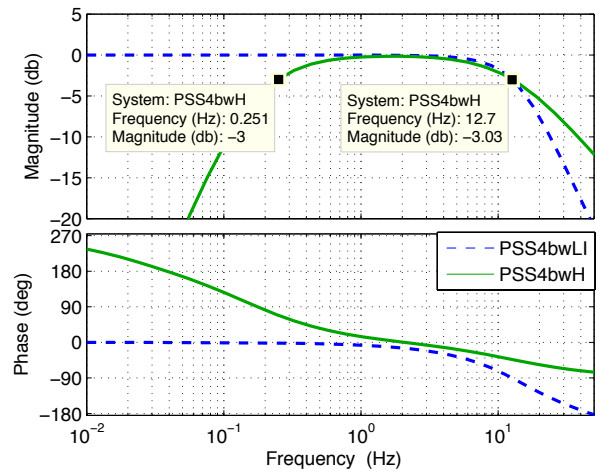
Figure 3-13: Bodé plot of PSS4B input transducers.

Breaking down the structure into smaller parts, makes it possible to easier analyse the behaviour of this multi-band structure. By only looking at two of the blocks in one of the three bands will make the mathematics easier. A block diagram of this simplification is illustrated in Figure 3-14.

$$H = \frac{Out}{In} = \frac{1+T_1 s}{1+T_2 s} - \frac{1+T_3}{1+T_4}$$

$$H = \frac{(1+T_1 s)(1+T_4 s)}{(1+T_2 s)(1+T_4 s)} - \frac{(1+T_3 s)(1+T_2 s)}{(1+T_2 s)(1+T_4 s)}$$

$$H = \frac{1+(T_1+T_4)s+T_1 T_4 s^2 - 1 - (T_3+T_2)s - T_3 T_2 s^2}{(1+T_1 s)(1+T_4 s)}$$
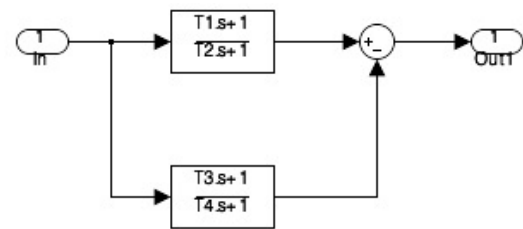
Figure 3-14: A simple differential filter.

$$H = \frac{(T_1+T_4-T_3-T_2)s+(T_1 T_4-T_3 T_2)s^2}{(1+T_1 s)(1+T_4 s)} = \frac{(T_1+T_4-T_3-T_2)s+\left(1+\dfrac{T_1 T_4-T_3 T_2}{T_1+T_4-T_2-T_3}s\right)}{(1+T_1 s)(1+T_4 s)}$$

Zeros: $s = -\dfrac{T_1 T_4 - T_3 T_2}{T_1 + T_4 - T_2 - T_3}$ Poles: $s = -\dfrac{1}{T_2}$ $s = -\dfrac{1}{T_4}$

The time constants decides whatever this structure is a high pass or a band pass filter. One special situation, which is utilized in the IEEE Std. 421.5 document [1], is when $T_3 = T_2$ and $T_1 = (T_2 T_3)/T_4 = (T_2)^2/T_4$. The transfer function will then be reduced as following:

$$H_{red.} = \frac{\left(\dfrac{(T_2)^2}{T_4}+T_4-2T_2\right)s \cdot \left(1+\dfrac{\dfrac{(T_2)^2}{T_4}T_4-(T_2)^2}{\dfrac{(T_2)^2}{T_4}+T_4-(T_2)^2}s\right)}{(1+T_2 s)(1+T_4 s)} = \frac{\left(\dfrac{(T_2)^2}{T_4}+T_4-2T_2\right)s}{(1+T_2 s)(1+T_4 s)}$$

The structure has now become a band-pass-filter with the centre frequency between the two corner frequencies $1/T_2$ and $1/T_4$. These corner frequencies can be chosen to give a wanted phase response at a specific frequency. The steepness of the phase response increases by decreasing the differences between T_2 and T_4. Figure 3-15 illustrates a frequency response of H_{red}, where two different sets of time constants are used. The dashed curve indicates a steeper phase response compared to the solid line, where the differences between the time constants is larger. Adding a gain in front of the differential filter in Figure 3-14 can increase the low magnitude-response presented in Figure 3-15. Equal gains will keep the phase-response fixed while the magnitude increases.
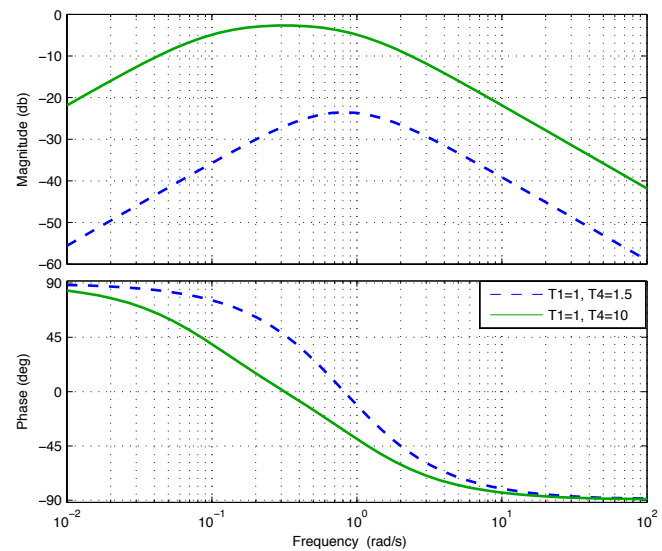
Figure 3-15: Bodé plot of the reduced filter with two different sets of time constants.

PSS4B has three sets of these differential filters (low-, intermediate-, and high frequency oscillations). At the end of the PSS4B structure these filters are added together. This summation will result in a more complex transfer function. When using IEEE typical data set (calculated from the equations 3.19 – 3.22), the frequency response of the PSS4B without the transducers will result in the curves to the left in Figure 3-16. Same principal model as for PSS2B is used to find the total frequency response of the PSS4B. (Total result from the parameter calculations is found in the simulation descriptions in chapter 5). The PSS4B output signal is presented as a black solid line, while the other lines are the different internal band-structures. Illustration indicates that the phase lift in the frequency range from 0.05 to 4 Hz is around 45 degrees. This is a much more stable phase response, in that specific range, than achieved with the other PSS structures presented in this thesis. When taking the input transducers into account, the bodé plot to the right in Figure 3-16 is created. The phase response of the output signal (V_{ST}) is still around 45 degrees for frequencies between approximately 0.05 to 4 Hz and the transducers does not seem to disturb the PSS much. Grondin (et.al) performs a similar bodé-plot and analysis in their article *" Modelling and closed-loop validation of a new PSS concept, the Multi-Band PSS"* [3]
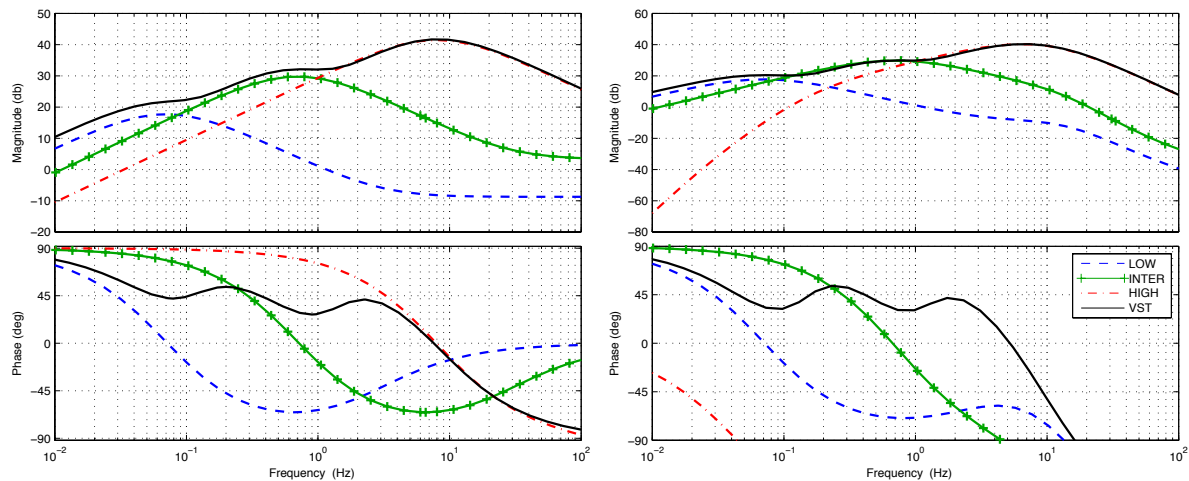
Figure 3-16: Bodé-plot of PSS4B. Left diagram: Without transducers. Right diagram: With transducers.

Another approach to tune the multi-band stabilizer is to disconnect the lower branch of each band, and use the upper branch as a regular lead/lag-filter in addition to a gain. Each of the different bands can be tuned separately according to the actual network oscillations. This is a much simpler tuning procedure where the tuning of the lead/lag-filters can be done similar to the procedure used in the dual-input PSS (PSS2B). First step is to find the critical oscillation modes in the network. Then one of the three bands in the PSS4B can be assigned to each of the oscillation modes where the damping will be improved. Disconnecting two of the three bands makes it possible to tune the third band to give a maximized damping of the selected oscillation mode. The goal is to move the selected eigenvalue straight to the left in the complex plane. Next step is to tune one of the other bands according to another oscillating eigenvalue.

4 Simulation Tool, SIMPOW

The stability analysis of a power network is a difficult procedure when calculating by hand. A computer programme called SIMPOW, developed and operated by the Swedish company STRI AB, performs therefore the stability simulations in this project. Since the system matrix of a large power system can become very large, it is more convenient to perform the stability analysis by using the computer programme. The simulation programme linearizes the system around an arbitrary state, in order to perform a linear analysis. Out of this it is possible to generate eigenvalues, perform modal analysis and make a frequency scan or a data scan. SIMPOW using the quick-response-method (QR-method) to uncover the eigenvalues, and the eigenvalues could be improved by using the inversed iteration method to get a more accurate solution. The modal analysis is a tool that detects which parts of the network that is oscillating against each other. This information is obtained from the eigenvectors in the electrical system. In a frequency scan the system is excited by a sinusoidal source with varying frequency and the system response can be studied. The data scan indicates the movement of the eigenvalues when ramping one of the system parameters [18].

SIMPOW has also an ability to perform a time domain analysis of the system, where variation of different system parameters can be plotted over a time period. This analysis can in many cases strengthen the results found in the linear analysis and different fault scenario can be implemented [18].

It is often a benefit to have the ability to implement different regulator structures in the simulation programme. SIMPOW uses a coding language named Dynamic Simulation Language - code (DSL-code). A DSL-code can be generated automatically by drawing the block diagram of the regulator structure in a code-generating programme. This coding programme is called HYDRAW and makes the programming work a lot easier. In some cases the programmer must be able to understand and read the code in order to make corrections. A generated programme code can be compiled in a library, which can contain different regulator models. By doing this different DSL-codes can be used together during the simulations.

When working with simulation tools it is important to determine the base values used in the p.u. system. SIMPOW uses p.u. base-values, according to the descriptions in the user manual: [18] "

- *One p.u. field current is the field current which would theoretically be required to produce one p.u. stator voltage, i.e. rated voltage, on the air-gap line at open-circuit rated speed steady-state conditions.*

- *One p.u. field voltage is the corresponding field voltage at the field winding temperature to consider (usually 75 or 100 degrees centigrade). "*

This means that when the machine is running at no load, the current in the field windings produce a certain terminal voltage. This voltage has no saturation and is mentioned as the air-gap voltage. The value of the field current that is producing nominal terminal voltage at no-load is set as the base value in SIMPOW.

5 Simulation descriptions

The simulation work is divided into different tasks, and a short intro is here presented:

- Analysis of the Voith Hydro's Thyricon® Excitation System.
    - Uncover the effect of generator voltage in the Thyricon® Excitation System.
    - Tuning of the Thyricon® Excitation System parameters according to a 100 MVA hydro machine.

- Build a five-generator two-area network model containing one hydro power plant at 100 MVA in addition to four 900 MVA turbo generators.
    - Analyse different oscillation modes when Thyricon® Excitation System (without a PSS) is installed in the 100 MVA machine.

- Implementation of the dual input PSS model (PSS2B) in the excitation system of the 100 MVA machine.
    - Tuning of the PSS's lead/lag-parameters and gain, according to the two-area network model.
    - Analyse the contribution of this PSS at overall damping in the system.

- Implementation of the multi-band PSS model (PSS4B) in the excitation system of the 100 MVA machine.
    - Loading the PSS4B with IEEE sample data and analyse the overall damping in the system.
    - Tuning of the PSS4B parameters according to the actual oscillations in the two-area network model, and analyse the overall damping in the system.

- Comparing the performance of PSS2B and PSS4B, and detect pros and cons of each stabilizer structure.

5.1 Analysis of Voith Hydro's Thyricon® Excitation system

In the pre-project of this master thesis a four-generator two-area network was analysed, and one of the generating units was simulating a hydro power plant at 900 MVA. This generator

was equipped with a very simplified version of the Thyricon® Excitation System, delivered by Voith Hydro. This system is a static excitation system where thyristors are used to produce a DC excitation voltage. The applied excitation system was basically modelled as a PID-regulator, where the D-part was disconnected. Additionally a simple gain and a time constant were representing the thyristor rectifier. Further explanation about the four-generator network can be found in the pre-project of this thesis. A PID controller will generally give a good and fast regulation of the voltage after a disturbance. The Norwegian grid operator, Statnett, has a PID-regulator as a requirement in every voltage regulators above 1 MVA [10].

In this master thesis the Thyricon® Excitation System is further analysed and the model is upgraded. Thyricon is a static excitation system where the generator stator voltage is rectified by a thyristor bridge. This DC excitation voltage is injected to the rotor windings through slip rings, and the rotor becomes excited. As the excited rotor rotates inside the stator, an AC voltage is generated at the stator terminals. Deviations in the stator voltage will directly affect the excitation voltage, and by skipping this contribution in the model may give a result that is incorrect. Different versions of the Thyricon® Excitation System is therefore modelled and compared, in order to study the contribution of a deviation in the stator voltage. One model with and one model without a multiplication of the generator voltage and exciter output are studied. The goal is to locate the effect of implementing this multiplication in the excitation system. A full description of the Thyricon® Excitation System, with all its limiters and stabilizers, is placed in the appendix. Figure 5-1 shows the exciter main structure, which is the base for the exciter modelled in the simulation programme of this master thesis. The different exciter models, applied in this master thesis, are recreated in a DSL-code programme, named HIDRAW, and these block diagrams are illustrated later in this chapter.

Figure 5-1: Thyricon® Excitation System, main structure [2].

Some of the limiters, mentioned in the full description, are skipped in the models applied in this thesis. These exclusions make the simulation work a bit easier, where the main focus is the damping of small signal oscillations. The integration block still contains some limiters (1 and -1), and additionally two other limiters are implemented. These are located right in front of the thyristor bridge and is the over excitation limiter (OELf) and the minimum field current limiter (MFCL). Together these four limiters form an *anti-wind up* system in the excitation system. All these limiters are initially set equal to one, as a given value by Voith Hydro.

At the end of the exciter structure, illustrated in Figure 5-1, a thyristor bridge block is implemented. This block is shown in Figure 5-2 and contains a gain and a time constant. The final excitation voltage is produced by the thyristors, which rectifies the generator stator AC-voltage. Typical values for the model of the thyristor bridge is given by Voith Hydro, where the gain (*Kbr*) is set to four and the time constant (*Tbr*) is in a range from 1.4 ms to 1.7 ms. Dips in the stator voltage will affect the excitation voltage, and this contribution can be

Figure 5-2: Block diagram of the thyristor bridge [2].

modelled by forwarding the generator voltage (*Ug*) and multiply it by the output signal. The next two sub-chapters explain the models that are used to study the effect of this multiplication.

5.1.1   Excitation system without multiplication of generator voltage (AVR1)

Figure 5-3: HIDRAW block diagram of Thyricon® Excitation System without multiplication of generator voltage at output, currently named AVR1.

First version of the excitation system (illustrated in Figure 5-3) is a block diagram that not contains a forwarding of the generator stator voltage (*VC* in Figure 5-3). The excitation voltage (*UF*) is now not depending on the generator terminal voltage.

5.1.2   Excitation system with multiplication of generator voltage (AVR2)

The second version of the excitation system includes the generator voltage-forwarding loop, and the block diagram is illustrated in Figure 5-4. Generator voltage (*VC*) is multiplied by the output of the excitation system (*Ubr*) and forms the final output signal (*UF*). In this structure the excitation voltage is clearly dependent on the generator stator voltage, where a disturbance in stator voltage will also create a direct disturbance at the field voltage. This system is theoretically more realistic, compared to the system where the forwarding loop is skipped.

Figure 5-4: HIDRAW block diagram of Thyricon® Excitation System with multiplication of generator voltage at output, named AVR2.

5.1.3   Simulations

These two different excitation systems are one by one implemented in the 900 MVA hydro generator of the four-generator network, used in the pre-project of this master thesis and also described in [11]. The reason for using this network is that it was well known at the time when the exciter models was created and tested, but the results are also applicable in a more advanced electrical network. A simple single-input PSS is implemented and tuned according to each exciter model. Same tuning procedure as used in the pre-project (the pole placement approach) is also used for this PSS. A root locus plot is then created for both exciter models, and the results are compared. Differences between the root locus plots tells how large the voltage-forwarding loop will contribute, and these simulations will detect the needs of implementing this block in the exciter model.

5.2 Tuning process of the voltage regulator

For further tuning of the two different excitation systems, explained in the previous chapter, the models are implemented in a smaller 100 MVA hydro generator. This generating unit is

later implemented in a five generator two-area network, which will be the applied network thru the rest of master thesis. The hydro generator model is inserted in an isolated network where the PID regulator of the excitation system is tuned. The generator is now only connected to a small electrical load, which will require a production of 0.001 p.u. This small value is only set in order to be able to solve the load flow equations. A voltage response of the generator is then performed, where a step in the reference voltage creates a disturbance. This method is described in a document made by Statnett (FIKS [10]), where the overshoot, rise-time and oscillations of the voltage-response can be identified for different settings of the PID-parameters. FIKS minimum requirements of a step response in a static excitation system are explained below [10].

- Less than 0.5 second to reach 90 % of the steady state value after a step of 5 %.
  - Step from 100% to 95% of base voltage →90 % = 0.955 p.u.
  - Step from 95 % to 100% of base voltage → 90 % = 0.995 p.u.
- Not an oscillating response
- Overshoot less than 15 % of the step

5.2.1   Simulations

Changing the voltage reference signal from 1 p.u to 0.95 p.u. after t=1 second performs the dynamic simulation. At steady state condition the reference is once more changed, but now from 0.95 p.u. to 1.0 p.u. To be able to implement this step-response test in the computer simulation tool, some corrections have to be made to the programme code of the excitation system (DSL-code). Further details around these corrections are given in the appendix. The response from a static excitation system is relative fast, and the derivative part of the PID regulator is therefore disconnected in this tuning procedure. A derivative block might be more useful when the voltage regulator is connected to a rotating exciter that has a larger time constant [15]. In the beginning of the tuning process, the voltage regulator is loaded with relatively "gentle values", which will give a relative slow step response. PI-parameters are then further tuned to better fulfil the FIKS requirements. Both versions of the Thyricon® Excitation System is tuned with the same parameters, and the result is later compared. Based on these simulations the differences between the two versions of the excitation system are further analysed. A small variation in the step response will be acceptable, and the most realistic voltage regulator model will be used in the rest of the master thesis.

5.3 The five-generator network

5.3.1 Network descriptions

The pre-project of this master thesis presented a four-generator network model that was heavily loaded and contained both inter-area and local oscillations. This network model is the base for the five-generator network developed in this master thesis. The original four-generator network is a fictive network that is made to illustrate the dynamics of an electrical power network. This base is copied from the textbook "Power System Stability and Control", written by Pradha Kundur [11], and is a well known two-area network model. All the generators in this four-generator model are large (900 MVA), and in order to make the commission more realistic a smaller generator at 100 MVA is implemented. This new generator is located near generator G2 and forms the new five-generator network. Figure 5-5 describes the new network model that can simulate a commission process of one single hydro generator.
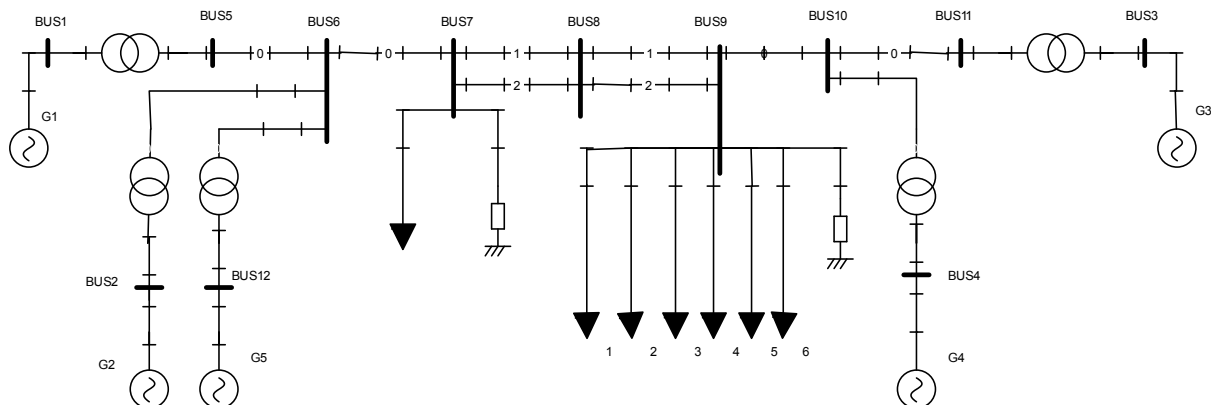
Figure 5-5: Five-generator network. G1, G2, G3, G4 are 900MVA turbo generators, while G5 is a smaller 100MVA hydro generator.

Figure 5-5 illustrates a single line diagram of the network, which is modelled in the computer simulation tool (SIMPOW). As seen in the figure, the network consists of five generators that are interconnected. Generator G2 and G5 are connected to generator G1 with a short line and forms one region (Area 1). The two other generators, generator G3 and G4, forms a second region (Area 2). In the middle of the network (BUS8) Area 3 is located. Generator G3 is the swing bus and it has a fixed voltage of 20.6 kV and an angle of -6.8 degrees. The voltage level in the transmission system has a value of 230 kV, and is operated at a frequency of 60 Hz.

The appendix contains a complete load flow analysis, and this indicates that area 1 exports and area 2 imports active power under normal state of operation. An active power flow of approximately 400 MW is transmitted from left to the right thru the tie line in the model. The long distance between the two areas generates a voltage in BUS8 that is below the limit, and the network is now heavily loaded. A disturbance may, under these conditions, lead to oscillations and system instability. There are clearly two areas in the network that is connected together by a weak tie grid, and this will easily lead to network stability problems. To provoke instability there is a possibility to make a three-phase short circuit at area 3, or by switching off some of the loads connected to BUS7 or BUS9. The active load at BUS9 is divided into smaller parts, for the reason to be able to trip a small load, and then analyse the network oscillations. A full overview of the loads is found in the appendix of this master thesis.

Four of the generators in the system have an equal rating of 900 MVA and 20 kV, but there are some differences in the inertia. The fifth generator is a smaller unit at 100 MVA. An own table in the simulation code describes the saturation in the machines, and this describes the terminal voltage as the field current rises. All the large generators in the network (900 MVA) are modelled as turbo generators with a round rotor. Voith Hydro is only working with hydro generators and most of them have a salient pole rotor. Generator G5 is therefore modelled as a salient pole generator, where a non-uniform reluctance between the rotor and stator appears. The resulting reactance's in the salient pole generator is therefore different from the ones in the round rotor machines [6]. All the large synchronous generators are modelled as *Type 1* in the computer simulation tool. This means that they have one field winding, one damper winding in d-axis and two damper windings in q-axis. The salient pole generator is modelled as *Type 2*, which means a generator with one field winding, one damper winding in d-axis and one damper winding in q-axis [18]. The appendix contains tables of the parameters for the generators, lines, transformers and the loads used in this five-generator network.

The different generating units in the network are connected to different turbine/governor models. An approximate model of a steam turbine with a single reheat (ST1) is connected to the turbo generators, and a general speed-governing model (SG1) regulates the speed of these turbines. A classical penstock hydro turbine model (HT1) generates the torque at the hydro generator, and the governor named DSLS/HYGOV regulates the speed. All these models are already implemented in the simulation software, and the parameters is chosen as typical

values. One important difference between a steam turbine and a hydro turbine is that the hydro turbine has two different droop parameters. A step in the water gate position of a hydro turbine will not give an instant increase in the power output of the turbine, but rather a small drop. The water flow in the penstock cannot increase instantaneously, so the velocity of the flow in the turbine will initially decrease after a gate opening. After a short delay the water flow in the penstock has the time to accelerate, and the power output of the turbine can increase. To handle this phenomenon the hydro governing model has two different droop parameters. This compensates for the water flow to catch up after a step in the gate position. One droop parameter reducing the gain after fast changes (called transient- or temporary-droop) and one droop parameter for slower changes in the gate opening (called permanent droop) [6]. The different models and parameters for turbine and governor are further described in the appendix. SINTEF Energy Research has given the parameter values as typical values for a turbine governing system.

5.3.2 Simulations

Under commissioning of generators it is usually difficult to tune the PSS at the inter-area oscillation mode, and only the local oscillation mode is often taken into consideration [19]. The simulation work in this document will identify the inter-area oscillations in addition to the local oscillations. Both modes are taken into consideration, and the goal is to increase the damping of the local as well as the inter-area oscillation mode in this five-generator network.

Initially the network is not containing any power system stabilizers, and at this stage the different network oscillations modes is analysed. The computer simulation programme includes a modal analysis tool and by using this, at the most critical eigenvalues, the different oscillation modes will be uncovered. These modes can then further be treated individually, in order to increase the damping. All eigenvalue analysis is, during this master thesis, performed at the initially state.

The different network oscillations are also described by performing a time domain analysis. To start the oscillations in this heavy loaded network, a 3-phase short circuit connection is introduced in BUS7. This fault is only present in 0.05 seconds and then it is totally removed. No other change is made in the electrical system, and the fault can be considered as an automatic re-connection. 0.05 seconds is a really short duration, and the fault represents a small disturbance of the system.

The next step in the step in this master thesis is to start improving the system stability by implementing different power system stabilizer´s in the network.

5.4 Implementation of the dual input PSS model (PSS2B)

In order to increase the damping of the system oscillations, the dual input stabilizer (PSS2B) is implemented in the hydro generator of the five-generator network. This generator is much smaller than the other generators in the network, and the lack of thrust will only result in smaller performance of damping of inter-area oscillations. In spite, it is always favourable to increase rather than decrease the damping of these oscillations after installing a PSS.

PSS2B is implemented in the computer simulation programme as a DSL-code, and the block diagram of this code is presented in Figure 5-6. System frequency and electrical power of the machine is the input parameters of this stabilizer structure.
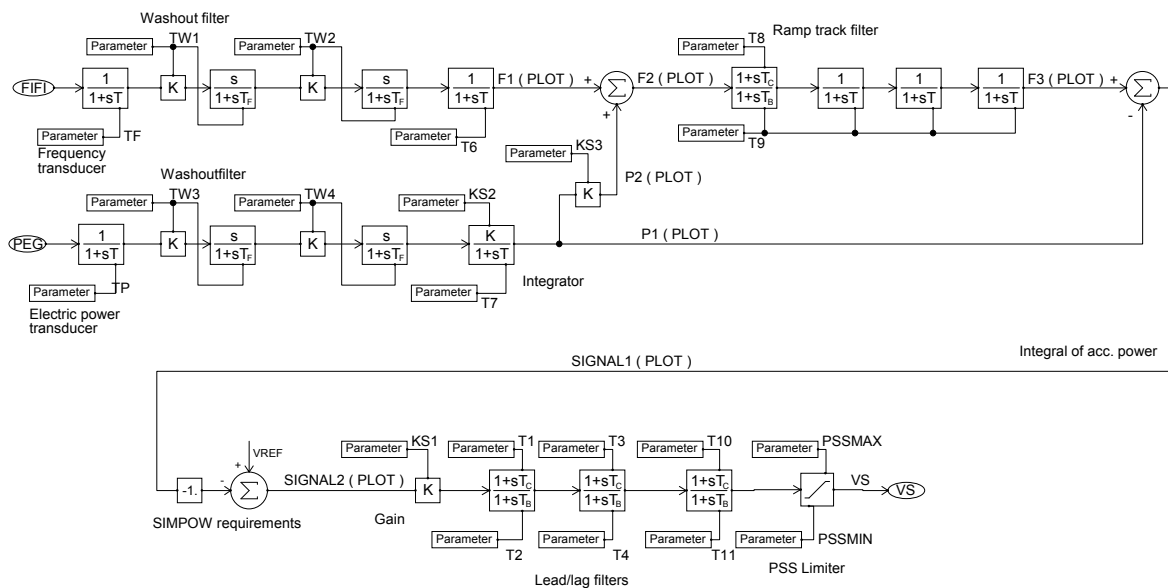
Figure 5-6: HIDRAW block diagram of PSS2B stabilizer structure.

SIGNAL1, located in the middle of the block diagram, is the synthesised integral of accelerating power signal, and the blocks in front of this signal is mentioned as the PSS2B transducer. This transducer has parameters that will not change from situation to situation, except from the gain *KS2*, which is dependent on the generator inertia. Table 5-1 describes the chosen parameters in the transducer part of the PSS2B.

Table 5-1: PSS2B transducer parameters given by Voith Hydro.

TF	TP	Tw1=Tw2=Tw3=Tw4	T6	T7	KS2=T7/2H	KS3	T8	T9
0.02	0.02	3	0	3	0.5137*	1	0.4	0.1

*100MVA generator, inertia: H=2.92.

5.4.1   Simulations

To verify that the PSS2B-transducer acts in a proper way, the integral of accelerating power signal is compared with the actual rotor speed of the machine. A well-adjusted transducer has an integral of accelerating power signal that follows the speed variations accurately. This test is performed in the beginning of the simulation work, and the following task is to tune the lead/lag-filters and gain so the overall damping is maximized. This procedure is based on a pole placement approach and tuning of lead/lag-filters, the same procedure as for a single input stabilizer. Theory part of this master thesis explains this in more detail and it is additionally explained in the previous chapter of this master thesis.

The next simulation is a time domain analysis where the three-phase short circuit connection is implemented at the tie line connection. This fault starts some oscillations in the generator speed and the implementation of a well-tuned PSS2B will optimally reduce these oscillations. The PSS output signal is additionally plotted in order to illustrate the overall behaviour of the PSS. Another time domain analysis is also performed, where a load of 500 MW at BUS9 is disconnected. This small disturbance produces a shift in the load flow, and the power generated by generator G5 will start to oscillate. The goal of this test is to detect the contribution of PSS2B in the hydro generator during regular operation of the network. Optimally the PSS must not disturb this regular operation, in any great concern.

5.5   Implementation of the multi-band PSS model (PSS4B)

A multi-band stabilizer (PSS4B) is, during this part of the simulation work, implemented in the hydro generator of the five-generator network. HIDRAW, the DSL-coding programme, is also used to implement this stabilizer, and the PSS4B block diagram is presented in Figure 5-7. The input signals in the upper two bands are the rotor speed, while the lower band uses the generator power as an input signal. These signals are passing through transducer models, which is similar to the models presented in the theory of this master thesis.

5.5.1 Loading the PSS4B structure with sample data given by IEEE

First step in the simulations, performed with this stabilizer structure, is to implement and load it with IEEE data, described in IEEE Std. 421.5. This data set is additionally described in the theory part of this master thesis, and a complete table of the chosen parameters is listed in Table 5-2. PSS4B is commonly used to achieve damping of oscillations in a wide frequency range and the IEEE data will approximately give a phase shift of 45 degrees from 0,1 Hz to 4 Hz. A simple time domain analysis of generator speed and stabilizing signal indicates the outcome of this PSS data set. The goal of this test is to see if the stabilizer gives an acceptable damping only by simply load it with the sample data.
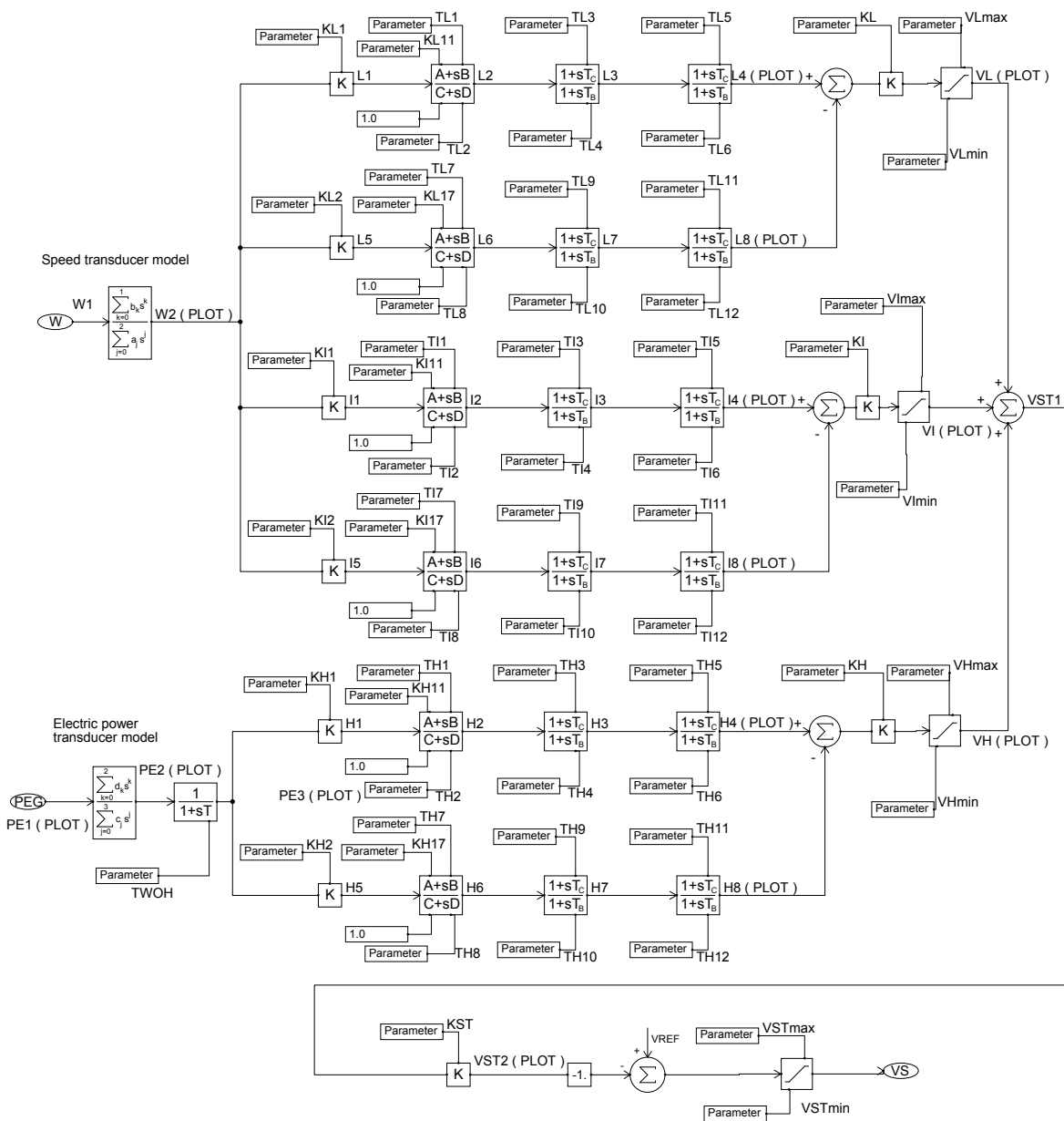
Figure 5-7: HIDRAW block diagram of PSS4B stabilizer structure.

Table 5-2: List of parameters of PSS4B, according to IEEE sample data.
(Parameters not mentioned in this table are set equal to 1)

l-band		i-band		h-band	
KL=7.5	FL=0.07 Hz	KI=30	FI=0.7 Hz	KH=120	FH=8 Hz
VL_{max}=0.075	VL_{min}=-0.075	VI_{max}=0.6	VI_{min}=-0.6	VH_{max}=0.6	VH_{min}=-0.6
$TL1$=1.73	$TL7$=2.075	$TI1$=0.173	$TI7$=0.2075	$TH1$=0.01513	$TH7$=0.01816
$TL2$=2.075	$TL8$=2.491	$TI2$=0.2075	$TI8$=0.2491	$TH2$=0.01816	$TH8$=0.02179
$KL1=KL2=KI1=KI2=KH1=KH2$=66, VST_{max}=0.15, VST_{min}=-0.15					

5.5.2   Tuning of the PSS structure based on the actual network oscillations

The next step is to tune the stabilizer more accurately, based on the actual oscillation modes in the electrical network. A more exact tuning procedure is here performed in five different cases. All cases are based on pole placement and root locus plots of eigenvalues. Setting the internal branch-gains *KL2, KI2* and *KH2* in Figure 5-7 to zero disconnects the lower branch of the three bands in PSS4B. Only the top branch is now used in the tuning processes, and initially only a simple washout block in the top branch is implemented. All the band-gains (*KL, KI, KH* in Figure 5-7) are initially set to zero and the other filters are initially set to not give any phase shift. By increasing one of the band-gains, the contribution from that specific branch is found and the need of a lead/lag-filter is identified based on a pole placement approach. The tuning process is now simplified, where the lead/lag-filters and gains for each band are tuned separately, and in different orders.

At the end of each case, a complete eigenvalue analysis is performed in order to assure that all eigenvalues in the system has acceptable values. Each case contains also time domain analysis, where a 3-phase short circuit, with duration of 0.05 seconds, is introduced in BUS8. The speed of generator G5 is analysed and additionally the PSS output signal. The time domain analyses of each case are plotted together with the situation where no PSS is implemented in the system. By comparing these graphs the improvement of the damping of speed oscillations is highly visible. Limiter values of the PSS4B are set equal to the limiter values used for the PSS2B. The reason is that this makes it possible to later compare the results of the respective time domain analysis, and the overall performance of each stabilizer structure. An overview of the different cases is now listed in Table 5-3 and a more detailed description is presented below.

Table 5-3: Overview of PSS4B tuning procedures.

Tuning procedure	Step 1	Step 2
Case 1	h-band is tuned according to the local oscillation mode	i-band is tuned according to the inter-area oscillation mode
Case 2	h-band is tuned according to the inter-area oscillation mode	i-band is tuned according to the local oscillation mode
Case 3	i-band is tuned according to the inter-area oscillation mode	h-band is tuned according to the local oscillation mode
Case 4	i-band is tuned according to the local oscillation mode	h-band is tuned according to the inter-area oscillation mode
Case 5	Same as case 4, but different gain	Same as case 4

Case 1

First step of case 1 is to tune the high frequency band (h-band) according to the local oscillation mode, and secondary tune the intermediate frequency band (i-band) to maximize the damping in the inter-area mode. The transducer of the h-band is specially designed to handle the highest oscillation frequencies, and the i-band is designed to handle the lowest frequencies. Tuning approach of case 1 utilize this natural allocation of frequencies according to each band.

This tuning procedure is starting with increasing the gain of the high frequency band (Kh), and thereby a root locus analysis of the most critical eigenvalues is performed. By using the same method of tuning and implementing lead/lag-filters as described for the PSS2B, the h-band is tuned to correct the initial angle of the movement of the local oscillation mode. The gain is then set to a reasonable value that increases the absolute damping of this mode, without highly disturbing the oscillating frequency. Next step is to adjust the inter-area oscillation mode by tuning the intermediate frequency band (i-band). By increasing the gain of the i-band (Ki), the initial angle of the movement of the inter-area mode is uncovered. This angle is the base of the tuning of the lead/lag-filters in the i-band.

Case 2

The tuning-order of case 2 is similar to case 1 where the h-band is tuned as the first step. Only difference from case 1 is that the h-band is here tuned according to the inter-area oscillation mode, and the i-band is then tuned to maximize the damping of the local oscillation mode. This approach is a more unnatural choice, but the result can uncover the importance of allocating the right frequencies to each band.

Case 3

The tuning order of case 3 are directly shifted compared to case 1, where the i-band is tuned first according to the inter-area oscillation mode, and the h-band is tuned according to the local oscillation mode. This approach will illustrate the differences of initially focusing on the inter-area mode, compared to start with the local mode.

Case 4

Case 4 is similar to case 3, where the i-band is tuned before the h-band. The difference is that the i-band is tuned according to the local oscillation mode. Next step is to tune the h-band according to the inter-area oscillation mode.

Case 5

Case 5 has the same tuning procedure like case 3, besides from choosing different gains of the i-band. The point of this test is to uncover the result of choosing a higher gain, in order to maximize the damping of the local oscillation mode. As a final step is the h-band tuned to improve the damping of the inter-area oscillation mode.

5.5.3   Final choice of tuning the PSS4B

In order to find the best solution of tuning the PSS4B, the results from the different cases are compared. First the improvements of the eigenvalues are examined, and the cases which gives acceptable results is further compared in time domain analysis. A load of 500 MW is then disconnected at BUS9, and the time response of the active and reactive power is analysed for each case.

5.6 PSS2B vs. PSS4B

The parameters that gave the best results of the two different stabilizer structures, PSS2B and PSS4B, are in this chapter compared in an eigenvalue analysis and also in different time domain analysis. The same disturbances as used in the previous chapters are also used to compare the performance of each stabilizer structure.

6 Results

6.1 Analysis of Voith Hydro's Thyricon® Excitation System

NB! This subchapter utilizes the four-generator two-area network explained in the pre-project of this master thesis. The network is used only to compare the two different versions of Thyricon® Excitation System, explained in chapter 5, and the results also applies in a more advanced network.

Eigenvalue progress is analysed as a single input stabilizer is tuned in two different versions of Thyricon® Excitation System. The stability performance of each setup identifies the contribution of directly multiplying the generator voltage with the output signal of the excitation system.

6.1.1   Without multiplication of generator voltage at exciter output, AVR1

Excitation system named AVR1 from chapter 5 is installed in generator G2 of the four-generator network. The exciter is equipped with a single input PSS, and initially no lead/lag-filter are implemented in the structure. First step of the tuning procedure, of this single input stabilizer, is to increase the gain and make a root locus plot of the most critical eigenvalues. These plots are illustrated in Figure 6-1 and Figure 6-2, where the inter-area mode at 0.62 Hz and the local mode at 1.08 Hz are present. Implementation of a PSS in generator G2 will not affect other eigenvalues in the system in a noticeable scale. The angle of the linear root locus plot of the inter-area and local mode is calculated, based on the mathematical function of the linear line (y). These angles and the respective frequency of each eigenvalue are used as the base for calculating the time constants of the second order lead/lag-filter. Mathematical expressions of these calculations are further explained in the theory part of this master thesis.
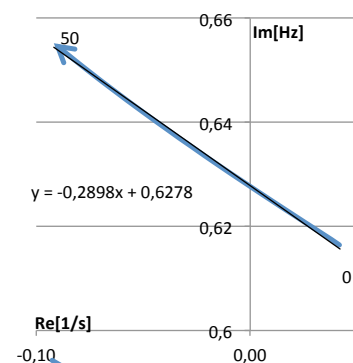
Figure 6-1: Root locus of inter-area mode.
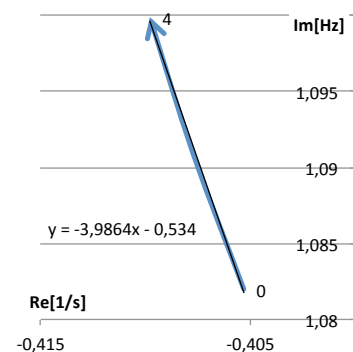
Figure 6-2: Root locus of local mode.

The lead/lag-filter of the PSS can now be tuned according to two different cases. Case 1 is a tuning procedure based on the inter-area mode and case 2 is based on the local mode. The lead/lag filter time constants are referred to the stabilizer presented in Figure 3-4 from the theory part of this master thesis.

Case 1:
Angle of root locus plot of inter-area modus at 0.61 Hz:

$$\angle = \arctan(-0.2874 \cdot 2 \cdot \pi) = -61° \rightarrow 61°$$

Time constants of a second order lead/lag-filter:
T1=T3=0.4565, T2=T4=0.1491

Case 2:
Angle of root locus plot of local modus at 1.08 Hz:

$$\angle = \arctan(-0.39864 \cdot 2 \cdot \pi) = -87.7° \rightarrow 87.7°$$

Time constants of a second order lead/lag-filter:
T1=T3=0.3459 T2=T4=0.0628
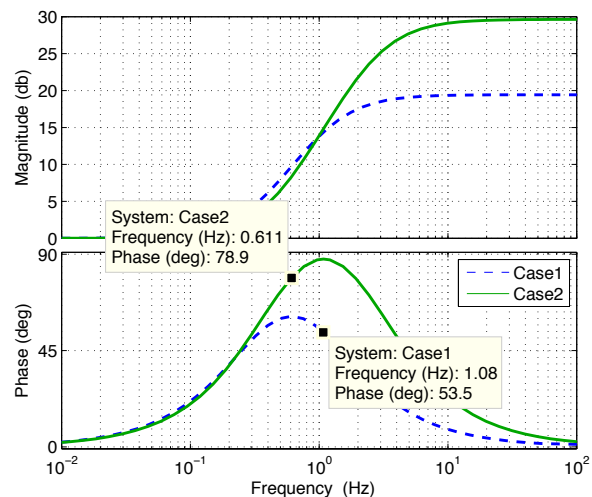
Figure 6-3: Bodé plot of lead/lag-filters

Bodé plots in Figure 6-3 indicates that the filter in case 1 will undercompensate for the local mode of 1.08 Hz. The optimal compensation is here calculated to 87.7 degrees and the filter designed for 0.61 Hz will give a phase lead of 53.5 degrees. The filter in case 2 will overcompensate the phase in the inter-area mode. By implementing these time constants in the lead/lag-filters and increasing the stabilizer gain gives the root locus plot presented in Figure 6-4. The eigenvalue relocations are basically in a direction towards the left and they become more damped as the PSS gain is increased. Both cases give a horizontal relocation of all eigenvalues, and case 2 gives the best performance. A gain equal to 12 increases the relative damping of the local mode to a value way above 10 %, while the inter-area mode will achieve a relative damping that is at 5 %.
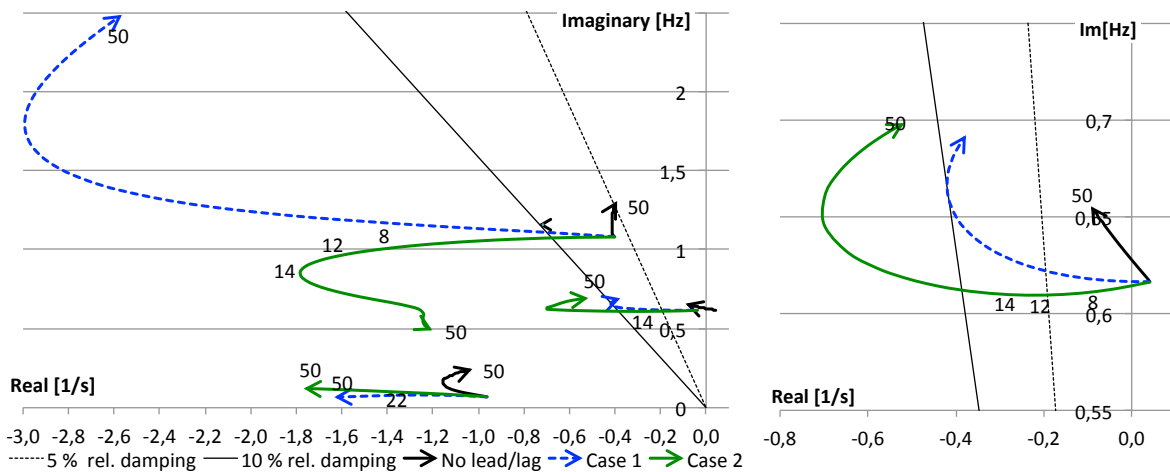
Figure 6-4: Root locus plot of the most critical eigenvalues in the system. PSS1A is installed in AVR1 in generator G2 and is tuned according to the cases. Right graph is a zoom up at the inter-area mode.

6.1.2   With multiplication of generator voltage at exciter output, AVR2

This exciter is first loaded with the same PSS parameters used for AVR1 (case 1 and case 2), and next the PSS is tuned specific according to AVR2. Calculations and bode-plot of these cases (Case 3 and Case 4) are left in the appendix. A result of the integration of these filters is presented in the root locus plot in Figure 6-5, where the gain of the single input PSS is increased. The graphs indicate that the multiplication of generator voltage has great influence at the pole placements.
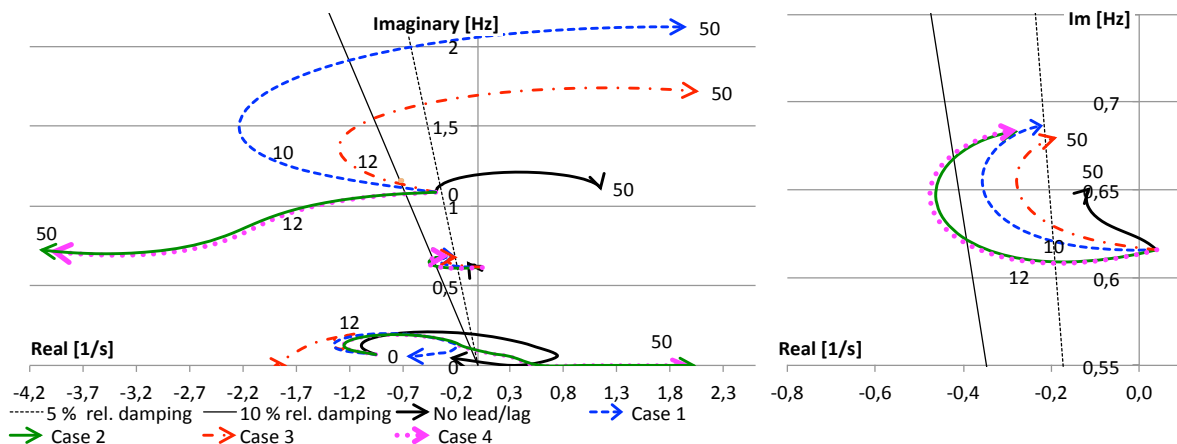
Figure 6-5: Root locus plot of the most critical eigenvalues in the system. PSS1A is installed in AVR2 in generator G2 and is tuned according to the cases. Right graph is a zoom up at the inter-area mode.

When the lead/lag-filter is tuned according to the inter-area mode (case 1 & case 3) the eigenvalues is initially moving to the right in the complex plane. At around a gain of 15 they bend off and rapidly starting to move towards the right part of the complex plane. The

maximum damping obtained in this case is lower compared to the result from AVR1 in the previous subchapter. When the lead/lag filter is tuned according to the local oscillation mode (case 2 & case 4) the eigenvalues is moving in a more favourable direction, and the damping gets higher for both local and inter-area mode. Overall the tuning of AVR2 is more troublesome compared to AVR1, since the eigenvalues tends to easily move towards the left part of the complex plane.

6.2 Tuning of the PID regulator of Thyricon® Excitation System

The PID-part of the excitation systems is here further tuned, according to a step in reference voltage. To handle this voltage step the DSL-code must be modified, and further explanation of these DSL-file corrections is placed in the appendix. Excitation system named AVR1 and AVR2, explained in the simulation description, is loaded with two sets of PID-parameters. One set has parameters that have relative gentle values, while the other set has a set of more "aggressive" values. The exact parameter values are found in Table 6-1.

By initially loading the excitation system named AVR1 with so-called "gentle" parameters the voltage overshoot, illustrated as a blue dashed line in Figure 6-6, is measured to:

$$\frac{1.004 - 1.0}{0.05} = 0.08 \rightarrow 8\% \ .$$

The response is not oscillating and it takes about 0.8 second to reach 90 % of the step. This is a voltage response that is too slow compared to the given restrictions. The parameters are then

Figure 6-6: Voltage step response of AVR1 and AVR2.

adjusted to give a result that practically gives no overshoot and to take about 0.4 seconds to reach 90 % of the step. This "adjusted" settings gives a voltage response that is within the requirements. When the variation of generator voltage is directly taken into account, by multiplication of stator voltage at AVR output, the step response gives a higher voltage overshoot, but not a higher rise-time. The result of the step responses, presented in Figure 6-6, shows clearly that AVR1 gives less overshoot compared to AVR2. The complete results

of the step response test are also presented in Table 6-1, and the overall difference between the excitation systems is not enormous.

Table 6-1: Step-response performance of the different excitation systems with two sets of parameters

Excitation sys.	AVR1		AVR2	
PI-parameters	"Gentle" Kp=5, Ti=2	Adjusted Kp=10, Ti=7	"Gentle" Kp=5, Ti=2	Adjusted Kp=10, Ti=7
Overshoot (max 15 %)	~0 %	8 %	2 %	12 %
Rise time (max 0.5 s)	0.8 s	0.4 s	0.8 s	0.4 s
Oscillations	-	-	-	-

AVR2 is the most correct representation of Voith Hydro's Thyricon® Excitation system, and it is used in the following simulations. It is loaded with the adjusted parameters presented in Table 6-1 in the following simulations.

6.3 Analysis of the five-generator network

The excitation system that includes the multiplication of the generator voltage (AVR2) is installed in the hydro generator of the five-generator network. A PSS is not initially implemented in the network, but it will be implemented in the small generator in the following chapters of this master thesis. Eigenvalue diagram, presented in Figure 6-7, explains the system oscillation when no PSS is installed. The eigenvalue at ~0.62 Hz is the worst damped eigenvalue, and it is located considerable close to the imaginary axis. At around 1.1 Hz two other eigenvalues is located, and at approximately 1.6 Hz the last critical eigenvalue is found. These four eigenvalues will highly contribute to oscillations in the network.
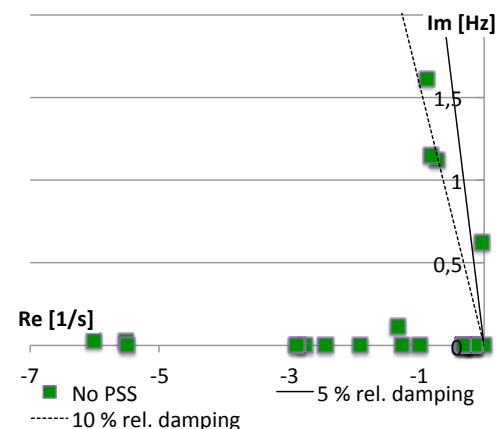
Figure 6-7: Most critical eigenvalues in the network.

One solid line and one dashed line are drawn in the diagram to indicate the relative damping of 5 % and 10 %, respectively. A higher oscillating frequency (imaginary axis) requires more absolute damping (real axis), in order to be considered as well damped [6]. The modal analysis of the five-generator network (Figure 6-8) indicates that the network is struggling with four oscillation modes.
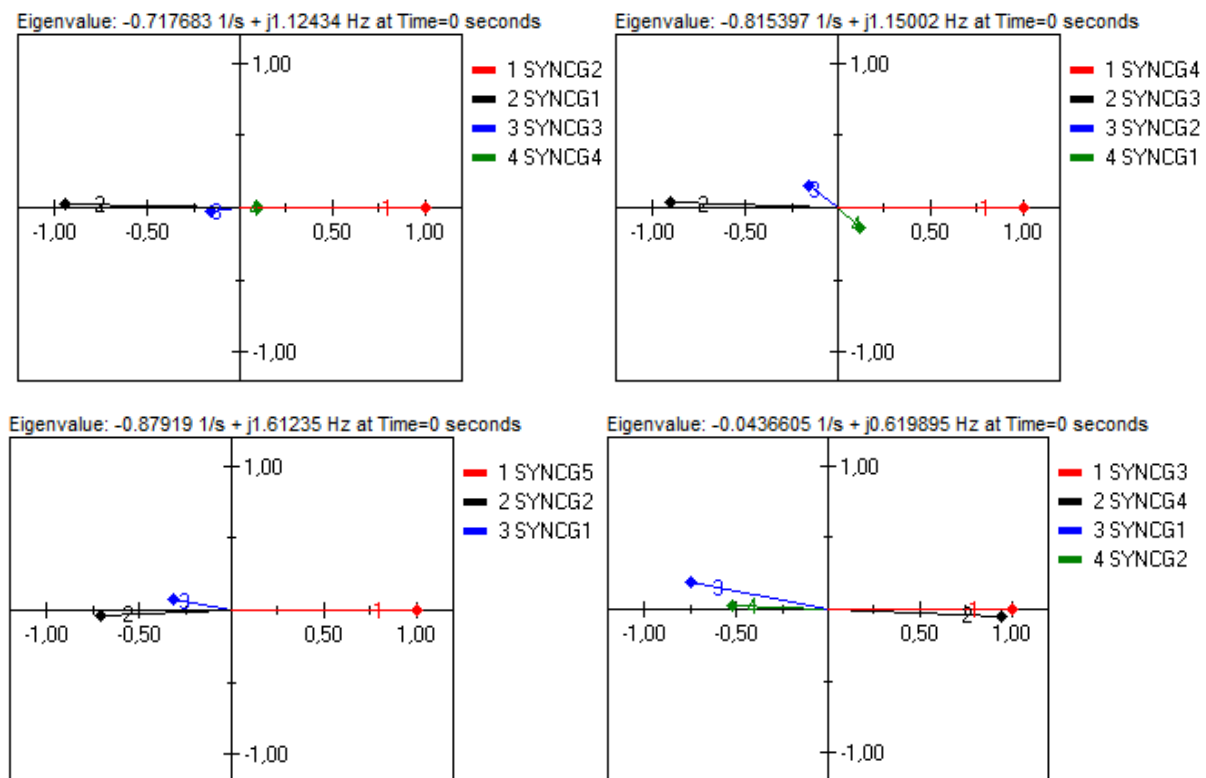
Figure 6-8: Modal analysis of the five-generator network.

At around 0.62 Hz the inter-area oscillation mode clearly appears, where generator SYNCG1 and SYNCG2, from area 1, oscillates against generator SYNCG3 and SYNCG4, from area 2. The smaller hydro generator, SYNC G5, is not present in Figure 6-8 at this mode. The reason is that the contribution from this generator is small, and the vector will not be visible when it is plotted together with the larger generators. Table 6-2 displays the complete list of all generators that contribute in the respective oscillation modes. The table shows that the small contribution from generator SYNCG5 is present also in the inter-area mode. It is not expected that this small generator will be able to highly improve the inter-area oscillations in the network [4].

Each area has also one local oscillation mode between the large turbo generators at approximately 1.124 Hz and 1.15 Hz. The hydro generator does not take any considerable part in these oscillation modes. An additional local oscillation mode appears between the hydro generator and the two larger turbo generators in area 1. The oscillation frequency of this mode is at 1.61 Hz, and the hydro generator is the reference of this mode (magnitude of 1.0 and angle of 0 degrees). Damping of this oscillation mode will highly increase by correct control of the hydro generator.

Table 6-2: Vectors (magnitude and angle) of kinetic energy represented in the eigenvalues.

Eigenvalue ([1/s], [Hz]): -0.71771, 1.1243				Eigenvalue ([1/s], [Hz]): -0.81539, 1.15			
Generator	Area	Magnitude	Angle [°]	Generator	Area	Magnitude	Angle [°]
SYNC G1	1	0.94582	178.22	SYNC G1	1	0.18938	-49.855
SYNC G2	1	1.0000	0.0000	SYNC G2	1	0.21498	135.66
SYNC G3	2	0.15743	-169.43	SYNC G3	2	0.90916	177.74
SYNC G4	2	0.094176	-0.85834	SYNC G4	2	1.000	0.000
SYNC G5	1	0.013682	47.095	SYNC G5	1	0.0056527	-178.06
Eigenvalue ([1/s], [Hz]): -0.04358, 0.61987				Eigenvalue ([1/s], [Hz]): -0.8796, 1.6125			
Generator	Area	Magnitude	Angle [°]	Generator	Area	Magnitude	Angle [°]
SYNC G1	1	0.11173	165.48	SYNC G1	1	0.32915	-165.73
SYNC G2	1	0.51883	177.39	SYNC G2	1	0.70653	-177.28
SYNC G3	2	1.000	0.00	SYNC G3	2	0.023592	142.64
SYNC G4	2	0.94625	-2.782	SYNC G4	2	0.05005	-175.93
SYNC G5	1	0.035099	171.38	SYNC G5	1	1.000	0.000

Table 6-3 displays two of the most critical eigenvalues in the system, which can be improved by the hydro generator. Additionally the relative damping of these are calculated according to equation 3.10 from the theory part of this master thesis. Generator G5 is later used to improve the damping of these two eigenvalues.

Table 6-3: Critical eigenvalues that can be improved by generator G5.

Stabilizer	Oscillation mode	Eigenvalue [1/s], [Hz]	Relative damping [ζ]
No PSS	Local	(-0.8796, 1.6125)	8.65 %
	Inter-area	(-0.0436, 0.6198)	1.12 %

The oscillations mentioned above can also be shown in a time domain analysis, illustrated in Figure 6-9, where a 3-phase short circuit at BUS8 is present for 0.05 seconds. Suddenly in the aftermath of the disturbance the more high frequent local oscillations is present. These oscillations are damped, and thereby replaced by an oscillation with a lower frequency. After approximately 5 seconds only the inter-area oscillations remains, where generator G1, G2 and G5 (Area 1) clearly oscillates against generator G3 and G4 (Area 2).
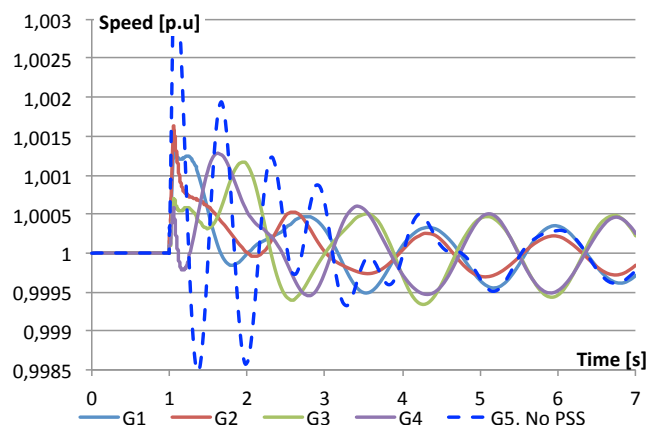
Figure 6-9: Time response of the generator speeds after a 3-phase short circuit fault at BUS8.

This oscillation is considerable poorly damped. The blue dashed line in Figure 6-9 indicates that G5 struggles with the toughest oscillations in the network. An installation of a PSS at this unit seems to be a good choice.

6.4 Implementing a dual input stabilizer (PSS2B)

6.4.1   Analysis of the input transducers

PSS2B stabilizer is implemented in generator G5 of the five-generator network and a 3-phase short circuit, with duration of 0.05 second, starts the oscillations presented in Figure 6-10. The integral of accelerating power signal is compared to the actual rotor speed in Figure 6-10, and this is slightly leading a bit in the first oscillations. After approximately five seconds the integral
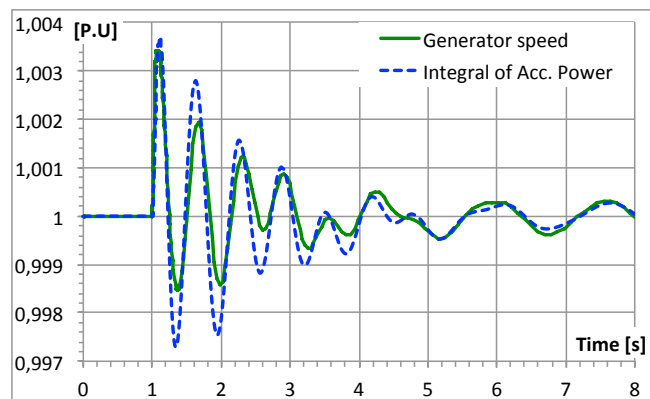
Figure 6-10: Time domain analysis of actual generator speed and PSS2B synthesised speed.

of accelerating power signal is directly following the generator speed signal. The overall variation between the two signals is considerable low, and the integral of accelerating power can be used as an input-signal to the lead/lag-filter and gain part of the stabilizer. The integral of accelerating power signal can now be considered as an equivalent speed signal, as described in the theory of this PSS [4].

6.4.2   PSS2B lead/lag-filter and gain

By increasing the gain of the stabilizer in the range 0<KST<2, and with a step of 0.5, the eigenvalues are relocated according to Figure 6-11. The linear part of this movement indicates the needs of phase compensation. Three different cases of tuning the lead/lag-blocks are now performed. All these cases are based on the respective eigenvalue frequency and the initial angle of the root locus plot in Figure 6-11. The lead/lag-filter in case 1 is tuned at the inter-area mode, the filter in case 2 are tuned at the local mode, and the filter in case 3 are tuned as a compromise between those two modes.
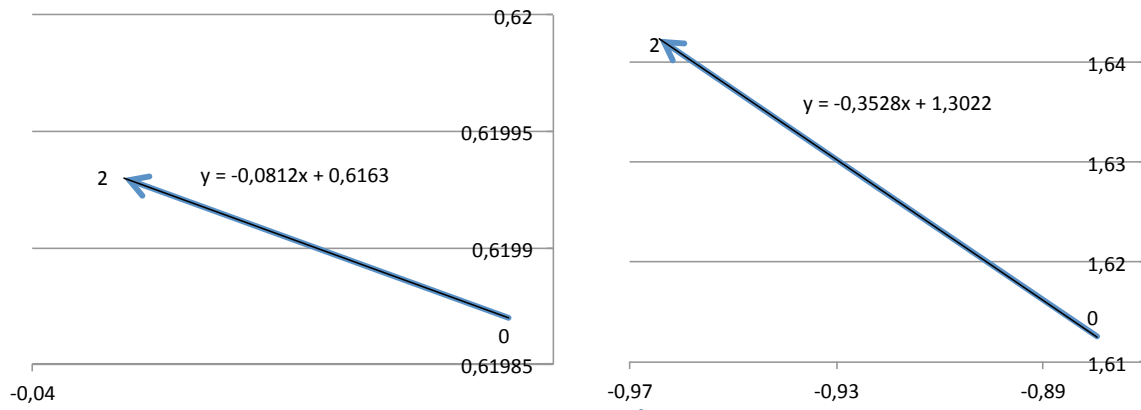
Figure 6-11: Initial root locus plot. 0<KST<2, step=0.5. y is the mathematical expression of the linear line. Left: Inter-area mode. Right: Local mode.

An expression of the linear line (y in Figure 6-11) is computed and the slope of this expression is used to find the initial angle, referred to the real axis.

Case 1.

Angle of the relocation of the inter-area mode starting at 0.62 Hz:

$$\arctan(-0.0812 \cdot 2 \cdot \pi) = -27° \rightarrow 27°$$

Case 2.

Angle of the relocation of the local mode starting at 1.61 Hz:

$$\arctan(-0.3528 \cdot 2 \cdot \pi) = -65.7° \rightarrow 65.7°$$

Case 3.

A compromise between case 1 and case 2.

Set to 50 degrees at 1.7 Hz.
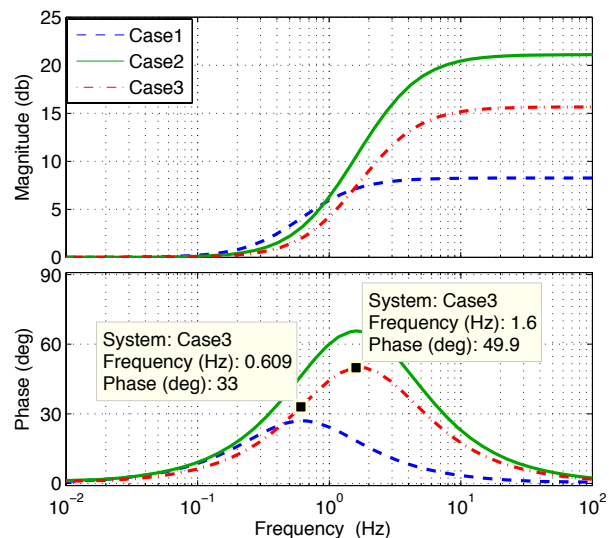
Figure 6-12: Bodé-plot of the three different tuning cases.

These angles and frequencies are used to compute the respective time constants of the lead/lag-filters. (Formulas and procedure is found in the theory part of this master thesis). The filter of each case is further analysed in the bodé-plot in Figure 6-12. This plot indicates that the lead/lag-filter tuned at the local mode (Case 2) gives a phase compensation of 46 degrees at the inter-area mode (0.61 Hz). This compansation is too strong compared to the optimal value in that spesific frequency. Inter-area mode is the base of calculating the time constants of case 1, and the resulting bodé-plot indicates a phase adjustment at the local mode (1.6 Hz) that is approximatly 18 degrees. This is a compensation that is much weaker than wanted in this spesific frequency. Case 3 is chosen to be a compromise between those two cases, and the

bodé-plot indicates a maximum phase response of 50 degrees at 1,7 Hz. This filter is produsing a phase lead of about 33 degrees at the inter-area mode, and a phase lead near to 50 degrees at the local mode. Table 6-4 displays the tuning data of the lead/lag-filters used in the following eigenvalue analysis.

Table 6-4: PSS2B lead/lag-filter parameters.

Adjustment			Parameters	
	Freq.	Angle	T1=T3	T2=T4
No lead/lag	-	-	1	1
Case 1	0.62 Hz	27	0.3256	0.2024
Case 2	1.61 Hz	65.7	0.1815	0.0538
Case 3	1.7 HZ	50	0.147	0.0596

By implementing the different parameters, presented in Table 6-4, and by increasing the stabilizer gain from 0 to 50 the eigenvalues will move according to the plot in Figure 6-13. The black solid arrow is the root locus plot where no lead/lag-filter is installed, and the initially movement is clearly not in parallel with the real axis. Suddenly it bends off, and the damping decreases. By introducing the filters described in the different cases, the oscillation mode at 1.61 Hz gets heavily affected. Lead/lag-filter described in case 2 gives an absolute damping (real axis) of approximately 3.1 before the curve bends off, and the damping decreases. Case 3, the compromise solution, gives also an increased damping of the local mode at 1,61 Hz, but it
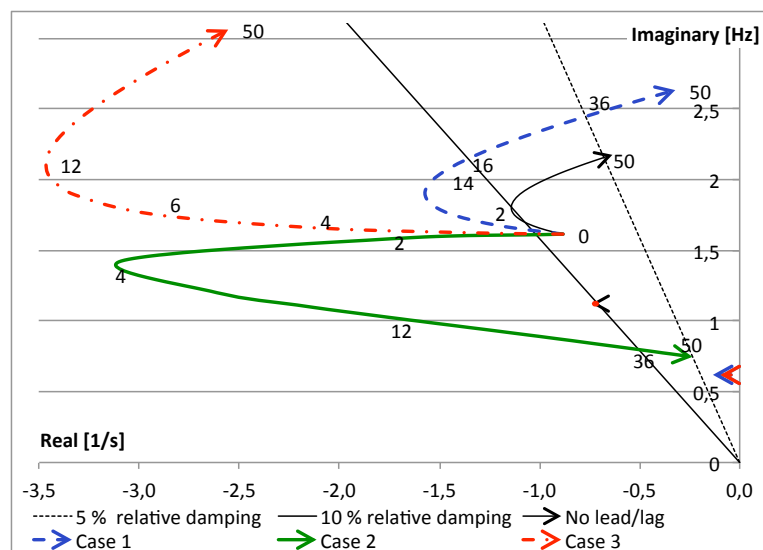
Figure 6-13: Root locus of the most critical eigenvalues. Stabilizer gain is increased in the range 0<KS1<50.

requires a higher gain compared to case 2. Maximum value of the absolute damping is 3.5, and this occurs when the gain is set equal to 12. The other oscillation modes are not responding in the same scale, and only the inter-area mode at 0.62 Hz has a noticeable movement at all.

By zooming up on the inter-area mode the root locus of this mode becomes more clearly. When tuning the lead/lag-filter according to case 1 the eigenvalue is moving in a curve that

has an initially horizontal direction, as expected from the calculations. The damping increases in the whole range and stops at approximately 0.14, where the gain is 50. This gain is too high when the local oscillation mode (Figure 6-13) is taken into consideration. The result of implementing the

Figure 6-14: Zoom up at the inter-area mode.

lead/lag filter presented in case 2 gives a relocation of the inter-area mode that is pointing downwards in the complex plane. The compromise solution (case 3) achieves a better result compared to case 2, where the oscillatory frequency is more or less unchanged.

By choosing a PSS gain equal to 12 and a lead/lag-filter according to case 3, the local mode (starting at 1.61Hz) has moved to its point of maximum damping. Here is the absolute damping approximately 3.5 and the frequency is 2.1 Hz. The inter-area oscillating frequency has decreased, while the absolute damping of this eigenvalue has increased. Figure 6-15 displays the most critical eigenvalues in the system, the ones closest to the imaginary axis, where the green dots is the result without a PSS, and the blue dots is the result where PSS2B is implemented. The eigenvalue starting at 1.6
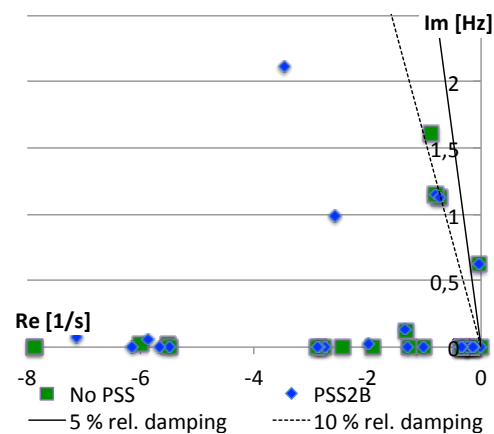
Figure 6-15: Most critical eigenvalues in the system with and without PSS2B.

Hz is moving rapidly to the left by implementing PSS2B and the damping of this local mode has increased. An other eigenvalue has appeared close to 1 Hz as an adverse effect of implementing PSS2B. The eigenvalue related to the inter-area mode is not improved considerable, but the relative damping is calculated to 1.3 % (Table 6-5). This is a small improvement compared to the relative damping of 1.12 % obtained in the situation where no PSS was installed.

Table 6-5: Resulting eigenvalues of case 3 and a gain of 12.

Stabilizer	Oscillation mode	Eigenvalue [1/s], [Hz]	Relative damping [ζ]
No PSS	Local	(-0.8796, 1.6125)	8.65 %
	Inter-area	(-0.0436, 0.6198)	1.12 %
PSS2B, Case 3	Local	(-3.4664, 2.1099)	25.3 %
	Inter-area	(-0.0506, 0.61976)	1.30 %

6.4.3   Time domain analysis

The reduction of system oscillations is also illustrated in a time domain analysis, presented to the left in Figure 6-16. Hydro generator G5 is relative small compared to the other production units in the system, and the inter-area oscillation mode is not highly reduced by implementing a PSS in this generating unit. To totally get the best performance in both modes, the gain is set equal to 12 and the lead/lag-filter described as case 3 is implemented. The local oscillation mode appears right after the system has started to oscillate, and the blue-dashed line indicate that these oscillations are well damped compared to the situation where no PSS is implemented. At around 3 seconds only the inter-area oscillations remains, and the damping of these oscillations are not noticeable improved. The analysis indicates that these oscillations will at least not increase and eventually they will die out. The PSS output signal is additionally plotted in Figure 6-16, and a gain equal to 12 makes the output signal saturate for 1,5 periods. A limiter at the PSS output is set equal to ±0.05 and the scale of this graph is located to the right in the plot window. The saturation is acceptable, and it indicates that the PSS is working properly without stressing the excitation system. The result of the time domain analysis indicates that the overall damping of speed oscillations is better when the PSS2B is implemented.
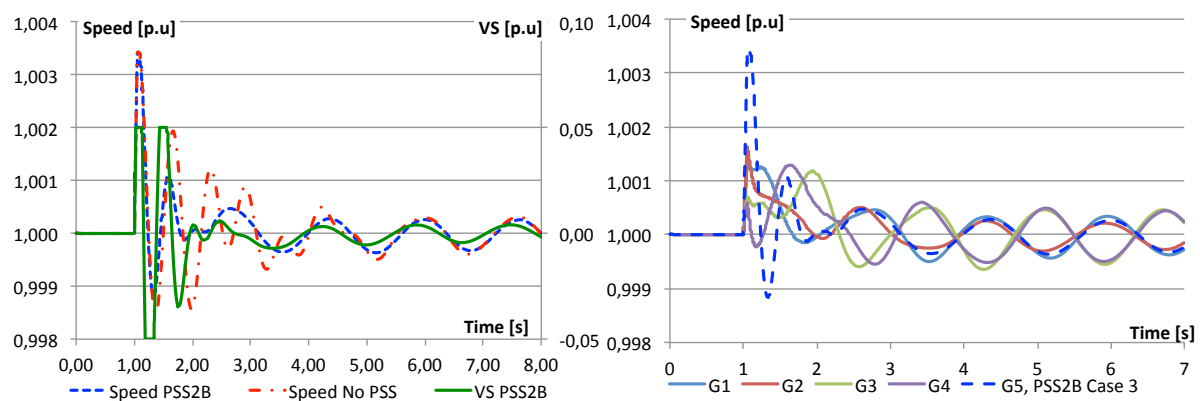
Figure 6-16: Left: Time response of the speed in generator G5 and PSS2B output signal (VS). PSS tuned as Case 3 and Ks=12. Right: Time response of generator speed the whole network.

By looking at the time domain response of the whole network, presented to the right in Figure 6-16, the local mode at generator G5 is well damped. The local oscillations between generator G1&G2 and between generator G3&G4 is not easy to locate, but these are also acting instantaneously when the fault is removed. At around 3 seconds the inter-area oscillations are clearly present, and these are not well damped.

Another time domain analysis is performed where a load of 500 MW is disconnected at BUS9. Figure 6-17 illustrates that active power, delivered by generator G5, starts to oscillate against a lower value, and the implementation of PSS2B has only marginally effect on the damping of this oscillation. PSS2B gives a response of the reactive power that is more fluctuating compared to the situation where PSS2B is disconnected. The peak value is near to 0.5 p.u, and this aggravation of reactive power response is a prise to pay for the increased damping of the system oscillations.
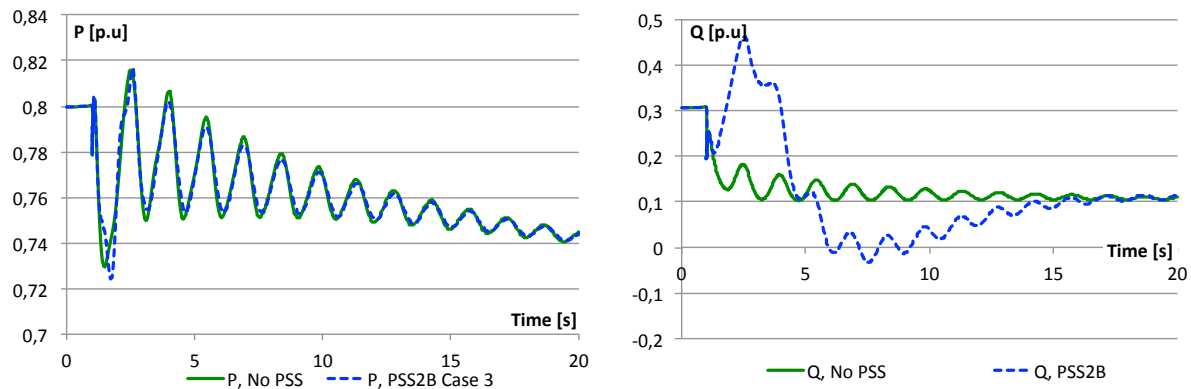
Figure 6-17: Time domain analysis, where 500 MW at BUS9 is disconnected. PSS2B is installed in generator G5 and tuned according to case 3.

6.5 Implementing a multi-band stabilizer (PSS4B)

6.5.1   Loading the PSS4B structure with sample data given by IEEE

Power system stabilizer PSS4B is here tuned and installed in the hydro generator (G5) of the five-generator network, according to the sample data given by IEEE (Table 5-2). This implementation will give eigenvalues according to the left plot in Figure 6-18, and this indicates that two of them have less relative damping than 5 %. Based on this analysis, the electrical system is worse damped and a fault in this state of operation will give stronger oscillations compared to a system without a PSS.

The result of a time domain analysis (right graph in Figure 6-18) shows that the damping of the speed oscillations (blue-dashed line) is reduced when the PSS4B is implemented and loaded with the sample data, given in IEEE Std. 421.5 [1]. The speed of generator G5 will also oscillate with a higher frequency compared to the situation where the PSS is turned off (red dash-dotted line). Signal *VS* (the green solid line) is the output signal from the PSS, and the figure indicates that the PSS is clearly stressed. The stabilizer will not act as wanted and

thereby increase the damping. The stressed PSS results in a stressed excitation system and the speed of the generator is highly disturbed. PSS output limiter is set according to IEEE example data equal to 0.15. This value gives a time domain result that is difficult to compare with the result from PSS2B, which has a limiter value of 0.05. There is a need of extra tuning of this multi-band PSS, in order to improve the damping of the system oscillations and also make it comparable with the dual-input PSS.
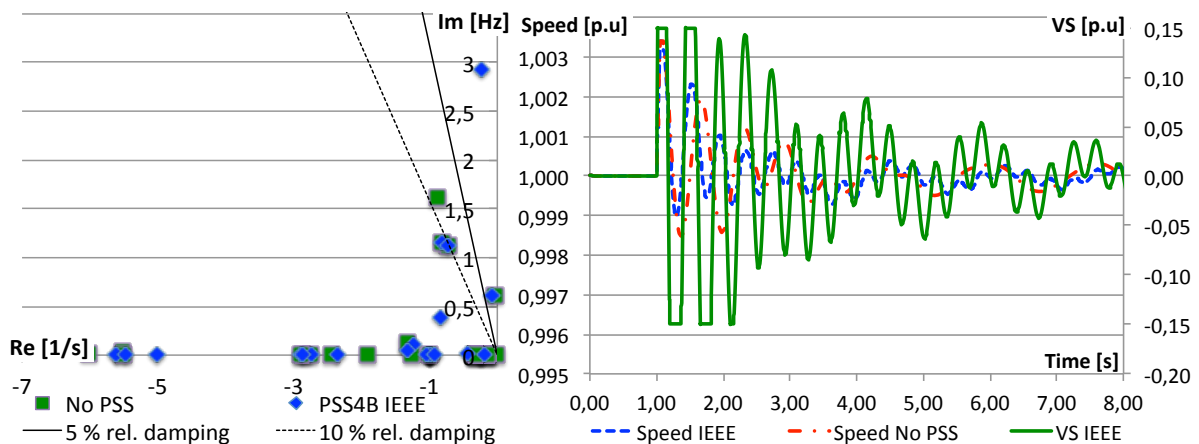
Figure 6-18: PSS4B with IEEE example parameters is installed in generator G5. Left: Critical eigenvalues in the network. Right: Time response of rotor speed and PSS output signal (VS) after a 3-phase short circuit has occurred in the network.

6.5.2   Tuning of the PSS4B structure based on the actual network oscillations

Complete lists of PSS4B parameter values and eigenvalues of each case are found in the appendix of this master thesis.

Case 1

Parameter *Kh* of PSS4B is increased with steps of 0.5, in order to find the initial angle of the root locus plot of the local and inter-area eigenvalue. Figure 6-19 displays the initially eigenvalue relocations, and a mathematical expression of the linear line. The angles of these lines are calculated blow:

Angle of the relocation of the local mode, starting at 1.6125 Hz:

arctan(2π·-1.049)=81.37° (lead)

Angle of the relocation of the inter-area mode, starting at 0.61987 Hz:

arctan(2π·0.0667)=22.74° (lag)
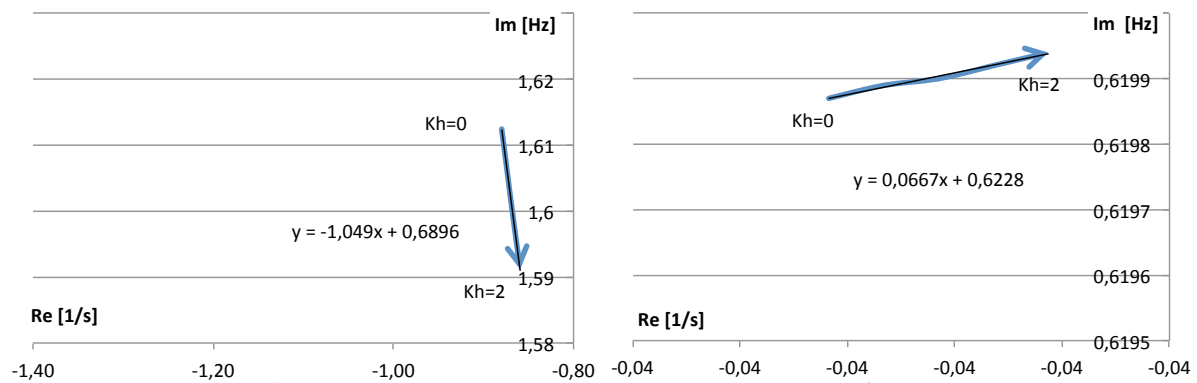
Figure 6-19: Initial root locus of local and inter-area oscillation mode. 0<*Kh*<2, step 0.5.

Both oscillation modes need a negative gain in order to move to the left in the complex plane. To correct the root locus graph in an initial straight horizontal direction, the local mode needs a lead of 81.37 degrees and the inter-area mode needs a lag of 22.74 degrees. The lead/lag-filter in the high frequency band of PSS4B is tuned first and according to the local oscillation mode. Time constants are calculated by using the same formulas as used in previous chapters of this master thesis. The curves in Figure 6-20 show the result of implementing different lead/lag-filters and gains. Black solid lines are the results of increasing the gains (*Kh* and *Ki*) from 0 to 50 without any lead/lag compensation at all. These curves are the bases for calculating the time constants of the lead/lag-filters. Curve named *step 1* in Figure 6-20, displays the result of implementing the lead/lag-filter designed according to the local mode. The time constants of these filters are listed in the summary table, Table 6-6. Unlike the situation where no lead/lag-filter is included is the root locus plot of the local oscillation mode (illustrated in the left plot of Figure 6-20) initially pointing to the left in the complex plane. Increasing the gain (*Kh*) results in eigenvalue relocation and a lower oscillatory frequency. *Kh* is selected equal to -4, since a lower value will highly change the oscillating frequency. This value is large enough to give a satisfying damping of the local oscillation mode, and this is the starting point of *step 2* in the tuning procedure.
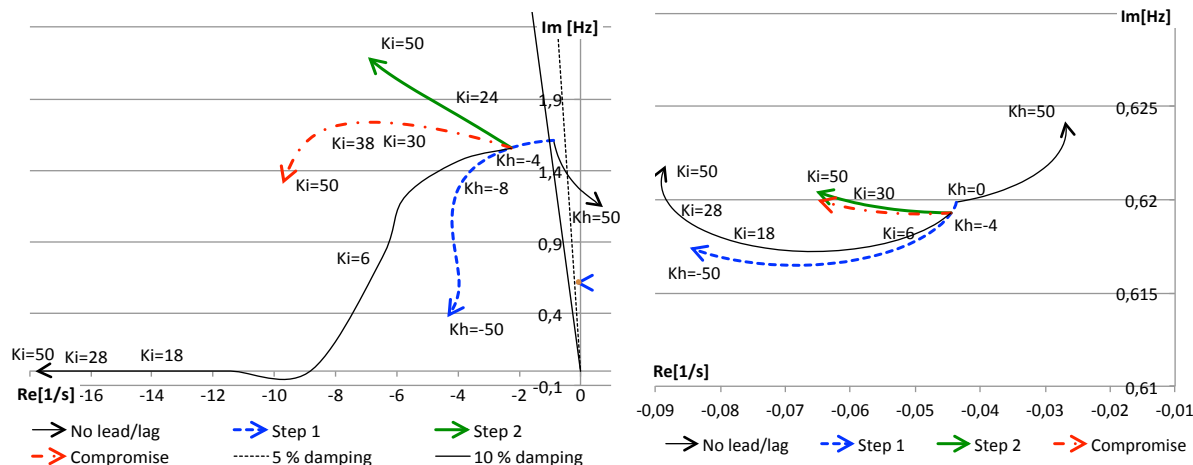
Figure 6-20: Root locus plots of local mode and inter-area mode, performed in case 1.

Right plot in Figure 6-20 is a zoom up at the inter-area oscillation mode and this graph is also pointing to the left, but initially not as straight as the local mode. This movement is corrected in step 2 by implementing the i-band of PSS4B. Step 2 is performed after the gain and lead/lag-filter, found in step 1, is implemented, and the i-band is now tuned to give a favourable eigenvalue relocation of the inter-area oscillation mode. This mode needs an initially lead of 60°, and this angle is found by the same procedure as used in step 1. The result of implementing the lead/lag-filter time constants of step 2 is shown as green solid lines in Figure 6-20. As the figure indicates will the inter-area eigenvalue now initially move straight to the left, while the local eigenvalue will move with an angle upwards in the complex plane. In order to try to totally get a better result, a compromise of tuning the lead/lag-filter at the local and inter-area oscillation mode is made. Frequency responses of these three different lead/lag-filters are presented in Figure 6-21. One of the filters in the frequency response is tuned at the local mode, one is tuned at the inter-area mode, and the last filter is tuned as a compromise between those two oscillation modes. This compromise, illustrated as the red, dash-dotted line, compensates with 52.5° at the inter-area mode and 31.2° at the local mode. After including this compromise filter in the i-band of PSS4B, the root locus plot indicates a more horizontal movement of both eigenvalues. In spite of this gives the compromise solution not a
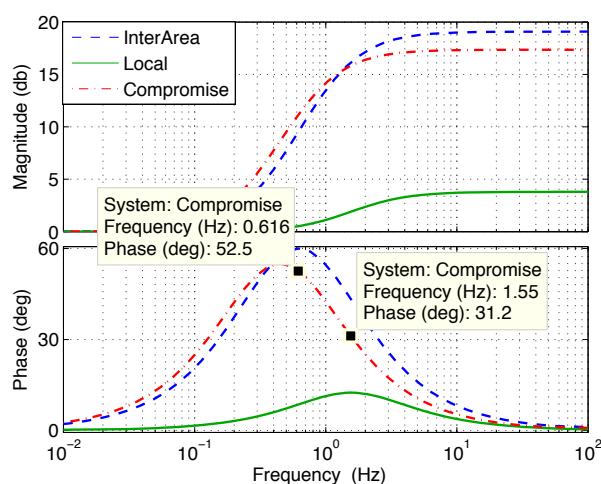
Figure 6-21: Bodé plot of the lead/lag filters used in Step 2.

better damping, compared to the situation where no lead/lag-filter is implemented. The final choice of step 2 is to not implement a lead/lag filter in the i-band at all, since this solution gives the best damping. By choosing a gain of the i-band equal to 28, and without implementing a lead lag filer in the i-band, a grate damping of both modes is obtained without considerable stressing the PSS. The final selection of case 1 is a lead/lag-filter in the h-band tuned at the local mode, and no lead/lag filter in the i-band. A summary of this tuning procedure is presented in Table 6-6.

Table 6-6: Summary of the tuning process presented in case 1.

	Step 1	Step 2
Tuning order	h-band is tuned according to the local oscillation mode	i-band is tuned according to the inter-area oscillation mode
Wanted compensation	1.6125 Hz (local mode): 81.37° lead	0.6193 Hz (inter-area mode): 47.83° lead
Compromise	-	0.8 Hz, 50° lead
Chosen compensation	1.6125 Hz (local mode): 81.37° lead	No lead/lag
Lead/lag-filter time constants	$Th3=Th5=0.215$ $Th4=Th6=0.0453$	$Ti3=Ti5=1$ $Ti4=Ti6=1$
Gain	$Kh=-4$	$Ki=28$
Resulting eigenvalues	Local mode ([1/s], [Hz]): (-16.415, 0.00) → ζ=100% Inter-area mode ([1/s], [Hz]): (-0.0878, 0.61978) → ζ=2.25 %	

A time domain analyses of the PSS output signal (*VS*) and generator speed are illustrated to the right in Figure 6-22, and to the left a plot of the initially eigenvalues is presented.
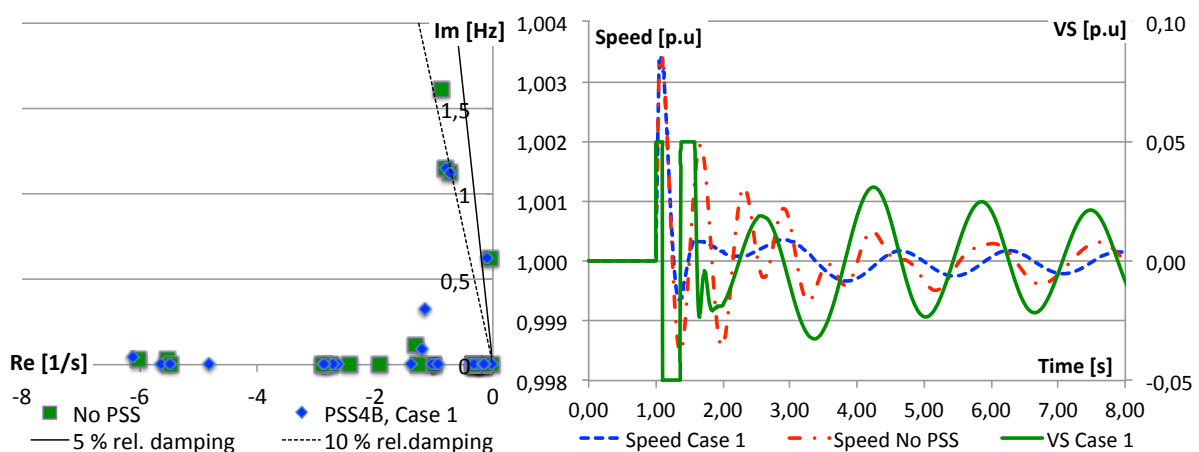
Figure 6-22: PSS4B is installed in generator G5 and tuned according to case 1. Left: Most critical eigenvalues in the network, with and without PSS4B. Right: Time domain analysis where a 3-phase short circuit with duration of 0.05 seconds is present at BUS8 in the network.

After one second a 3-phase short circuit is introduced at BUS8, and the duration is 0.05 seconds. This fault starts the oscillations in the electrical network, and the output signal of the PSS reaches suddenly the respective limiter value (±0.05) for 3 times. The speed plot

indicates that the implementation of PSS4B, tuned according to Case 1 (blue dashed line), gives increased damping of the oscillation, compared to the situation where no PSS is present (red dash-dotted line). The high frequency oscillations are removed and only the inter-area oscillation remains. The damping of these oscillations is also increased compared to the situation where no PSS is installed.

Case 2

First step in case 2 is to tune the lead/lag-filter in the h-band, according to the initial angle of the movement of the inter-area oscillation mode. Increasing the Kh will relocate the eigenvalue, related to the inter-area mode, to the right in the complex plane. The damping of this mode is then decreasing (See Figure 6-23). This movement is corrected in the opposite direction by choosing a gain that rather decreases from 0 to -50. In order to correct the relocation of the eigenvalues related to the inter-area mode, the lead/lag filter must cause a phase lag of 22.74° at 0.62 Hz (See Figure 6-19). This angle is calculated in the previous case. The eigenvalue of the local oscillation mode is moving towards the imaginary axis, and a compromise is made in order to totally get a better response. The compromise uses only a negative gain with no lead/lag-filter in the high-frequency branch. This gives a better result in both local and inter-area oscillation modes, and the gain (Kh) is selected equal to -50, in order to maximize the damping of the inter-area mode. Absolute damping of the inter-area mode is now increased to approximately 0.06 1/s. The eigenvalue related to the local mode has moved upwards in the complex plane with a final value of approximately 2 Hz, and it has no improvement of the damping. This is the starting point of step 2 in the tuning procedure of case 2.
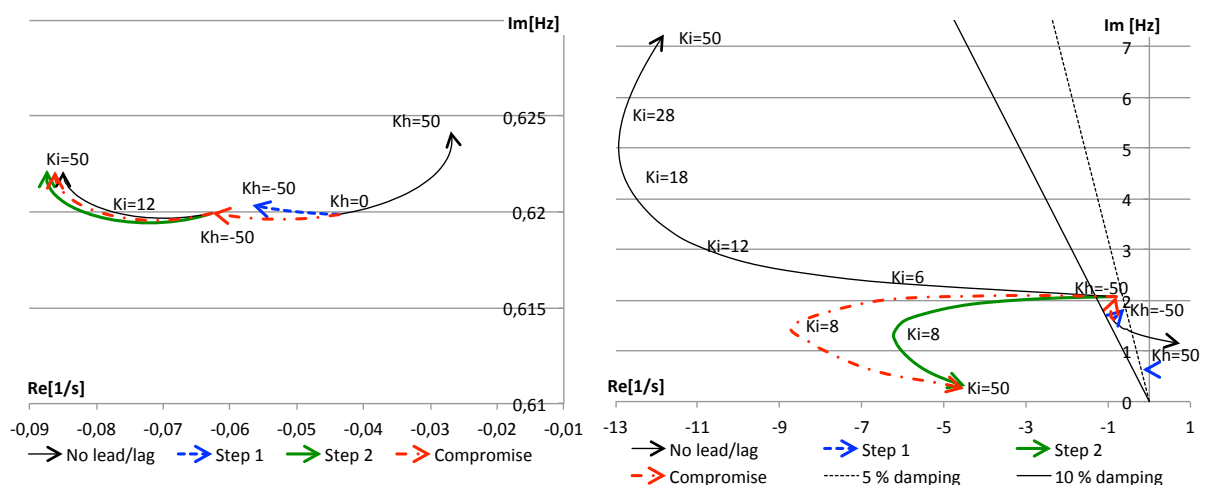
Figure 6-23: Root locus plots of inter-area mode and local mode, performed in case 2.

Step 2 in this case utilizing the i-band of PSS4B to increase the damping of the local oscillation mode. The h-band is now held to the fixed values explained in step 1. An increased *Ki* gives a root locus plot that pointing in a favourable direction, but with a leading angle of 17.77°. Introducing a phase-leading filter at this value corrects the angle, and the result of this implementation is illustrated as the green solid line in Figure 6-23. The implementation causes only a smaller difference in the inter-area mode, compared to the situation where no lead/lag-filter is present in the i-band. A compromise solution is illustrated as the red dash-dotted line in Figure 6-23, where a lower angle of 9° gives increased damping of the local mode. The relocation of the local mode bends off and starts to decrease at around an absolute damping of 8 1/s. This filter and gain is the final solution of step 2. Table 6-7 is a summary of the tuning process of case 2 and contains the chosen parameters.

Table 6-7: Summary of the tuning process presented in case 2.

	Step 1	**Step 2**
Tuning order	h-band is tuned according to the inter-area mode	i-band is tuned according to the local mode
Wanted compensation	0.61987 Hz (inter-area mode): 22.74 ° lag in neg. dir.	1.62 Hz (local mode): 17.77° lead
Compromise	0.61987 Hz (inter-area mode): 0° and a neg.dir.	1.62 Hz (local mode): 9° lead
Chosen compensation	0.61987 Hz (inter-area mode): 0° and a neg.dir.	1.62 Hz (local mode): 9° lead
Lead/lag-filter time constants	$Th3=Th5=1$ $Th4=Th6=1$	$Ti3=Ti5=0.0836$ $Ti4=Ti6=0.0714$
Gain	$Kh=-50$	$Ki=8$
Resulting eigenvalue	Local mode ([1/s], [Hz]): (-8.6772, 1,5177) → ζ=67.3 % Inter-area mode ([1/s], [Hz]): (-0.0709, 0.6196) → ζ=1.82 %	

The result of the time domain analysis, where a 3-phase fault is introduced, indicates that this tuning procedure will also give an acceptable result. The instantaneously high frequent oscillations are removed, and the inter-area oscillation has an increased damping. PSS output signal reach the limiter value for three times and does not stress the excitation system.
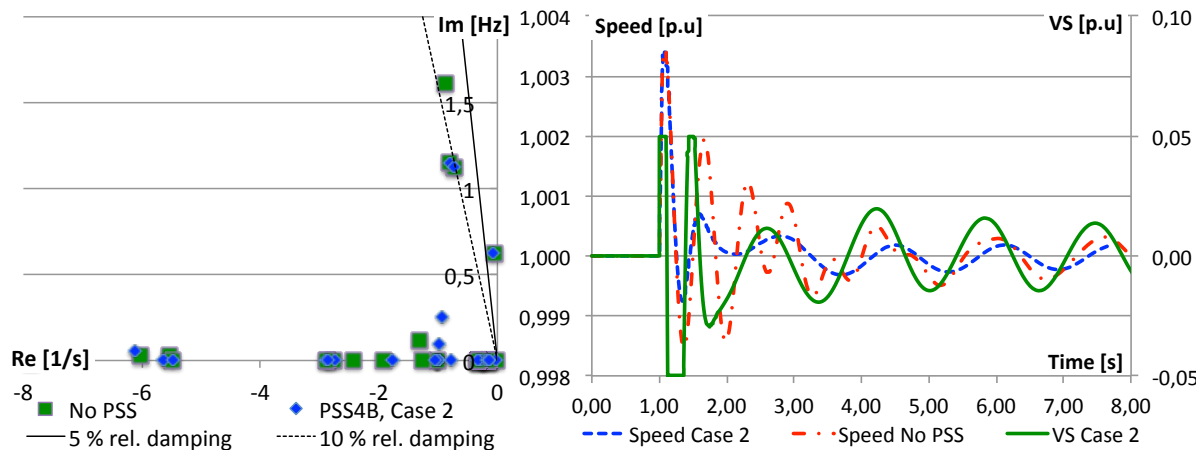
Figure 6-24: PSS4B is installed in generator G5 and tuned according to case 2. Left: Most critical eigenvalues in the network. Right: Time domain analysis where a 3-phase short circuit appears for 0.05 seconds at BUS8.

Case 3

The tuning procedure presented here, in case 3, starts with tuning the i-band, and the initial angles of the inter-area and local oscillation mode are uncovered. Ki is increased in steps of 0.5 in order to find the initial angles the relocation of each oscillation mode.

Angle of the relocation of the local mode, starting at 1.6125 Hz:

$$\arctan(2\pi \cdot 0.002) \approx 0°$$

Angle of the relocation of the inter area mode, starting at 0.61987 Hz:

$$\arctan(2\pi \cdot 0.0667) = 68.9° \text{ (lag)}$$
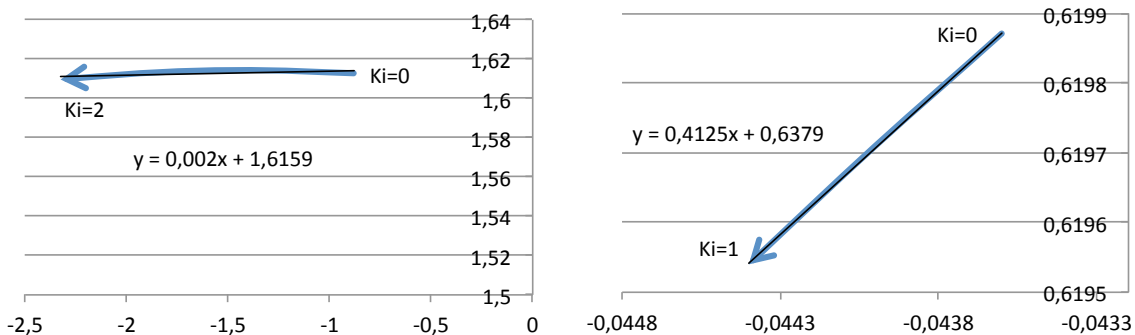
Figure 6-25: Initial root locus plots of local and inter-area oscillation mode, respectively.

Step 1 of case 3 adjusts the inter-area oscillation mode to move straight to the left in the complex plane. A lead/lag-filter, that produces a lag of 68.9° at 0.62 Hz, is implemented in the i-band, and the result is presented as the blue dashed line in Figure 6-26. The response at the local oscillation mode is small, and a compromise is made to get increased effect of the damping of the local mode. This lead/lag-filter produces a lag of 30° at 0.62 Hz, and the result

of implementing this compromise-filter shows increased damping of both oscillation modes. The gain of the i-band is now set equal to 26, which is the starting point of step 2.
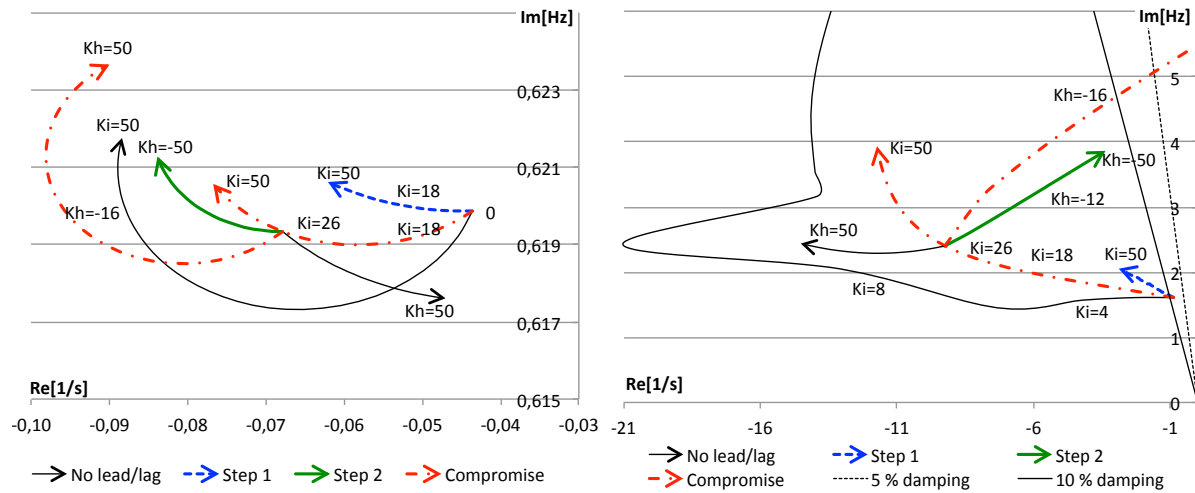
Figure 6-26: Root locus plots of inter-area mode and local mode, performed in case 3.

By increasing *Kh* the eigenvalue related to the inter-area mode is moving to the right, and the local mode eigenvalue moves almost straight to the left. Forcing the inter-area mode to initially move to the left in the complex plane, shown as green solid lines in Figure 6-26, results in a local mode that is moving to the right and upwards. The damping of this mode is now reducing. A compromise is made where a lag of 30° acts at 0.62 Hz, and this compromise improves the damping of the inter-area mode even more. The eigenvalue related to the local mode is still moving towards the imaginary axis when the gain is increased. To increase the damping of the inter-area mode, and also achieve a relative damping of the local mode that is close to 10 %, the gain of the h-band is set to -16. These results and tuning parameters are also explained in Table 6-8.

Table 6-8: Summary of the tuning process presented in case 3.

	Step 1	Step 2
Tuning	i-band is tuned according to the inter-area mode	h-band is tuned according to the local mode
Wanted compensation	0.61987 Hz (inter-area mode), 68.9 ° lag	1.62 Hz (inter-area mode), 46° lead in neg. dir.
Compromise	0.61987 Hz (inter-area mode), 30 ° lag	0.691 Hz (local mode), 90° lead in neg.dir.
Chosen compensation	0.61987 Hz (inter-area mode), 30 ° lag	0.691 Hz (local mode), 90° lead in neg. dir.
Lead/lag-filter time constants	*Ti3=Ti5*=0.197 *Ti4=Ti6*=0.3345	*Th3=Th5*=0.6197 *Th4=Th6*=0.1063
Gain	*Ki*=26	*Kh*=-16
Resulting eigenvalue	Local mode ([1/s], [Hz]): (2.8098, 4.7456) → ζ=9.38 % Inter-area mode ([1/s], [Hz]): (0.0958, 0.6199) → ζ=2.47 %	

A time domain analysis of generator speed and PSS output signal (right graph in Figure 6-27) indicates that the output signal reaches the limiter value four times and the PSS is more stressed compared to the other cases until now. The overall damping of speed oscillations is acceptable, where the inter-area oscillation is clearly decreasing and the local mode is only visible in the first seconds after the disturbance has occurred. The inter-area mode is visible from 3 seconds, and these are better damped when PSS4B is installed and tuned according to case 3. The eigenvalue analysis, oriented to the left in Figure 6-27, shows that one high frequency eigenvalue has appeared near to 5 Hz. This has a relative damping that is below 10 %.
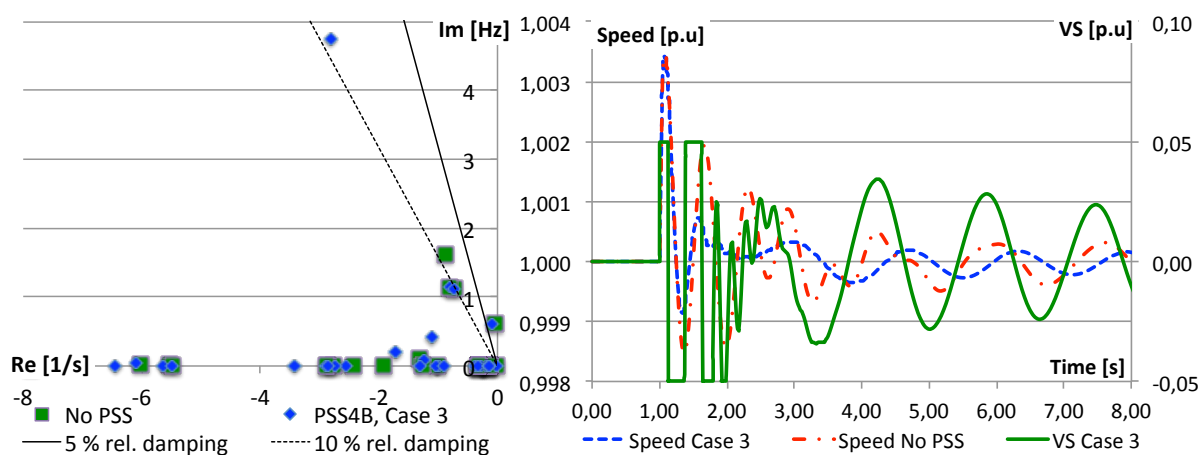
Figure 6-27: PSS4B is installed in generator G5 and tuned according to case 3. Left: Most critical eigenvalues in the network. Right: Time domain analysis where a 3-phase short circuit appears for 0.05 seconds at BUS8.

Case 4

The tuning presented in case 4 take advantage of the already good relocation of the eigenvalue related to the local oscillation mode when no lead/lag-filter is installed, and the gain of the i-band is increased. The first step in this case is to set this Ki equal to 4, and then tune the inter-area mode as a second step by using the h-band for the PSS4B. The black solid line in Figure 6-28 indicates that both eigenvalues moves to the right when *Kh* is increased, and the damping of these modes decreases. By rather decreasing the gain, the initial relocation of the inter-area eigenvalue points in a straight horizontal direction away from the imaginary axis. The movement of the local mode is initially pointing upwards and turning against the imaginary axis. There is a large difference between the responses of the respective oscillating modes, and a compromise is made where a lead/lag-filter is designed to produce a lead of 45°

at 0,62 Hz. This compromise filter is implemented in the h-band, and by setting the gain at -8 gives the best result of this case.
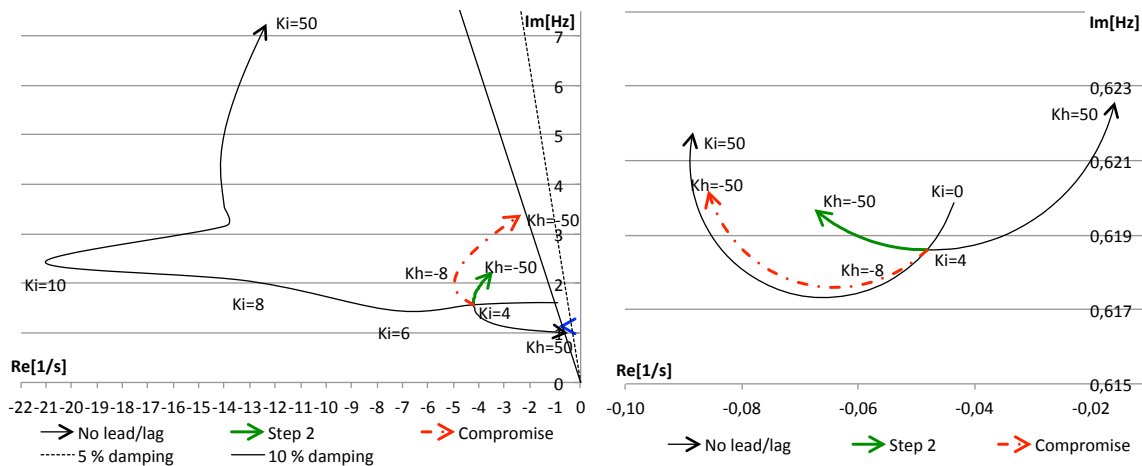
Figure 6-28: Root locus plots of local mode and inter-area mode, performed in case 4.

Table 6-9 is listing a summary of the tuning process of case 4, and this presents the chosen parameters.

Table 6-9: Summary of the tuning process presented in case 4.

	Step 1	Step 2
Tuning	i-band is tuned according to the local mode	h-band is tuned according to the inter area mode
Wanted compensation	1.6125 Hz (local mode): 0 °	0.619 Hz (inter-area mode): 180°
Compromise	-	0.619 Hz (inter-area mode): 45° lead
Chosen compensation	1.6125 Hz (local mode): 0 °	0.619 Hz (inter-area mode): 45° lead
Lead/lag-filter time constants	*Ti3=Ti5=1* *Ti4=Ti6=1*	*Th3=Th5=0.3851* *Th4=Th6=0.1719*
Gain	*Ki=4*	*Kh=-8*
Resulting eigenvalue	Local mode ([1/s], [Hz]): (-4.9100, 2.1395) → ζ=34.30 % Inter-area mode ([1/s], [Hz]): (-0.0573, 0.6178) → ζ=1.48 %	

The result of the time domain analysis, presented in to the left in Figure 6-29, shows an output signal that hits the limiter value (0.05) twice, and the PSS is not in a stressed operation. Damping of inter-area oscillations is practically the same with and without the PSS, but the local oscillations is effectively decreased. This analysis supports the results of the eigenvalue analysis, where the local mode has obtained an increased damping, while the inter-area mode has only a smaller improvement.
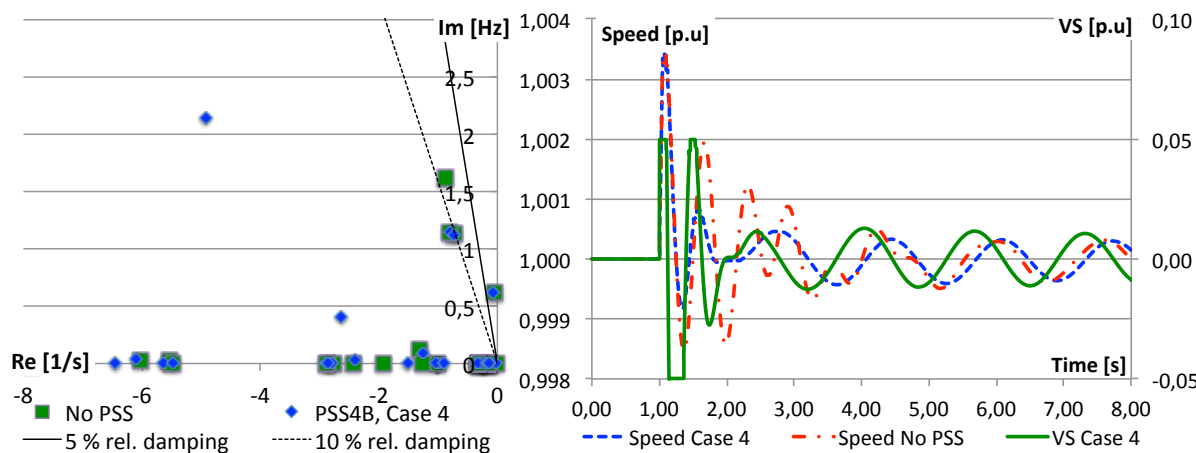
Figure 6-29: PSS4B is installed in generator G5 and tuned according to case 4. Left: Most critical eigenvalues in the network. Right: Time domain analysis where a 3-phase short circuit appears for 0.05 seconds at BUS8.

Case 5

Case 5 uses the same i-band setup as case 4, besides of a gain equal to 10. At this point the root locus movement is shifting from moving to the right to start pointing to the left in the complex plane, and the absolute damping is maximized. At this point the two oscillation modes will start moving in different directions by increasing the gain of the h-band. The damping of the local mode increases slightly, while the damping of the inter-area mode decreases rapidly, in relation to the respective scales of the graphs.
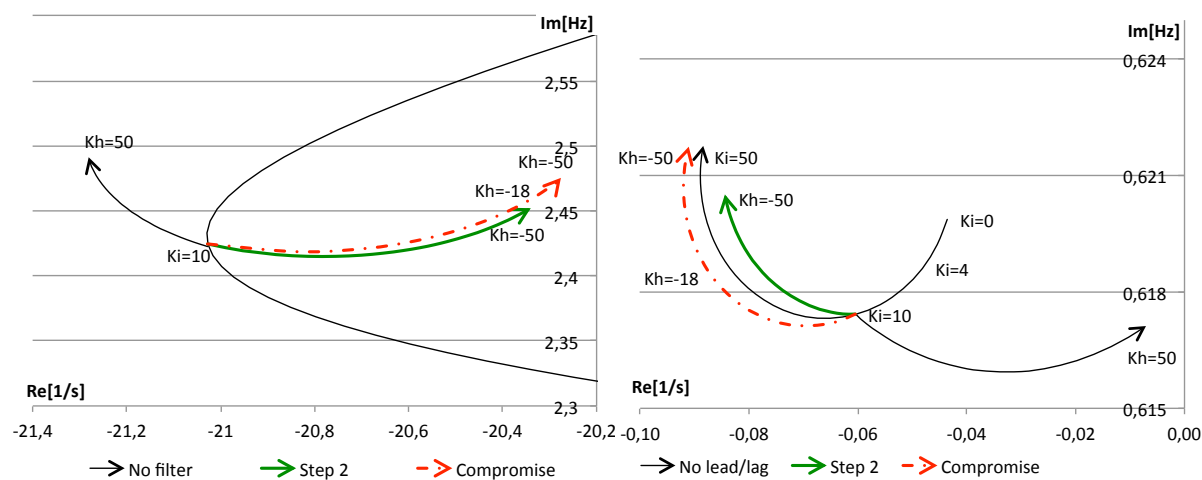
Figure 6-30: Root locus plots of a zoom up of the local mode and the inter-area mode preformed in case 5.

Kh is now rather decreased towards -50, in order to force the inter-area mode in a rightwards direction. Additionally a lead of 37.5° at 0.6174 Hz is implemented, and the result is an initially straight movement of the inter-area mode. The local mode is now moving to the left, but not in a considerable scale. In order to get a better response of the inter-area mode, a lead

of 60° at 0.6174 Hz is tested as a compromise. This filter gives an increased damping in the inter-area mode, compared to the filter that gives an initially straight relocation of the eigenvalue. The compromise filter is the final choice, and *Kh* is set equal to -18. This maximizes the absolute damping of the inter-area mode, without highly disturbing the oscillating frequency. These results are also presented in Table 6-10, as a summary of case 5.

Table 6-10: Summary of the tuning process in presented in case 5.

	Step 1	**Step 2**
Tuning	i-band is tuned according to the local mode	h-band is tuned according to the inter-area mode
Wanted compensation	1.6125 Hz (local mode), 0 °	0.6174 Hz (inter-area mode), 37,5° in neg. dir.
Compromise	-	0.6174 Hz (inter-area mode), 60 ° lead
Chosen compensation	1.6125 Hz (local mode), 0 °	0.6174 Hz (inter-area mode), 60° lead
Lead/lag-filter time constants	*Ti3=Ti5=1* *Ti4=Ti6=1*	*Ti3=Ti5=0.4465* *Ti4=Ti6=0.1488*
Gain	*Ki*=10	*Kh*=-18
Resulting eigenvalues	Local mode ([1/s], [Hz]): (-20.365, 2.4540) → ζ=79.72 % Inter-area mode ([1/s], [Hz]): (-0.0868, 0.6184) → ζ=2.23 %	

The resulting eigenvalue analysis (right plot in Figure 6-31) shows that no new eigenvalues has obtained a poor damping. A time domain analysis of the solution presented in case 5 is plotted to the right in Figure 6-31 and this shows an PSS output signal that reaches the limiter value four times. The local oscillation mode that has obtained an increased damping, while the damping of the inter-area mode is not highly improved.
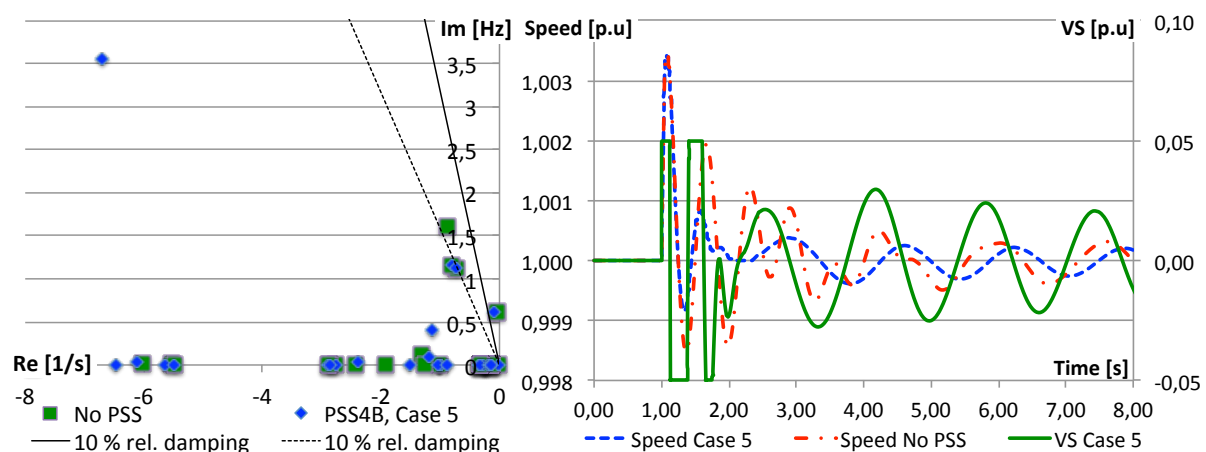

Figure 6-31: PSS4B is installed in generator G5 and tuned according to case 5. Left: Most critical eigenvalues in the system. Right: Time domain analysis where a 3-phase short circuit appears for 0.05 seconds at BUS8.

6.5.3   Final choice of tuning of the PSS4B

The eigenvalues of the respective cases in the previous chapter is compared in order to find the case that obtains the initially best eigenvalue performance. According to Table 6-11 gives case 1 the best eigenvalue performance, where the local mode is completely removed and the eigenvalue related to the inter-area mode obtains a relative damping of 2.25 %. Only case 3 obtains a relative damping of the local mode that is below 10 %, and this is basically not a preferred tuning method of the PSS4b. All remaining cases are basically methods that can be used to tune the PSS4B. These cases (case 1, 2, 4 and 5) are further compared in order to pinpoint the best method of tuning the PSS4B.

Table 6-11: Resulting eigenvalues of the local and inter-area oscillation mode of each tuning method.

Tuning	Oscillation mode	Eigenvalue ([1/s], [Hz])	Relative damping ζ
Case 1	Local	(-16.415, 0.0000)	100 %
	Inter-area	(-0.0878, 0.6198)	2.25 %
Case 2	Local	(-8.6772, 1,5177)	67.3 %
	Inter-area	(-0.0709, 0.6196)	1.82 %
Case 3	Local	(2.8098, 4.7456)	9.38 %
	Inter-area	(0.0958, 0.6199)	2.47 %
Case 4	Local	(-4.9100, 2.1395)	34.30 %
	Inter-area	(-0.0573, 0.6178)	1.48 %
Case 5	Local	(-20.365, 2.4540)	79.72 %
	Inter-area	(-0.0868, 0.6184)	2.23 %

A new time domain analysis is now performed where a load of 500 MW at BUS9 is disconnected. The power response where PSS4B is installed and tuned according to the respective cases is presented in Figure 6-32 and Figure 6-33. Green solid lines in the figures are the response of no PSS installed in the excitation system, and the blue dashed lines are the response where PSS4B is installed. Generally, after implementing the PSS4B, the oscillations of the active power are clearly unbalanced in the first seconds after the disturbance has occurred. As the time goes, the damping of the active power oscillations is increasing, and the oscillations are finally dying out. Case 1 and case 5 obtains the initially most disturbed power response, but after approximately 5 seconds they are well damped. Out of the four cases tested in this analysis is case 1 the case that best damps the oscillations of active power, while case 4 has no considerable improvement of the damping of the active power oscillations.
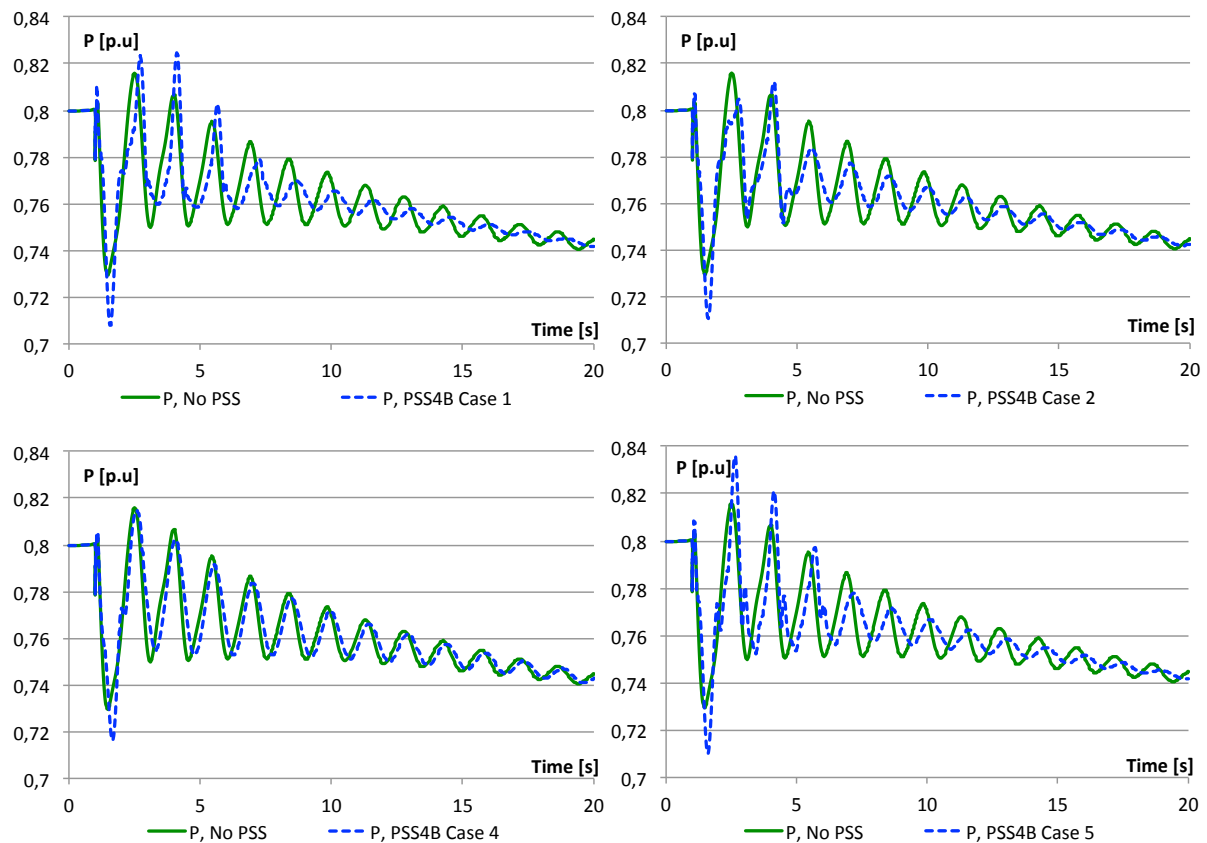
Figure 6-32: Time domain response of active power of generator G5 when PSS4B is installed and tuned according to case 1, case 2, case 4 and case 5.

A result of the reactive power response, illustrated in Figure 6-33, indicates that PSS4B is clearly disturbing the regulation of reactive power in generator G5. All cases gives an oscillation that is less damped, compared to the situation where no PSS is installed. Suddenly, after the loss of active power in BUS9, the PSS is working against this "disturbance", and generator G5 is forced to deliver more reactive power to the grid. The amount of reactive power reaches a maximum peak value in case 1 and in case 2, where approximately 0.45 p.u. is delivered to the grid. Case 1 obtains the overall heaviest oscillations of reactive power, but within approximately 12 seconds the reactive power is oscillating around the steady state value. Case 4 is the case with the least oscillations of reactive power. This case has a peak value of approximately 0.36 p.u and this case obtain the best overall damping of reactive power, out of the four cases presented here.
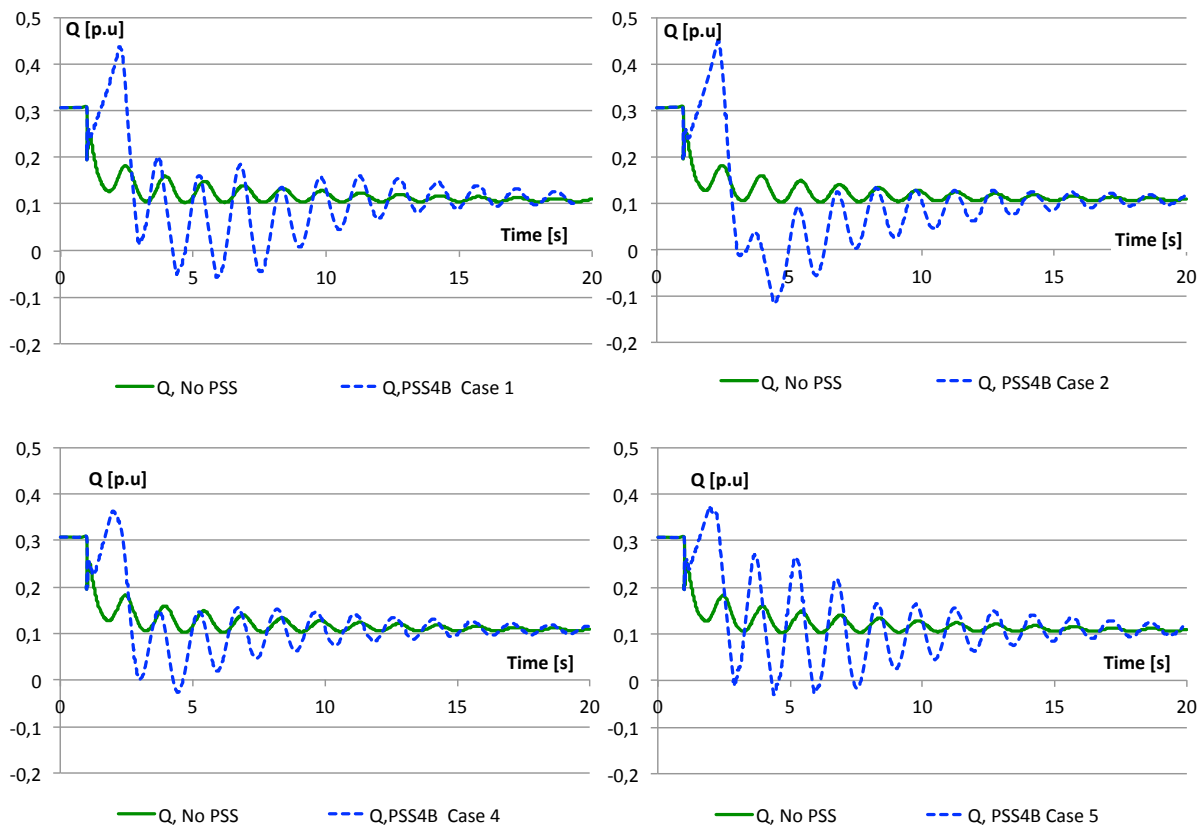
Figure 6-33: Time domain response of reactive power of generator G5 when PSS4B is installed and tuned according to case 1, case 2, case 4 and case 5.

6.6 PSS2B vs. PSS4B

PSS4B tuned according to case 1 obtained the best overall result in the previous chapter, and it is here compared to the performance PSS2B. First the rotor speed response is compared, where the same 3-phase short circuit as used in the previous chapters is introduced. As Figure 6-34 illustrates will a tuning of PSS4B according to case 1, give a better damping of both high and low frequency rotor oscillations, compared to the results from PSS2B. The red dash-dotted curve illustrates the situation where no PSS is installed, and initially after the

Figure 6-34: Time response of rotor speed where a small signal disturbance is introduced.

disturbance a high frequency oscillation appears. This oscillation is well damped by the PSS2B, while the PSS4B setup completely removes this oscillation. Also the low frequency

inter-area oscillation, in the range from approximately four to eight seconds, is better damped in the case where PSS4B is installed. This improvement is not very noticeable in the time domain analysis, presented in Figure 6-34, but the results of a eigenvalue analysis in Table 6-12 illustrates the difference more precisely. Both PSSs gives increased damping of the critical eigenvalues in the system, but an installation of PSS4B results in much higher relative damping, compared to the situation where PSS2B is installed.

Table 6-12: Eigenvalues related to the local and inter-area oscillation mode in the network, when different PSSs are installed in the hydro generator of the five-generator network.

Stabilizer	Oscillation mode	Eigenvalue ([1/s], [Hz])	Relative damping [ζ]
No PSS	Local	(-0.8796, 1.6125)	8.65 %
	Inter-area	(-0.0436, 0.6198)	1.12 %
PSS2B	Local	(-3.4664, 2.1099)	25.3 %
	Inter-area	(-0.0506, 0.61976)	1.30 %
PSS4B	Local	(-16.415, 0.0000)	100%
	Inter-area	(-0.0878, 0.6198)	2.25 %

The performance of each stabilizer is also compared in another time domain analysis, where the active load at BUS9 is disconnected. Active and reactive power response at generator G5 is plotted in Figure 6-35, where PSS2B and PSS4B are implemented one by one.
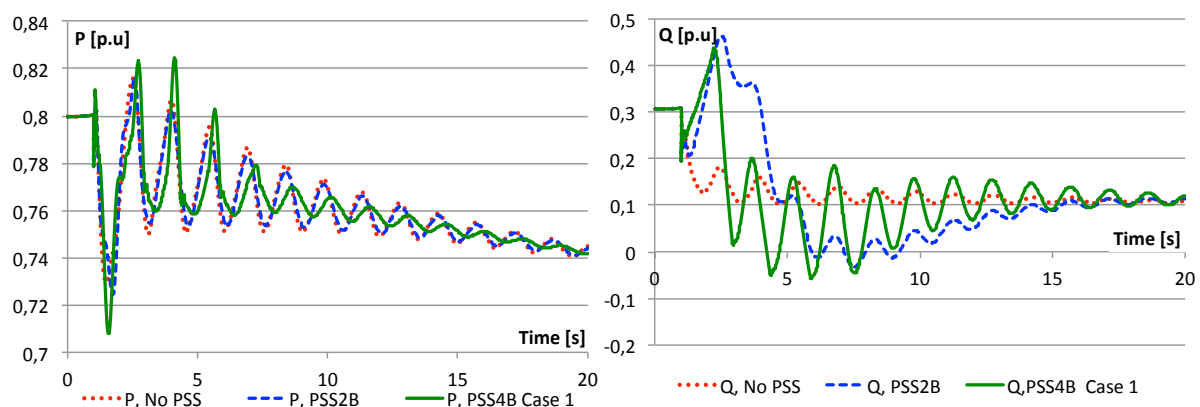
Figure 6-35: Time domain response of active and reactive power of generator G5. PSS4B and PSS2B are respectively implemented in the excitation system of the generator.

PSS4B gives increased damping of the active power oscillations, compared to the situations where no PSS is installed, and also compared to when PSS2B is installed. The active power generation is initially disturbed and a higher peak value is obtained when PSS4B is implemented, compared to the other setups. In spite is the final damping higher and a steady state value is faster obtained. The response of reactive power is also more disturbed when PSS4B is installed. A more aggressive oscillation is now present compared to the situation

where no PSS and PSS2B are installed. This oscillation starts to oscillate around the steady state value, and it is finally damped out.

The variation of reactive power is directly related to variation in generator voltage, and the same pattern of the reactive power (Figure 6-35) can be seen in Figure 6-36. This figure illustrates the variation of generator voltage after the disconnection of the 500 MW load in BUS9. Both PSS2B and PSS4B give peak values below 1.06 p.u. and above 0.98 p.u. PSS4B gives a more oscillatory response compared to PSS2B, and it gives also a shorter period of voltage overshoot.
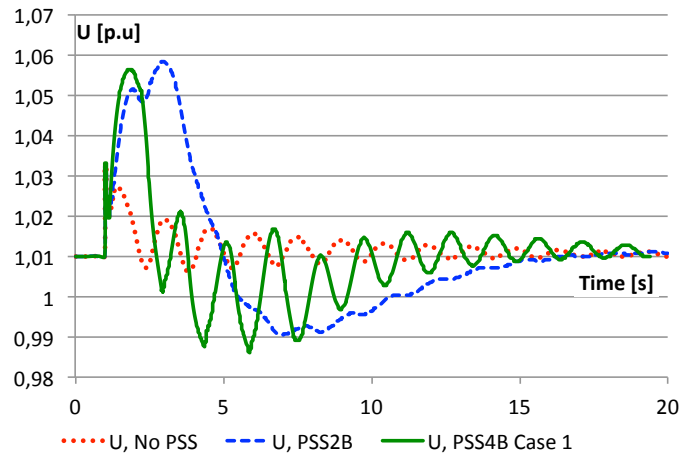
Figure 6-36: Time response of generator voltage after a reduction of loading.

7 Discussion

7.1 The contribution of generator voltage in the excitation system

The pre-project of this master thesis was using a simplified model of Thyricon® Excitation System, where the multiplication of generator voltage and exciter output signal was not implemented (AVR1). During this master thesis, a study of the contribution from a varying generator voltage is performed, and the simplified model of Thyricon® Excitation System is upgraded to contain a multiplication block at the output of the exciter (AVR2). The difference of the performance between the exciter models (with and without multiplication of generator voltage at exciter output) is distinctive. The simple excitation system (AVR1) gives an eigenvalue response that is more stable compared to the excitation system that contains the contribution from a varying stator voltage. A root locus plot of a varying PSS gain is created, and the main deviation between AVR1 and AVR2 is that the eigenvalues of AVR2 is tending to be more destabilized. Tuning of the PSS in AVR2 is more brittle, where a small change in the lead/lag-filter time constants gives a considerable change in the eigenvalue relocations.

The test, performed in this master thesis, shows the importance of including the contribution of a varying generator voltage in the exciter model. A disturbance of the generator stator voltage will also affect the DC field voltage, delivered by the thyristors in the excitation system. It is important to include this contribution in the excitation system, in order to simulate the most realistic situation. The upgraded version of the excitation system (AVR2) is therefore used in the rest of the master thesis, where more advanced PSS's are installed and tuned.

For even more detailed simulations, where for instance transient stability is investigated, the models of the excitation system has to be upgraded even more. All the protection circuits and limiter structures, presented in the original model description [2], must then be implemented in order to give a representative result.

7.2 Analysis of the five-generator network

In this master thesis a five-generator two-area network is established, based on the well-known four-generator network "Kundur's Two Area System" [11, 20]. A smaller hydro

generator is installed, and this obtains a heavier oscillation compared to the larger turbo machines. This is because the rotor inertia of this machine is smaller compared to the other inertias in the system. The swing equation explains this phenomenon. A modal analysis of this five-generator network is performed, and it indicates that hydro generator take a considerable part of one of the local oscillation modes. Correct control of this unit will highly improve the damping of this oscillation mode. The hydro generator is not highly represented in the modal analysis of the inter-area oscillation mode, and correct control of this unit will not effectively improve the damping of this mode. One essential factor is that the improved damping of the local oscillation mode must not destabilize the inter-area oscillation mode, but rather improve the damping as much as possible.

7.3 Tuning of the PSS2B

The dual-input stabilizer is quick and easy to tune, where it has only one lead/lag-structure and a one associated gain. Frequency and electrical power is measured and used as input signals in an advanced transducer structure, where the integral of accelerating power is computed. This synthesized signal has, in this mater thesis, a time response that is more or less in phase with the rotor speed, and this signal is used as an input to the lead/lag-structure. The advantage of this stabilizer is that it would not introduce a phase lag at lower frequencies, and it does not destabilize the exciter oscillation mode as the gain is increased [4, 14]. This advantage is not further illustrated in this master thesis, and the reason is that the network does not contain any torsional oscillations.

Theoretically a higher limiter value could be set, in order to achieve an increased damping of the rotor oscillations. Kundur explains in [11] that a maximum PSS output limit of 0.1 to 0.2 is acceptable if the generator terminal voltage is limited to its maximum allowable value, usually 1.12 to 1.15 p.u. Voith Hydro gives the PSS limiter values used in this thesis and these are relative strict values [2]. These limiters prevent the PSS of highly disturbing the voltage regulation under normal operation conditions.

In order to give a satisfying result of both oscillating modes, a compromise solution of the lead/lag-filter time constants has to be made. A disadvantage of this compromise is that it gives not an optimal improvement of the oscillation modes. This drawback is more present in networks containing a wide spectre of oscillation modes, since the lead/lag filter cannot cover

a wide range of frequencies. To increase the damping of the inter-area mode the stabilizer gain can be increased, but a major side effect of this is that the local oscillation mode becomes less damped. This is clearly illustrated in the root locus plot, where the eigenvalues of each oscillation mode moves in opposite directions as the stabilizer gain is increased above the chosen value. The need of this compromise lead/lag compensation is the drawback of the dual-input stabilizer, where none of the oscillation modes gets an optimal damping.

7.4 The different tuning procedures of PSS4B

A PSS4B stabilizer is a complicated structure, and it can be tuned in many ways. The first tuning method, performed in this master thesis, is to implement the whole structure and tune it according to the sample data presented in the IEEE standard [1]. The procedure focusing at centre frequencies and associated gain values, and the phase response of the PSS is not further commented. It seems that this procedure is more convenient in a network containing a wider spectre of oscillation modes. Results from loading the PSS4B with IEEE sample data indicates that it must be tuned more specifically in order to act appropriate in this network.

PSS4B consists of 3 separate bands that are designed to handle 3 different oscillation modes. One of the branches of each band is here disconnected, and the reason is that the structure is now much simpler. Each band is tuned one by one as a well-known lead/lag structure. Tuning of lead/lag-filters is successfully performed in the previous chapter, where the PSS2B is implemented. The following tuning procedure is divided into 5 different cases. Each of the 5 cases has different order of which band, and of which oscillation mode that is tuned first. This is done in order to find an effective tuning technique. In case 1 the h-band of the stabilizer is tuned first, so the damping of the local oscillation mode is improved. Secondary the i-band is tuned to give an improvement of the lower frequency inter-area mode. This tuning technique gives the best damping of the local oscillation mode, where the eigenvalue analysis gives a non-oscillating eigenvalue. The damping of the inter-area mode is additionally improved, where the relative damping is at the second best value ever achieved in this master thesis. The other tuning techniques are generally more troublesome, and in some cases will the eigenvalue relocations go in opposite directions as the band gains are increased.

The results from the eigenvalue analysis are also presented in time domain analysis of generator speed. At case 1 is practically only the inter-area oscillation is present and this test

shows that it is a correlation between the eigenvalue analysis and the time domain analysis. To further test the robustness of the network a disconnection of an active load is performed. Results indicate an increased damping of the active power oscillations after implementing the PSS4B, which is tuned according to case 1. The reactive power delivered by generator G5 is more fluctuating, but the oscillations decreases and the steady state value is finally found. A price to pay of increased damping of rotor oscillations is increased variations of reactive power in the machine. The peak values of reactive power are not higher, but the damping of these oscillations is reduced. An explanation of this can be that the control of the generating unit is more active, in order to damp the rotor oscillation, and therefore will also the reactive power in the machine fluctuate.

Case 4 is the case that gives the lowest disturbance in reactive power, after the disconnection of the active load. Damping of oscillations in active power is then not increased considerable and so is the oscillation of the rotor speed. This is similar to the damping of the inter-area mode, found in the eigenvalue analysis.

7.5 PSS4B vs. PSS2B

The tuning of the multi-band stabilizer that achieves the overall best performance is case 1, and this stabilizer is now compared to the tuned dual-input stabilizer. In the dual-input stabilizer, the lead/lag-filter must be tuned as a compromise between the actual oscillation modes present in the network. This solution gives not an optimal result. The result of comparing the time domain analysis of the rotor oscillations indicates that the multi-band stabilizer will give an overall best damping of the oscillation modes.

The inter-area oscillation mode is though not highly improved, neither by installation of PSS2B or by PSS4B. This phenomena is also described in [11] where an effective alternative solution could be an installation of a static VAR compensation and/or by control of HVDC converters (if present). Generator G5 is a small generating unit, and its ability to improve the inter-area mode is limited. By installing a PSS in one of the other (larger) generating units, the inter-area oscillation mode may probably be better damped. The pre-project of this master thesis presents such a solution with great results.

An instantaneously decrease of the generator loading is performed, and both stabilizers give a disturbed regulation of reactive power (and voltage), compared to the situation where no PSS is installed. An increased damping of rotor oscillations results in a higher level of reactive power oscillations. PSS4B is clearly more active in the aftermath of a disturbance of the network operation condition. This can also be seen in the time plot of the PSS output signal. Variations of the reactive power are also seen in the response of generator voltage, which shows a voltage overshoot of 1.06 p.u. This overshoot is within the given regulations of 110 % (EN 50160) and cannot be considered as a voltage swell [21]. The voltage level can be considered as stable when it stays inside a limit of ±0.5 % of system voltage, and both stabilizers are reaching this value at approximately the same time [21]. This oscillatory generator voltage is the price to pay for increased rotor stability in the network.

Table 7-1 and Table 7-2 describes some advantages and disadvantages about the respective PSS's.

Table 7-1: Pros and cons of PSS2B.

+	-
Well known in the market.	Single lead/lag-filter must be tuned as a compromise between all oscillatory modes in the system.
Simple tuning procedure.	Often only tuned at the local oscillation mode for one specific machine [19].
Handles a higher gain compared to a single input stabilizer, without destabilizing the exciter oscillation mode.	Cannot cover a large variation of oscillation frequencies in the network.

Table 7-2: Pros and cons of PSS4B.

+	-
Gives increased damping of both oscillation modes presented in this master thesis.	New in the market, and few really good papers are describing it.
Great tuning flexibility.	The complicated structure needs more tuning compared to older and simpler PSS structures.
Will theoretically be very useful in a system with a wide spectre of oscillation modes.	Have to be further benchmarked in the real world to ensure the theoretically good performance.

8 Conclusions

The best overall damping, obtained in this master thesis, occurs when the high frequency band (h-band) of the PSS4B is tuned first, and in order to improve the damping of the local oscillation mode. The intermediate frequency band (i-band) is then tuned as a second step, according to the inter-area oscillation mode. PSS4B has a complicated structure and the tuning process can, in the first glance, look troublesome. IEEE has proposed a method of tuning each band of the multi-band stabilizer, where a selection of three centre frequencies and associated gains are used as a base of the parameter settings. This method does not tune the phase shift directly, and the IEEE sample parameters gives not a good result in this master thesis. In a commission process, where the stabilizer has to deliver an exact phase response, the stabilizer has to be fine tuned in order to give an optimal result. Several simplifications of the PSS4B structure are here made, where parts of the stabilizer are disconnected. The lower branch of each band is disconnected, and the top branch is tuned as a regular lead/lag-filter. An input transducer of the h-band is specially designed to handle the high frequencies in the applied network, and the remaining bands have an input transducer that is optimized for the lower frequencies in the network. Results from the different tuning techniques, presented in this master thesis, indicate that it is an advantage that this design is exploited. The tuning order can be mixed, and the result indicates an improved damping. A drawback of these procedures is that they gives root locus plots and time domain analysis that are more troublesome. The oscillation modes in the network of this master thesis (local and inter-area) has a relative small frequency deviation, and a network containing a wider spectre of oscillation frequencies will probably obtain a greater advantage of implementing the PSS4B.

PSS4B gives higher tuning flexibility and better performance compared to PSS2B. The absolute damping of the inter-area oscillation mode obtains a value of 0.0506 1/s when using PSS2B, and the PSS4B gives a value of 0.0878 1/s. This oscillation mode is still poorly damped, and the reason is that the applied generator has a small participation of this mode. When the oscillatory frequency is taken into consideration the relative damping is computed, and PSS4B gives a value of 2.25 %, while PSS2B gives a relative damping of 1.3 %. This result indicates that PSS4B gives almost twice as good relative damping of the inter-area mode! PSS4B gives also a much better damping of the local oscillation mode, where the relative damping is 100 %, and the oscillation mode is completely damped. By way of comparison obtains PSS2B only a relative damping of 25 % for the local oscillation mode.

9 Further work

As a further work of this master thesis the multi-band stabilizer can be implemented in a network containing oscillations in a wider spectre. The multi-band stabilizer (PSS4B) is designed to handle oscillation modes in three different bands, and the network analysed in this master thesis contains only two modes of concern. These modes have a small variation of frequency (~ 1 Hz) and are local- and inter-area oscillation modes. It will usually be difficult to obtain an increased damping of all torsional-, local-, inter-area-, and global oscillation modåes in a network by implementing the traditional PSS's. These are oscillations with large frequency deviation (0.05 - 4 Hz) and the advanced structure of PSS4B can be tuned specific to cover this wide spectre. Utilizing the h-band of the PSS4B can reduce torsional oscillation modes in a generator, or reduce some of the local oscillation modes in the network. The l-band can reduce low frequency global oscillations in a network, and the i-band can be tuned to reduce the inter-area oscillation mode at around 0.5 Hz.

The stabilizers could additionally be tuned according to the other tuning approaches, explained in the theory part of this master thesis. These techniques are the damping torque approach and the frequency response approach. The complete network can then be implemented in another computer simulation programme, which can compute mathematical transfer functions, and the frequency response of the system can be detected.

The excitation system could be upgraded to contain all the protective circuits and limiters, described in the complete Thyricon® Excitation System model description [2], and a transient stability analysis of the network could be performed. This analysis would identify the performance of each PSS during large faults in the network.

In order to analyse the performance of PSS4B more deeply, the model could be implemented in a real world excitation system, and several commissioning tests could be performed.

References

[1]   IEEE, "IEEE Recommended Practice for Excitation System Models for Power System Stability Studies," in *IEEE Std 421.5-2005 (Revision of IEEE Std 421.5-1992)*, ed: IEEE, 2006, pp. 1-85.

[2]   D. Mota, "Models for Power System Stability Studies, Thyricon(R) Excitation System," Trondheim Patent, 2010.

[3]   R. Grondin, I. Kamwa, G. Trudel, L. Gerin-Lajoie, and J. Taborda, "Modeling and closed-loop validation of a new PSS concept, the multi-band PSS," *Power Engineering Society General Meeting, 2003, IEEE,* vol. 3, p. 1809, 13-17 July 2003 2003.

[4]   B. Pal and B. Chaudhuri, *Robust Control in Power Systems*. Boston, MA: Springer Science+Business Media, Inc., 2005.

[5]   W. G. Heffron and R. A. Phillips, "Effect of a Modern Amplidyne Voltage Regulator on Underexcited Operation of Large Turbine Generators," *Power Apparatus and Systems, Part III. Transactions of the American Institute of Electrical Engineers,* vol. 71, pp. 692-697, 1952.

[6]   J. Machowski, J. W. Bialek, and J. R. Bumby, *Power system dynamics: stability and control*. Chichester: Wiley, 2008.

[7]   E. C. C. C.-E. f. a. C. W. EU. (2008). *EU action against climate change*. Available: http://ec.europa.eu/climateaction/eu_action/index_en.htm

[8]   J. F. Manwell, J. G. McGowan, and A. L. Rogers, *Wind Power Explained - Theory, Designe and Application*, 1. edition ed.: John Wiley & Sons, 2002.

[9]   I. Kamwa, R. Grondin, and G. Trudel, "IEEE PSS2B versus PSS4B: the limits of performance of modern power system stabilizers," *Power Systems, IEEE Transactions on,* vol. 20, pp. 903-915, 2005.

[10]   Statnett. (2008). *Funksjonskrav i kraftsystemet*. Available: http://www.statnett.no/default.aspx?ChannelID=1416

[11]   P. Kundur, N. J. Balu, and M. G. Lauby, *Power system stability and control*. New York: McGraw-Hill, 1994.

[12]   K. Bjørvik and P. Hveem, *Reguleringsteknikk*. Trondheim: Høgskolen i Sør Trøndelag, Avd. for teknologi, Program for elektro- og datateknikk, 2007.

[13]   IEEE, "IEEE Guide for Identification, Testing, and Evaluation of the Dynamic Performance of Excitation Control Systems," in *IEEE Std 421.2-1990*, ed, 1990, p. 45.

[14]   G. R. Bérubé and L. M. Hajagos, "Accelerating-Power Based Power System Stabilizers," p. 10, Year not known.

[15]   K. Kiyong and R. C. Schaefer, "Tuning a PID controller for a digital excitation control system," *Industry Applications, IEEE Transactions on,* vol. 41, pp. 485-492, 2005.

[16]   A. Murdoch, S. Venkataraman, R. A. Lawson, and W. R. Pearson, "Integral of accelerating power type PSS. I. Theory, design, and tuning methodology," *Energy Conversion, IEEE Transactions on,* vol. 14, pp. 1658-1663, 1999.

[17]   N. Martins and L. T. G. Lima, "Eigenvalue and Frequency Domain Analysis of Small Signal Electromechanical Stability Problems," 1989.

[18]   STRI, "SIMPOW, Power System Simulation Software, USER MANUAL (Beta release)," vol. 10.2, ed, 2004.

[19]   D. Mota, "Project meeting in this master thesis," A. Hammer, Ed., ed. Trondheim, 2011.

[20]   J. Person and STRI, "Kundur's Two Area System," vol. 10.1, 1996.

[21]   Norges-vassdrags-og-energidirektorat. (2004). *Forskrift om leveringskvalitet i kraftsystemet*. Available: http://www.lovdata.no/cgi-wift/ldles?doc=/sf/sf/sf-20041130-1557.html

10 Appendix

1   Tuning of AVR2 in the four-generator network.

Figure 10-1: Determination of angles of root locus plot with AVR2 containing single input PSS.

Case 3:

Initial angle of inter-area modus at 0.61 Hz:

$$\angle = \arctan(2\pi \cdot -0.1765) = -47.95° \rightarrow 48°$$

Time constant of a second order lead/lag filter:
    T1=T3=0.3981, T2=T4=0.1676

Case 4:

Initial angle of local modus at 1.08 Hz:

$$\angle = \arctan(2\pi \cdot -4.159) = 87.8° \rightarrow 90°$$

Time constant of a second order lead/lag filter:
    T1=T3=0.3558, T2=T4=0.061
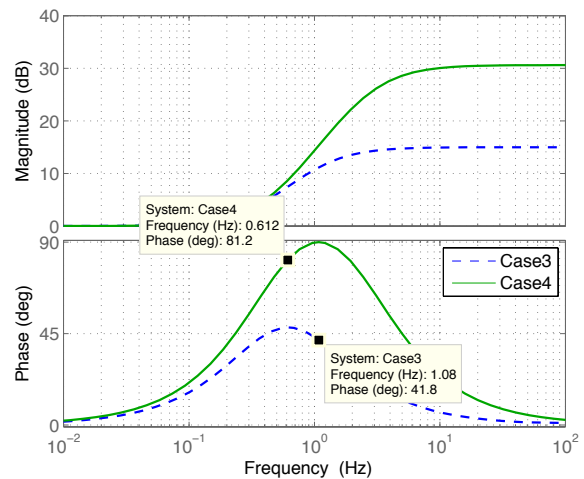
2   Parameters for the network components

Table 10-1: Generator data.

Parameters		Type 1 Round	Type 2 Sailient
Reactances	Direct-axis synchronous reactance (Xd)	1.8	1.1
	Quadrature-axis synchronous reactance (Xq)	1.7	0.8
	Direct-axis transient reactance (Xd')	0.3	0.25
	Quadrature-axis transient reactance (Xq')	0.55	-
	Direct-axis subtransient reactance (Xd'')	0.25	0.16
	Quadrature-axis subtransient reactance (Xq'')	0.25	0.25
	Leakage reactance in stator (Xa)		0.1
Time constants	Direct-axis transient open circuit time constant (Td0')	8.0 s	7.8 s
	Quadrature-axis transient open circuit time constant (Tq0')	0.4 s	-
	Direct-axis subtransient open circuit time constant (Td0'')	0.03 s	0.03 s
	Quadrature-axis subtransient open circuit time constant (Tq0'')	0.05 s	0.05 s
Others	Damping torque coefficient K_D (mechanical damping)	0	0
	A_{sat} (Saturation const. to define the saturation table)	0.015	0.015
	B_{sat} (Saturation const. to define the saturation table)	9.6	9.6
	Armature resistance (Ra)	0.0025	0.0018
	Inertia of G1 & G2 (H) = 6.5		
	Inertia of G3 & G4 (H) = 6.175		
	Inertia of G5 (H) = 2.92		

Table 10-2: Line data.

Nominal base voltage	230 kV
Nominal base power	100 MVA
Resistance (r)	0.0001 P.U/km
Reactance (x_L)	0.001 P.U/km
Susceptance (b_C)	0.00175 P.U/km

Table 10-3: Line lengths.

Line	Bus 5-6	Bus 6-7	Bus 7-8	Bus 8-9	Bus 9-10	Bus10-11
Lengths	25 km	10 km	110 km	110 km	10 km	25 km

Table 10-4: Transformer data.

U_{prim}	U_{sec}	Reactance	S_n	Off-nominal ratio
20 kV	230 kV	0.15 p.u	900 MVA	1.0

Table 10-5: Loads modelled as constant power for each area.

Area 1 (Bus 7)	Active load (P_L)	967 MW
	Capacitive load (X_c)	200 MVAr
	Inductive load (X_L)	100 MVAr
Area 2 (Bus 9)	Active load (P_{L-1})	767 MW
	Active load (P_{L-2})	500 MW
	Active load (P_{L-3})	250 MW
	Active load (P_{L-4})	125 MW
	Active load (P_{L-5})	50 MW
	Active load (P_{L-6})	25 MW
	Capacitive load (X_c)	350 MWAr
	Inductive load (X_L)	100 MVAr
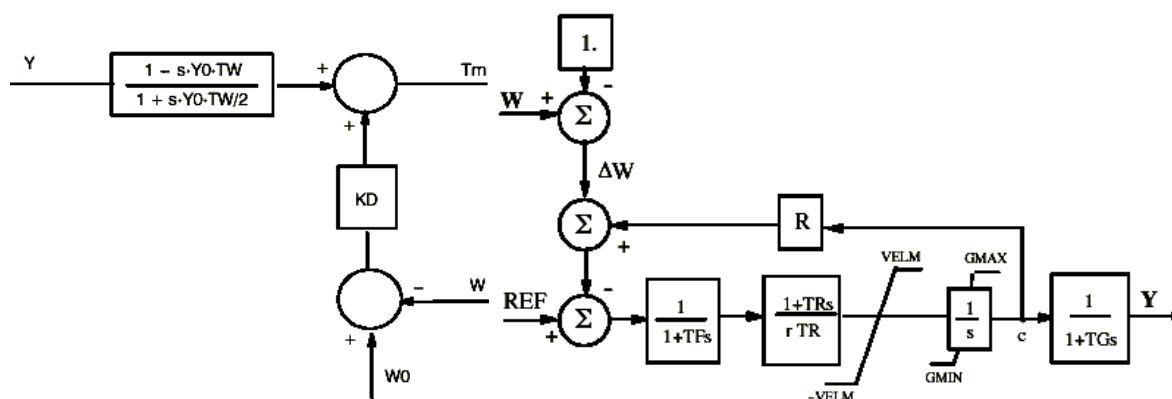
Figure 10-2: Left: penstock turbine model, HT1. Right: hydro governor, DSLS/HYGOV.

Table 10-6: Turbine and governor model description.

Turbine model			Governor model		
Shortening	Description	Value	Shortening	Description	Value
Y	Gate opening	-	Y	Gate opening	-
Y0	Initial gate opening	-	TG	Servo time const.	0.2
Tw	Water start time	1 s	TF	Filter time const.	0.05
Tm	Mech. torque	-	TR	Gov. time const.	5
KD	Turb. Damp. Const.	1 Nm/P.U	ΔW	Change in speed	-
W	Speed of machine	-	W	Speed of machine	-
W0	Nominal speed	-	R	Permanent droop	0.04
			r	Temporary droop	0.4
			VELM	Gate velocity limit	0.1
			GMAX	Max gate limit	1
			GMIN	Min. gate limit	0

*Parameters given by SINTEF as typical values

3   Parameters for the different cases of PSS4B, referred to the SIMPOW model.

Table 10-7: PSS4B Case 1. (Parameter not mentioned is set equal to 1).

KL11=KI11=KH11=KL1=KL2=KI2=KH2=0, VST$_{max}$=0.05, VST$_{min}$=-0.05					
TL1=TL2=TI1=TI2=TH1=TH2=3 (washout filters)					
VL$_{max}$=0.075	VL$_{min}$=-0.075	VI$_{max}$=0.6	VI$_{min}$=-0.6	VH$_{max}$=0.6	VH$_{min}$=-0.6
TL3=1	TL7=1	TI3=1	TI5=1	TH3=0.21535	TH5=0.21536
TL4=1	TL8=1	TI4=1	TI6=1	TH4=0.04538	TH6=0.04538
KL=0 (L-band disconnected)		KI=28		KH=-4	

Table 10-8: PSS4B Case 2. (Parameter not mentioned is set equal to 1).

KL11=KI11=KH11=KL1=KL2=KI2=KH2=0, VST$_{max}$=0.05, VST$_{min}$=-0.05					
TL1=TL2=TI1=TI2=TH1=TH2=3 (washout filters)					
VL$_{max}$=0.075	VL$_{min}$=-0.075	VI$_{max}$=0.6	VI$_{min}$=-0.6	VH$_{max}$=0.6	VH$_{min}$=-0.6
TL3=1	TL7=1	TI3=0.0836	TI5=0.0836	TH3=1	TH5=1
TL4=1	TL8=1	TI4=0.0714	TI6=0.0714	TH4=1	TH6=1
KL=0 (L-band disconnected)		KI=8		KH=-50	

Table 10-9: PSS4B Case 3. (Parameter not mentioned is set equal to 1).

KL11=KI11=KH11=KL1=KL2=KI2=KH2=0, VST$_{max}$=0.05, VST$_{min}$=-0.05					
TL1=TL2=TI1=TI2=TH1=TH2=3 (washout filters)					
VL$_{max}$=0.075	VL$_{min}$=-0.075	VI$_{max}$=0.6	VI$_{min}$=-0.6	VH$_{max}$=0.6	VH$_{min}$=-0.6
TL3=1	TL7=1	TI3=0.197	TI5=0.197	TH3=0.6197	TH5=0.6197
TL4=1	TL8=1	TI4=0.3345	TI6=0.3345	TH4=0.1063	TH6=0.1063
KL=0 (L-band disconnected)		KI=26		KH=-16	

Table 10-10: PSS4B Case 4. (Parameter not mentioned is set equal to 1).

KL11=KI11=KH11=KL1=KL2=KI2=KH2=0, VST$_{max}$=0.05, VST$_{min}$=-0.05					
TL1=TL2=TI1=TI2=TH1=TH2=3 (washout filters)					
VL$_{max}$=0.075	VL$_{min}$=-0.075	VI$_{max}$=0.6	VI$_{min}$=-0.6	VH$_{max}$=0.6	VH$_{min}$=-0.6
TL3=1	TL7=1	TI3=1	TI5=1	TH3=0.3851	TH5=0.3851
TL4=1	TL8=1	TI4=1	TI6=1	TH4=0.1719	TH6=0.1719
KL=0 (L-band disconnected)		KI=4		KH=-8	

Table 10-11: PSS4B Case 5. (Parameter not mentioned is set equal to 1).

KL11=KI11=KH11=KL1=KL2=KI2=KH2=0, VST$_{max}$=0.05, VST$_{min}$=-0.05					
TL1=TL2=TI1=TI2=TH1=TH2=3 (washout filters)					
VL$_{max}$=0.075	VL$_{min}$=-0.075	VI$_{max}$=0.6	VI$_{min}$=-0.6	VH$_{max}$=0.6	VH$_{min}$=-0.6
TL3=1	TL7=1	TI3=1	TI5=1	TH3=0.4465	TH5=0.4465
TL4=1	TL8=1	TI4=1	TI6=1	TH4=0.1488	TH6=0.1488
KL=0 (L-band disconnected)		KI=10		KH=-18	

4 Thyricon® Excitation System, main structure.

VOITH

Voith Hydro

4 Automatic Voltage Regulator

THYR-DDI_Excitation_Models_for_Power_System_Stability_Studies.doc
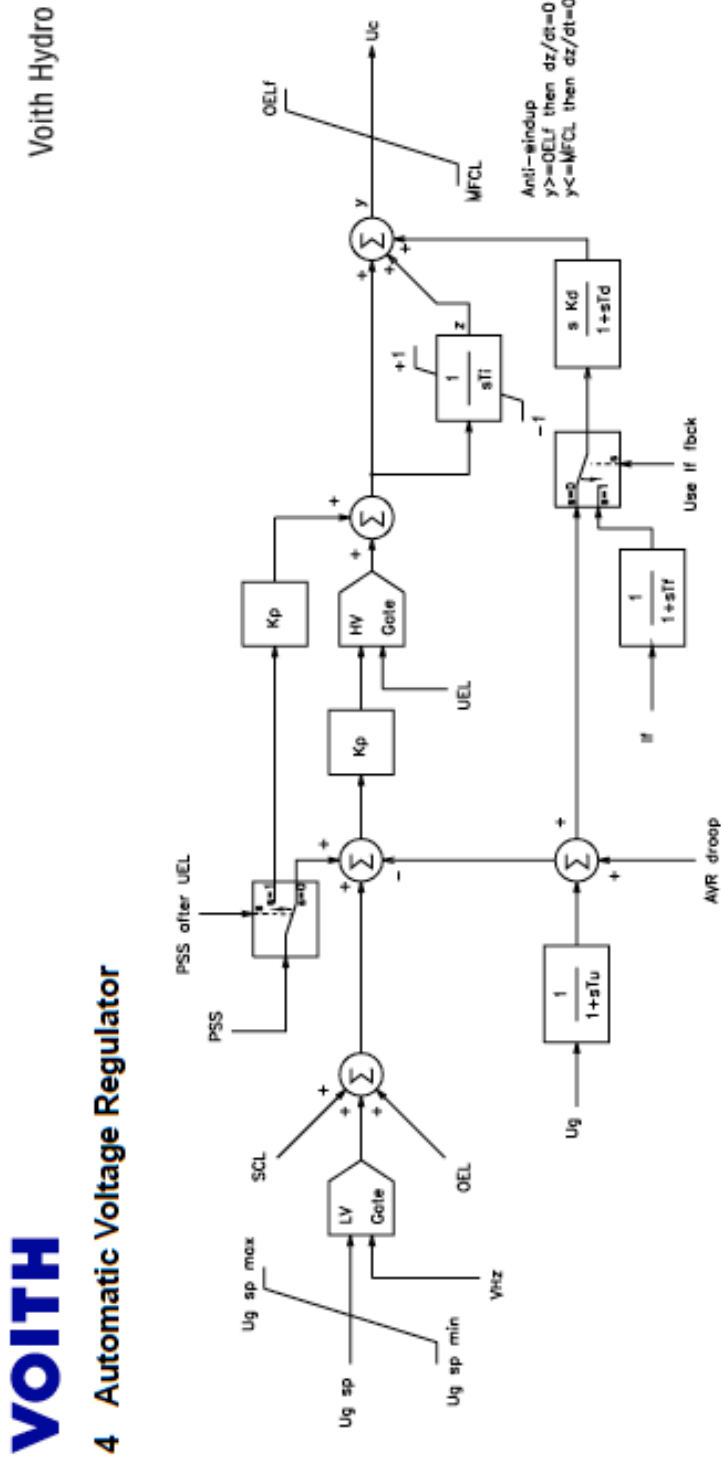
Parameters		Range	Typical Value	Adjusted	Comments
Ug sp max	Maximum allowed AVR setpoint	0,9 ~ 1,2	1,1		
Ug sp min	Minimum allowed AVR setpoint	0,7 ~ 1	0,9		
Tu	Transducer time constant	-	20ms		
Tf	Field current smoothing time constant	-	20ms		
Kp	Proportional gain	0,1 ~ 40	10		
Ti	Integral time	0,1 ~ 10s	2s		
Kd	Derivative gain	-40 ~ 0	0		
Td	Smoothing time constant	0,1 ~ 10s	5s		
Use If fdbck	Use If as feedback into the control loop	0 or 1	0		Only for brushless excitation systems
PSS after UEL	Use PSS after UEL	0 or 1	1		

Voith Hydro

VOITH

5 Thyristor Bridge
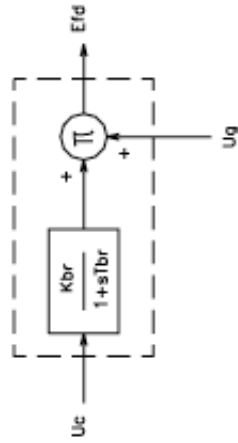
Parameters		Range	Typical Value	Adjusted	Comments
Kbr	Rectifier bridge gain	-	According to regional standards		The rectifier bridge gain is equal to the ceiling voltage divided by the air gap field voltage
Tbr	Rectifier bridge time constant	-	1,4ms or 1,7ms		The rectifier bridge time constant is usually adopted as 1/12 of the grid period

Notes:
- The rectifier bridge control signal "Uc" is either the output of the Automatic Voltage Regulator or the output of the Field Current Regulator.

THYR-DDL_Excitation_Models_for_Power_System_Stability_Studies.doc

5   Load flow analysis of the five-generator network:

Show Powerflow Result Jobid:KUN   **Optpow**

	Name	Region	Area	U p.u.	Remark	U kV	FI(u) Deg.	P1 MW	Q1 Mvar	P2 MW	Q2 Mvar	P3 MW	Q3 Mvar
1	BUS1	1	1	1.03		20.6	29.4477						
2	TR2 BUS1 BUS5 0							-700	-201.121	700	117.787	0	0
3	PROD G1							700	201.121	0	0	0	0
4	BUS2	1	1	1.01		20.2	19.6424						
5	TR2 BUS2 BUS6 0							-700	-273.355	700	181.089	0	0
6	PROD G2							700	273.355	0	0	0	0
7	BUS5	1	1	1.00387		230.889	22.9691						
8	LINE BUS5 BUS6 0							-700	-117.787	687.491	-3.0494	0	0
9	TR2 BUS1 BUS5 0							-700	-201.121	700	117.787	0	0
10	BUS6	1	1	0.971782		223.51	12.8158						
11	LINE BUS5 BUS6 0							-700	-117.787	687.491	-3.0494	0	0
12	LINE BUS6 BUS7 0							-1467.49	-197.89	1444.27	-32.713	0	0
13	TR2 BUS2 BUS6 0							-700	-273.355	700	181.089	0	0
14	TR2 BUS12 BUS6 0							-80	-30.6426	80	19.8511	0	0
15	BUS7	1	1	0.948008	** Low **	218.042	3.77542						
16	SHUN BUS7 0							1.90951E-007	179.744	0	0	0	0
17	LINE BUS6 BUS7 0							-1467.49	-197.89	1444.27	-32.713	0	0
18	LINE BUS7 BUS8 1							-238.634	-23.5155	231.585	-30.3007	0	0
19	LINE BUS7 BUS8 2							-238.634	-23.5155	231.585	-30.3007	0	0
20	LOAD BUS7 0							-967	-100	0	0	0	0
21	BUS12	1	1	1.01		20.2	19.8385						
22	TR2 BUS12 BUS6 0							-80	-30.6426	80	19.8511	0	0
23	PROD G5							80	30.6426	0	0	0	0
24	BUS3	1	2	1.03		20.6	-6.8						
25	TR2 BUS3 BUS11 0							-646.927	-166.424	646.927	96.3243	0	0
26	PROD G3							646.927	166.424	0	0	0	0
27	BUS4	1	2	1.01		20.2	-15.2582						
28	TR2 BUS4 BUS10 0							-700	-217.985	700	130.164	0	0
29	PROD G4							700	217.985	0	0	0	0
30	BUS9	1	2	0.963835		221.682	-30.0704						
31	SHUN BUS9 0							-3.86036E-006	325.142	0	0	0	0
32	LINE BUS9 BUS10 0							1317.67	-60.0575	-1336.4	-125.582	0	0
33	LINE BUS8 BUS9 1							-231.585	30.3007	224.663	-82.5425	0	0
34	LINE BUS8 BUS9 2							-231.585	30.3007	224.663	-82.5425	0	0
35	LOAD BUS9 1							-767	-100	0	0	0	0
36	LOAD BUS9 2							-500	-2.219E-006	0	0	0	0
37	LOAD BUS9 3							-250	-1.1095E-006	0	0	0	0
38	LOAD BUS9 4							-125	-5.54751E-007	0	0	0	0
39	LOAD BUS9 5							-75	6.09059E-007	0	0	0	0
40	LOAD BUS9 6							-50	1.3577E-008	0	0	0	0
41	BUS10	1	2	0.980854		225.596	-22.0214						
42	LINE BUS10 BUS11 0							636.405	-4.58258	-646.927	-96.3243	0	0
43	LINE BUS9 BUS10 0							1317.67	-60.0575	-1336.4	-125.582	0	0
44	TR2 BUS4 BUS10 0							-700	-217.985	700	130.164	0	0
45	BUS11	1	2	1.00852		231.959	-12.7578						
46	LINE BUS10 BUS11 0							636.405	-4.58258	-646.927	-96.3243	0	0
47	TR2 BUS3 BUS11 0							-646.927	-166.424	646.927	96.3243	0	0
48	BUS8	1	3	0.924299	** Low **	212.589	-13.3529						
49	LINE BUS7 BUS8 1							-238.634	-23.5155	231.585	-30.3007	0	0
50	LINE BUS7 BUS8 2							-238.634	-23.5155	231.585	-30.3007	0	0
51	LINE BUS8 BUS9 1							-231.585	30.3007	224.663	-82.5425	0	0
52	LINE BUS8 BUS9 2							-231.585	30.3007	224.663	-82.5425	0	0

6   Corrections of the DSL-file to implement a voltage step response in the AVR.

Excitation system is called THYRAVR6_PSS in the simulation file.

```
!! *--------   DSL Code Generator, Simpow   ---------------------
!! *
!! *           Name      : THYRAVR6_PSS
!! *           Explanation: Thyricon AVR, reconstructed.
!! *
!! *           DSL Code Generator, release 1.3, 2005-02-10.
!! *           Copyright STRI AB, Sweden.
!! *-------------------------------------------------------------
!! Department :
!! Designed by:
!! Checked by :
!! Approved by:
!! Date       :
!! *-------------------------------------------------------------

PROCESS THYRAVR6_PSS(KP,VC,KBR,TBR,
& OELf,MFCL,VS,IMIN,
& IMAX,TD,TI,KD,
& TU,UF,UF0, REFTAB)
EXTERNAL KP,VC,KBR,TBR
EXTERNAL OELf,MFCL,VS,IMIN
EXTERNAL IMAX,TD,TI,KD
EXTERNAL TU,UF0
EXTERNAL REFTAB                              !AH revisjon
!! End of external declarations.
REAL     KP,K1/*/,VC,KBR
REAL     TBR,OELf,MFCL,VS
REAL     IMIN,IMAX,TD,TI
REAL     KD,TU,Ug,V1
REAL     REF/*/,V2,UF0,V7
REAL     V4,V5,INTER_1
REAL     INTER_2,V3,V6,V8
REAL     UC,UBR,UF
INTEGER  CHECK_OF_LIMITS
REAL     REFX                                !AH revisjon
INTEGER  IREFTAB                             !AH revisjon
!! End of real and integer declarations.
STATE   IREFTAB/1/                           !AH revisjon
ARRAY   REFTAB(*,2)                          !AH revisjon
PLOT    VS,Ug,V3,V6
PLOT    V8,UC
STATE   V1,INTER_2,V6,UBR
STATE   CHECK_OF_LIMITS/0/
!! End of state declarations.
   IF (START) THEN
      K1=1.0
   ENDIF
!!Here starts the reftab
IF(TIME.GE/0/.0.)THEN
    IF (NROW(REFTAB) .EQ.1 .AND.             !AH revisjon REFTAB SEKVENS
&   REFTAB(1,1).EQ.-99999.AND.REFTAB(1,2).EQ.-99999.) THEN
    REFX=1.
    ELSE
    IF (IREFTAB.LT. NROW(REFTAB))THEN
   IF (TIME .GE/0/. REFTAB(IREFTAB+1,1))THEN
     IREFTAB=IREFTAB+1
     PRINT "DISCONTINUITY IN REFTAB"
```

```
     ENDIF
  ENDIF
  IF (IREFTAB.EQ. NROW(REFTAB)) THEN
    REFX = REFTAB(NROW(REFTAB),2)
  ELSE
    IF (REFTAB(IREFTAB+1,1)-REFTAB(IREFTAB,1) .NE/0/. 0.)THEN
      REFX = (REFTAB(IREFTAB,2)+(TIME-REFTAB(IREFTAB,1))*
&         (REFTAB(IREFTAB+1,2)-REFTAB(IREFTAB,2))/
&          (REFTAB(IREFTAB+1,1)-REFTAB(IREFTAB,1)))
    ELSE
     REFX= REFTAB(IREFTAB,2)
    ENDIF
  ENDIF
   ENDIF
ELSE
REFX=1.
ENDIF
!!! End of reftab
!! End of parameter setting and initiations of THYRAVR6_PSS.

!! Here starts the dynamic part of process THYRAVR6_PSS.
!! Multiplication of two signals.
   Ug=K1*Vc
!! First-order filter with filter constant TU.
   IF (START00) THEN
      V1=Ug
   ELSE
      V1: V1=Ug-TU*.D/DT.V1
   ENDIF
!! A signal subtracted to the reference, Reference.
   V2=REF*REFX-V1                                   !AH revisjon. *REFX
!! Summation of two signals.
   V7=VS+V2
!! Multiplication of two signals.
   V4=KD*V7
!! Filtered deriving function s/(1+sTD).
   INTER_1=V4/TD
   INTER_2: INTER_2=INTER_1-TD*.D/DT.INTER_2
   V5=INTER_1-INTER_2
!! Multiplication of two signals.
   V3=KP*V7
!! An integrator of non-wind-up type with integral time TI.
   IF (V6.GE.IMAX.AND.
&      V3.GE.0.AND..NOT.START) THEN
      V6=IMAX
      PRINT-I'V6 is at maximum limit.'
   ELSEIF (V6.LE.IMIN.AND.
&      V3.LT.0.AND..NOT.START) THEN
      V6=IMIN
      PRINT-I'V6 is at minimum limit.'
   ELSE
      V6: TI*.D/DT.V6=V3
      PRINT'V6 is within limits.'
   ENDIF
!! Summation of three signals.
   V8=V6+V3+V5
!! Limiter, MFCL <= UC <= OELf.
!! Checking the limits of the Limit function.
   IF (OELf.LT.MFCL) THEN
      STOP'The upper limit is lower than the lower limit.'
   ENDIF
```

```
      IF (V8.GE.OELf.AND..NOT.START) THEN
          UC=OELf
          PRINT-I'UC is at maximum limit.'
      ELSEIF (V8.LE.MFCL.AND..NOT.START) THEN
          UC=MFCL
          PRINT-I'UC is at minimum limit.'
      ELSE
          UC=V8
          PRINT'UC is within limits.'
      ENDIF
!! First-order filter with filter constant TBR
!! and the constant KBR in the numerator.
      IF (START00) THEN
          UBR=KBR*UC
      ELSE
          UBR: UBR=KBR*UC-TBR*.D/DT.UBR
      ENDIF
!! Multiplication of two signals.
      UF=UBR*Ug
!! Initial control of some of the block diagrams.
      IF (START) THEN
!! Checks start conditions by setting REF.
          REF: UF=UF0
!! A check of the filtered deriving function s/(1+sTD).
          IF (TD.LE.0) THEN
              STOP'Time constant TD in block s/(1+sTF) less or equal zero!'
          ENDIF
      ENDIF
!! End of initial control of some of the block diagrams.
!! Control of block diagram outputs within given limits.
      IF (.NOT.START.AND.CHECK_OF_LIMITS.EQ.0) THEN
!! An integrator of non-wind-up type with integral time TI.
!! This is a start-up check.
          IF (V6.GE.IMAX.AND.
&          V3.GT.0.OR.
&          V6.GT.IMAX) THEN
              STOP'V6 is at maximum limit.'
          ELSEIF (V6.LE.IMIN.AND.
&          V3.LT.0.OR.
&          V6.LT.IMIN) THEN
              STOP'V6 is at minimum limit.'
          ENDIF
          IF (V8.GE.OELf) THEN
              PRINT-I'UC is at maximum limit.'
          ELSEIF (V8.LE.MFCL) THEN
              PRINT-I'UC is at minimum limit.'
          ENDIF
          CHECK_OF_LIMITS=1
      ENDIF
!! End of control of block diagram outputs within given limits.
END
!! End of THYRAVR6_PSS.                    :-)
```

7   Complete list of eigenvalues No PSS:

```
Eigenvalue no      1: -0.200000      1/s ,    0.00000      Hz
Eigenvalue no      2:  -714.354      1/s ,    0.00000      Hz
Eigenvalue no      3:  -94.3743      1/s ,    0.00000      Hz
Eigenvalue no      4:  -95.4989      1/s ,    0.00000      Hz
Eigenvalue no      5:  -97.3306      1/s ,    0.00000      Hz
Eigenvalue no      6:  -97.2767      1/s ,    0.00000      Hz
Eigenvalue no      7:  -53.3239      1/s ,    0.00000      Hz
Eigenvalue no      8:  -45.9116      1/s ,    0.00000      Hz
Eigenvalue no      9:  -19.1186      1/s ,    3.35869      Hz
Eigenvalue no     10:  -19.1186      1/s ,   -3.35869      Hz
Eigenvalue no     11:  -41.5298      1/s ,    0.00000      Hz
Eigenvalue no     12:  -41.7052      1/s ,    0.00000      Hz
Eigenvalue no     13:  -39.1070      1/s ,    0.00000      Hz
Eigenvalue no     14:  -37.8297      1/s ,    0.00000      Hz
Eigenvalue no     15:  -37.1032      1/s ,    0.00000      Hz
Eigenvalue no     16:  -20.0850      1/s ,    2.45102      Hz
Eigenvalue no     17:  -20.0850      1/s ,   -2.45102      Hz
Eigenvalue no     18:  -27.9072      1/s ,    0.00000      Hz
Eigenvalue no     19:  -27.3198      1/s ,    0.00000      Hz
Eigenvalue no     20:  -21.7312      1/s ,    0.00000      Hz
Eigenvalue no     21:  -16.0720      1/s ,    0.00000      Hz
Eigenvalue no     22:  -15.6144      1/s ,    0.00000      Hz
Eigenvalue no     23: -0.879600      1/s ,    1.61249      Hz
Eigenvalue no     24: -0.879600      1/s ,   -1.61249      Hz
Eigenvalue no     25: -0.815394      1/s ,    1.15002      Hz
Eigenvalue no     26: -0.815394      1/s ,   -1.15002      Hz
Eigenvalue no     27: -0.717715      1/s ,    1.12435      Hz
Eigenvalue no     28: -0.717715      1/s ,   -1.12435      Hz
Eigenvalue no     29:  -10.3563      1/s ,    0.00000      Hz
Eigenvalue no     30:  -10.4174      1/s ,    0.00000      Hz
Eigenvalue no     31:  -10.0836      1/s ,    0.00000      Hz
Eigenvalue no     32:  -10.0730      1/s ,    0.00000      Hz
Eigenvalue no     33: -0.435859E-01 1/s ,    0.619871     Hz
Eigenvalue no     34: -0.435859E-01 1/s ,   -0.619871     Hz
Eigenvalue no     35:  -6.01405      1/s ,    0.238524E-01 Hz
Eigenvalue no     36:  -6.01405      1/s ,   -0.238524E-01 Hz
Eigenvalue no     37:  -5.52238      1/s ,    0.254884E-01 Hz
Eigenvalue no     38:  -5.52238      1/s ,   -0.254884E-01 Hz
Eigenvalue no     39:  -5.49319      1/s ,    0.00000      Hz
Eigenvalue no     40:  -1.32329      1/s ,    0.118996     Hz
Eigenvalue no     41:  -1.32329      1/s ,   -0.118996     Hz
Eigenvalue no     42:  -1.91834      1/s ,    0.00000      Hz
Eigenvalue no     43:  -2.43675      1/s ,    0.00000      Hz
Eigenvalue no     44:  -1.27182      1/s ,    0.00000      Hz
Eigenvalue no     45:  -2.76669      1/s ,    0.00000      Hz
Eigenvalue no     46:  -2.88993      1/s ,    0.00000      Hz
Eigenvalue no     47:  -2.86091      1/s ,    0.00000      Hz
Eigenvalue no     48: -0.284108      1/s ,    0.00000      Hz
Eigenvalue no     49: -0.188545E-01 1/s ,    0.00000      Hz
Eigenvalue no     50: -0.135757      1/s ,    0.00000      Hz
Eigenvalue no     51: -0.141785      1/s ,    0.00000      Hz
Eigenvalue no     52: -0.142467      1/s ,    0.00000      Hz
Eigenvalue no     53: -0.142452      1/s ,    0.00000      Hz
```

8   Complete list of eigenvalues PSS2B, case 3:

```
Eigenvalue no      1: -0.200000      1/s ,    0.00000      Hz
Eigenvalue no      2:  -1.00000      1/s ,    0.00000      Hz
Eigenvalue no      3:  -10000.0      1/s ,    0.00000      Hz
```

```
Eigenvalue no        4:   -714.349      1/s ,    0.00000      Hz
Eigenvalue no        5:   -99.9781      1/s ,    0.00000      Hz
Eigenvalue no        6:   -94.3742      1/s ,    0.00000      Hz
Eigenvalue no        7:   -95.4984      1/s ,    0.00000      Hz
Eigenvalue no        8:   -97.2767      1/s ,    0.00000      Hz
Eigenvalue no        9:   -97.3306      1/s ,    0.00000      Hz
Eigenvalue no       10:   -48.2378      1/s ,    1.23031      Hz
Eigenvalue no       11:   -48.2378      1/s ,   -1.23031      Hz
Eigenvalue no       12:   -50.9172      1/s ,    0.00000      Hz
Eigenvalue no       13:   -41.7051      1/s ,    0.00000      Hz
Eigenvalue no       14:   -41.5406      1/s ,    0.00000      Hz
Eigenvalue no       15:   -37.8560      1/s ,    0.00000      Hz
Eigenvalue no       16:   -36.9207      1/s ,    0.00000      Hz
Eigenvalue no       17:   -19.1296      1/s ,    3.37311      Hz
Eigenvalue no       18:   -19.1296      1/s ,   -3.37311      Hz
Eigenvalue no       19:   -50.0000      1/s ,    0.859940E-13 Hz
Eigenvalue no       20:   -50.0000      1/s ,   -0.859940E-13 Hz
Eigenvalue no       21:   -19.6762      1/s ,    2.60164      Hz
Eigenvalue no       22:   -19.6762      1/s ,   -2.60164      Hz
Eigenvalue no       23:   -27.9394      1/s ,    0.00000      Hz
Eigenvalue no       24:   -27.2960      1/s ,    0.00000      Hz
Eigenvalue no       25:   -20.4355      1/s ,    1.99512      Hz
Eigenvalue no       26:   -20.4355      1/s ,   -1.99512      Hz
Eigenvalue no       27:   -21.7043      1/s ,    0.00000      Hz
Eigenvalue no       28:   -3.46642      1/s ,    2.10989      Hz
Eigenvalue no       29:   -3.46642      1/s ,   -2.10989      Hz
Eigenvalue no       30:   -16.0708      1/s ,    0.00000      Hz
Eigenvalue no       31:   -15.5927      1/s ,    0.00000      Hz
Eigenvalue no       32:  -0.815695      1/s ,    1.15001      Hz
Eigenvalue no       33:  -0.815695      1/s ,   -1.15001      Hz
Eigenvalue no       34:  -0.718034      1/s ,    1.12328      Hz
Eigenvalue no       35:  -0.718034      1/s ,   -1.12328      Hz
Eigenvalue no       36:   -2.56048      1/s ,    0.981003     Hz
Eigenvalue no       37:   -2.56048      1/s ,   -0.981003     Hz
Eigenvalue no       38:   -10.4158      1/s ,    0.00000      Hz
Eigenvalue no       39:   -10.3554      1/s ,    0.00000      Hz
Eigenvalue no       40:   -10.0727      1/s ,    0.00000      Hz
Eigenvalue no       41:   -10.0849      1/s ,    0.00000      Hz
Eigenvalue no       42:  -0.505869E-01 1/s ,    0.619756     Hz
Eigenvalue no       43:  -0.505869E-01 1/s ,   -0.619756     Hz
Eigenvalue no       44:   -7.13722      1/s ,    0.824435E-01 Hz
Eigenvalue no       45:   -7.13722      1/s ,   -0.824435E-01 Hz
Eigenvalue no       46:   -6.16149      1/s ,    0.00000      Hz
Eigenvalue no       47:   -5.88458      1/s ,    0.610592E-01 Hz
Eigenvalue no       48:   -5.88458      1/s ,   -0.610592E-01 Hz
Eigenvalue no       49:   -5.47725      1/s ,    0.00000      Hz
Eigenvalue no       50:   -5.66213      1/s ,    0.00000      Hz
Eigenvalue no       51:   -2.74298      1/s ,    0.00000      Hz
Eigenvalue no       52:   -2.86098      1/s ,    0.00000      Hz
Eigenvalue no       53:   -2.89136      1/s ,    0.00000      Hz
Eigenvalue no       54:   -1.97086      1/s ,    0.269556E-01 Hz
Eigenvalue no       55:   -1.97086      1/s ,   -0.269556E-01 Hz
Eigenvalue no       56:   -1.34009      1/s ,    0.132208     Hz
Eigenvalue no       57:   -1.34009      1/s ,   -0.132208     Hz
Eigenvalue no       58:   -1.28065      1/s ,    0.00000      Hz
Eigenvalue no       59:  -0.328665      1/s ,    0.171102E-01 Hz
Eigenvalue no       60:  -0.328665      1/s ,   -0.171102E-01 Hz
Eigenvalue no       61:  -0.188545E-01 1/s ,    0.00000      Hz
Eigenvalue no       62:  -0.245562      1/s ,    0.00000      Hz
Eigenvalue no       63:  -0.135759      1/s ,    0.00000      Hz
Eigenvalue no       64:  -0.141785      1/s ,    0.00000      Hz
Eigenvalue no       65:  -0.142452      1/s ,    0.00000      Hz
```

```
Eigenvalue no       66: -0.142467      1/s ,    0.00000      Hz
Eigenvalue no       67: -0.332994      1/s ,    0.00000      Hz
Eigenvalue no       68: -0.333344      1/s ,    0.00000      Hz
Eigenvalue no       69: -0.333323      1/s ,    0.00000      Hz
```

9   Complete list of eigenvalues PSS4B, IEEE parameters:

```
Eigenvalue no        1: -0.200000      1/s ,    0.00000      Hz
Eigenvalue no        2: -1.00000       1/s ,    0.00000      Hz
Eigenvalue no        3: -1.00000       1/s ,    0.00000      Hz
Eigenvalue no        4: -1.00000       1/s ,    0.00000      Hz
Eigenvalue no        5: -1.00000       1/s ,    0.00000      Hz
Eigenvalue no        6: -1.00000       1/s ,    0.00000      Hz
Eigenvalue no        7: -1.00000       1/s ,    0.00000      Hz
Eigenvalue no        8: -1.00000       1/s ,    0.00000      Hz
Eigenvalue no        9: -1.00000       1/s ,    0.00000      Hz
Eigenvalue no       10: -1.00000       1/s ,    0.00000      Hz
Eigenvalue no       11: -1.00000       1/s ,    0.00000      Hz
Eigenvalue no       12: -1.00000       1/s ,    0.00000      Hz
Eigenvalue no       13: -1.00000       1/s ,    0.00000      Hz
Eigenvalue no       14: -1340.48       1/s ,    0.00000      Hz
Eigenvalue no       15: -714.509       1/s ,    0.00000      Hz
Eigenvalue no       16: -94.3783       1/s ,    0.00000      Hz
Eigenvalue no       17: -95.5075       1/s ,    0.00000      Hz
Eigenvalue no       18: -97.3308       1/s ,    0.00000      Hz
Eigenvalue no       19: -97.2766       1/s ,    0.00000      Hz
Eigenvalue no       20: -78.6428       1/s ,    0.00000      Hz
Eigenvalue no       21: -71.1943       1/s ,    0.00000      Hz
Eigenvalue no       22: -58.7861       1/s ,    0.00000      Hz
Eigenvalue no       23: -39.5240       1/s ,    3.30501      Hz
Eigenvalue no       24: -39.5240       1/s ,   -3.30501      Hz
Eigenvalue no       25: -50.1924       1/s ,    0.00000      Hz
Eigenvalue no       26: -48.9260       1/s ,    0.00000      Hz
Eigenvalue no       27: -41.7051       1/s ,    0.00000      Hz
Eigenvalue no       28: -41.5370       1/s ,    0.00000      Hz
Eigenvalue no       29: -37.8520       1/s ,    0.00000      Hz
Eigenvalue no       30: -37.0401       1/s ,    0.00000      Hz
Eigenvalue no       31: -19.1619       1/s ,    3.36531      Hz
Eigenvalue no       32: -19.1619       1/s ,   -3.36531      Hz
Eigenvalue no       33: -20.1701       1/s ,    2.47551      Hz
Eigenvalue no       34: -20.1701       1/s ,   -2.47551      Hz
Eigenvalue no       35: -27.9395       1/s ,    0.00000      Hz
Eigenvalue no       36: -27.3450       1/s ,    0.00000      Hz
Eigenvalue no       37: -0.235963      1/s ,    2.92876      Hz
Eigenvalue no       38: -0.235963      1/s ,   -2.92876      Hz
Eigenvalue no       39: -21.8407       1/s ,    0.00000      Hz
Eigenvalue no       40: -16.0568       1/s ,    0.00000      Hz
Eigenvalue no       41: -15.6052       1/s ,    0.00000      Hz
Eigenvalue no       42: -10.4187       1/s ,    0.00000      Hz
Eigenvalue no       43: -10.3570       1/s ,    0.00000      Hz
Eigenvalue no       44: -10.0831       1/s ,    0.00000      Hz
Eigenvalue no       45: -10.0732       1/s ,    0.00000      Hz
Eigenvalue no       46: -0.815882      1/s ,    1.15005      Hz
Eigenvalue no       47: -0.815882      1/s ,   -1.15005      Hz
Eigenvalue no       48: -0.724437      1/s ,    1.12312      Hz
Eigenvalue no       49: -0.724437      1/s ,   -1.12312      Hz
Eigenvalue no       50: -6.10337       1/s ,    0.452343E-01 Hz
Eigenvalue no       51: -6.10337       1/s ,   -0.452343E-01 Hz
Eigenvalue no       52: -5.00316       1/s ,    0.00000      Hz
Eigenvalue no       53: -5.62163       1/s ,    0.00000      Hz
Eigenvalue no       54: -5.47431       1/s ,    0.00000      Hz
```

```
Eigenvalue no       55: -0.850148E-01 1/s ,   0.619555      Hz
Eigenvalue no       56: -0.850148E-01 1/s , -0.619555      Hz
Eigenvalue no       57: -0.843710    1/s ,   0.392731      Hz
Eigenvalue no       58: -0.843710    1/s , -0.392731      Hz
Eigenvalue no       59:  -2.35870     1/s ,   0.00000      Hz
Eigenvalue no       60:  -2.73620     1/s ,   0.00000      Hz
Eigenvalue no       61:  -2.89188     1/s ,   0.00000      Hz
Eigenvalue no       62:  -2.86100     1/s ,   0.00000      Hz
Eigenvalue no       63:  -1.24715     1/s ,   0.114567     Hz
Eigenvalue no       64:  -1.24715     1/s , -0.114567     Hz
Eigenvalue no       65:  -1.33708     1/s ,   0.468503E-01 Hz
Eigenvalue no       66:  -1.33708     1/s , -0.468503E-01 Hz
Eigenvalue no       67:  -1.04041     1/s ,   0.00000      Hz
Eigenvalue no       68: -0.932842    1/s ,   0.00000      Hz
Eigenvalue no       69: -0.438746    1/s ,   0.128696E-01 Hz
Eigenvalue no       70: -0.438746    1/s , -0.128696E-01 Hz
Eigenvalue no       71: -0.272549    1/s ,   0.00000      Hz
Eigenvalue no       72: -0.188545E-01 1/s ,   0.00000      Hz
Eigenvalue no       73: -0.171226    1/s ,   0.00000      Hz
Eigenvalue no       74: -0.135746    1/s ,   0.00000      Hz
Eigenvalue no       75: -0.141785    1/s ,   0.00000      Hz
Eigenvalue no       76: -0.142452    1/s ,   0.00000      Hz
Eigenvalue no       77: -0.142467    1/s ,   0.00000      Hz
```

10 Complete list of eigenvalues PSS4B, case 1:

```
Eigenvalue no        1: -0.200000    1/s ,   0.00000      Hz
Eigenvalue no        2: -1.00000     1/s ,   0.00000      Hz
Eigenvalue no        3: -1.00000     1/s ,   0.00000      Hz
Eigenvalue no        4: -1.00000     1/s ,   0.00000      Hz
Eigenvalue no        5: -1.00000     1/s ,   0.00000      Hz
Eigenvalue no        6: -1.00000     1/s ,   0.00000      Hz
Eigenvalue no        7: -1.00000     1/s ,   0.00000      Hz
Eigenvalue no        8: -1.00000     1/s ,   0.00000      Hz
Eigenvalue no        9: -1.00000     1/s ,   0.00000      Hz
Eigenvalue no       10: -1339.67     1/s ,   0.00000      Hz
Eigenvalue no       11: -717.375     1/s ,   0.00000      Hz
Eigenvalue no       12: -94.3704     1/s ,   0.00000      Hz
Eigenvalue no       13: -95.4899     1/s ,   0.00000      Hz
Eigenvalue no       14: -97.3304     1/s ,   0.00000      Hz
Eigenvalue no       15: -97.2767     1/s ,   0.00000      Hz
Eigenvalue no       16: -79.8757     1/s ,   0.00000      Hz
Eigenvalue no       17: -68.5509     1/s ,   0.00000      Hz
Eigenvalue no       18: -12.7133     1/s ,   5.55589      Hz
Eigenvalue no       19: -12.7133     1/s , -5.55589      Hz
Eigenvalue no       20: -50.8848     1/s ,   0.00000      Hz
Eigenvalue no       21: -48.2374     1/s ,   0.00000      Hz
Eigenvalue no       22: -41.5367     1/s ,   0.00000      Hz
Eigenvalue no       23: -41.7051     1/s ,   0.00000      Hz
Eigenvalue no       24: -19.3333     1/s ,   3.38036      Hz
Eigenvalue no       25: -19.3333     1/s , -3.38036      Hz
Eigenvalue no       26: -37.8526     1/s ,   0.00000      Hz
Eigenvalue no       27: -37.0366     1/s ,   0.00000      Hz
Eigenvalue no       28: -20.3249     1/s ,   2.50144      Hz
Eigenvalue no       29: -20.3249     1/s , -2.50144      Hz
Eigenvalue no       30: -30.1825     1/s ,   0.00000      Hz
Eigenvalue no       31: -27.9358     1/s ,   0.00000      Hz
Eigenvalue no       32: -27.3443     1/s ,   0.00000      Hz
Eigenvalue no       33: -21.7090     1/s ,   0.00000      Hz
Eigenvalue no       34: -16.4154     1/s ,   0.00000      Hz
Eigenvalue no       35: -16.0209     1/s ,   0.00000      Hz
```

```
Eigenvalue no        36:  -15.5917        1/s ,    0.00000        Hz
Eigenvalue no        37:  -10.4194        1/s ,    0.00000        Hz
Eigenvalue no        38:  -10.3573        1/s ,    0.00000        Hz
Eigenvalue no        39:  -10.0829        1/s ,    0.00000        Hz
Eigenvalue no        40:  -10.0732        1/s ,    0.00000        Hz
Eigenvalue no        41: -0.815949        1/s ,    1.15005        Hz
Eigenvalue no        42: -0.815949        1/s ,   -1.15005        Hz
Eigenvalue no        43: -0.725084        1/s ,    1.12293        Hz
Eigenvalue no        44: -0.725084        1/s ,   -1.12293        Hz
Eigenvalue no        45:  -6.12400        1/s ,   0.490444E-01 Hz
Eigenvalue no        46:  -6.12400        1/s ,  -0.490444E-01 Hz
Eigenvalue no        47:  -5.63056        1/s ,    0.00000        Hz
Eigenvalue no        48:  -5.47573        1/s ,    0.00000        Hz
Eigenvalue no        49:  -4.82793        1/s ,    0.00000        Hz
Eigenvalue no        50: -0.878199E-01 1/s ,    0.619711        Hz
Eigenvalue no        51: -0.878199E-01 1/s ,   -0.619711        Hz
Eigenvalue no        52:  -1.16948        1/s ,    0.321128        Hz
Eigenvalue no        53:  -1.16948        1/s ,   -0.321128        Hz
Eigenvalue no        54:  -2.63094        1/s ,    0.00000        Hz
Eigenvalue no        55:  -2.70181        1/s ,    0.00000        Hz
Eigenvalue no        56:  -2.89290        1/s ,    0.00000        Hz
Eigenvalue no        57:  -2.86103        1/s ,    0.00000        Hz
Eigenvalue no        58:  -1.39552        1/s ,    0.00000        Hz
Eigenvalue no        59:  -1.21829        1/s ,   0.848072E-01 Hz
Eigenvalue no        60:  -1.21829        1/s ,  -0.848072E-01 Hz
Eigenvalue no        61:  -1.03868        1/s ,    0.00000        Hz
Eigenvalue no        62: -0.929053        1/s ,    0.00000        Hz
Eigenvalue no        63: -0.371486        1/s ,    0.00000        Hz
Eigenvalue no        64: -0.188546E-01 1/s ,    0.00000        Hz
Eigenvalue no        65: -0.267319        1/s ,    0.00000        Hz
Eigenvalue no        66: -0.333333        1/s ,    0.00000        Hz
Eigenvalue no        67: -0.171265        1/s ,    0.00000        Hz
Eigenvalue no        68: -0.135747        1/s ,    0.00000        Hz
Eigenvalue no        69: -0.141785        1/s ,    0.00000        Hz
Eigenvalue no        70: -0.142452        1/s ,    0.00000        Hz
Eigenvalue no        71: -0.142467        1/s ,    0.00000        Hz
Eigenvalue no        72:  -1.00000        1/s ,    0.00000        Hz
Eigenvalue no        73:  -1.00000        1/s ,    0.00000        Hz
Eigenvalue no        74:  -1.00000        1/s ,    0.00000        Hz
Eigenvalue no        75:  -1.00000        1/s ,    0.00000        Hz
Eigenvalue no        76:  -1.00000        1/s ,    0.00000        Hz
Eigenvalue no        77:  -1.00000        1/s ,    0.00000        Hz
```

11 Complete list of eigenvalues PSS4B, case 2:

```
Eigenvalue no         1: -0.200000        1/s ,    0.00000        Hz
Eigenvalue no         2:  -1.00000        1/s ,    0.00000        Hz
Eigenvalue no         3:  -1.00000        1/s ,    0.00000        Hz
Eigenvalue no         4:  -1.00000        1/s ,    0.00000        Hz
Eigenvalue no         5:  -1.00000        1/s ,    0.00000        Hz
Eigenvalue no         6:  -1.00000        1/s ,    0.00000        Hz
Eigenvalue no         7:  -1.00000        1/s ,    0.00000        Hz
Eigenvalue no         8:  -1.00000        1/s ,    0.00000        Hz
Eigenvalue no         9:  -1.00000        1/s ,    0.00000        Hz
Eigenvalue no        10:  -1.00000        1/s ,    0.00000        Hz
Eigenvalue no        11:  -1.00000        1/s ,    0.00000        Hz
Eigenvalue no        12:  -1340.16        1/s ,    0.00000        Hz
Eigenvalue no        13:  -715.651        1/s ,    0.00000        Hz
Eigenvalue no        14:  -94.3726        1/s ,    0.00000        Hz
Eigenvalue no        15:  -95.4948        1/s ,    0.00000        Hz
Eigenvalue no        16:  -97.3305        1/s ,    0.00000        Hz
```

```
Eigenvalue no      17:   -97.2767       1/s ,    0.00000       Hz
Eigenvalue no      18:   -79.9619       1/s ,    0.00000       Hz
Eigenvalue no      19:   -64.7839       1/s ,    0.00000       Hz
Eigenvalue no      20:   -51.3770       1/s ,    0.00000       Hz
Eigenvalue no      21:   -47.7966       1/s ,    0.00000       Hz
Eigenvalue no      22:   -41.5364       1/s ,    0.00000       Hz
Eigenvalue no      23:   -41.7051       1/s ,    0.00000       Hz
Eigenvalue no      24:   -37.8531       1/s ,    0.00000       Hz
Eigenvalue no      25:   -37.0342       1/s ,    0.00000       Hz
Eigenvalue no      26:   -19.2965       1/s ,    3.31854       Hz
Eigenvalue no      27:   -19.2965       1/s ,   -3.31854       Hz
Eigenvalue no      28:   -20.7957       1/s ,    2.45048       Hz
Eigenvalue no      29:   -20.7957       1/s ,   -2.45048       Hz
Eigenvalue no      30:   -11.0903       1/s ,    3.09721       Hz
Eigenvalue no      31:   -11.0903       1/s ,   -3.09721       Hz
Eigenvalue no      32:   -27.9740       1/s ,    0.00000       Hz
Eigenvalue no      33:   -27.3693       1/s ,    0.00000       Hz
Eigenvalue no      34:   -22.4334       1/s ,    0.00000       Hz
Eigenvalue no      35:   -16.0170       1/s ,    0.00000       Hz
Eigenvalue no      36:   -15.5735       1/s ,    0.00000       Hz
Eigenvalue no      37:  -0.815877       1/s ,    1.15004       Hz
Eigenvalue no      38:  -0.815877       1/s ,   -1.15004       Hz
Eigenvalue no      39:  -0.723134       1/s ,    1.12306       Hz
Eigenvalue no      40:  -0.723134       1/s ,   -1.12306       Hz
Eigenvalue no      41:   -10.4429       1/s ,    0.00000       Hz
Eigenvalue no      42:   -10.3653       1/s ,    0.00000       Hz
Eigenvalue no      43:   -9.14153       1/s ,    0.00000       Hz
Eigenvalue no      44:   -10.0747       1/s ,  0.823259E-03 Hz
Eigenvalue no      45:   -10.0747       1/s , -0.823259E-03 Hz
Eigenvalue no      46:   -8.01615       1/s ,    0.00000       Hz
Eigenvalue no      47:   -6.11412       1/s ,  0.555716E-01 Hz
Eigenvalue no      48:   -6.11412       1/s , -0.555716E-01 Hz
Eigenvalue no      49:   -5.62872       1/s ,    0.00000       Hz
Eigenvalue no      50:   -5.47513       1/s ,    0.00000       Hz
Eigenvalue no      51: -0.743193E-01 1/s ,    0.619772       Hz
Eigenvalue no      52: -0.743193E-01 1/s ,   -0.619772       Hz
Eigenvalue no      53:  -0.937658       1/s ,    0.256104       Hz
Eigenvalue no      54:  -0.937658       1/s ,   -0.256104       Hz
Eigenvalue no      55:   -2.73604       1/s ,    0.00000       Hz
Eigenvalue no      56:   -2.89187       1/s ,    0.00000       Hz
Eigenvalue no      57:   -2.86100       1/s ,    0.00000       Hz
Eigenvalue no      58:   -1.77287       1/s ,    0.00000       Hz
Eigenvalue no      59:  -0.986910       1/s ,  0.957609E-01 Hz
Eigenvalue no      60:  -0.986910       1/s , -0.957609E-01 Hz
Eigenvalue no      61:   -1.05217       1/s ,    0.00000       Hz
Eigenvalue no      62:  -0.780046       1/s ,    0.00000       Hz
Eigenvalue no      63:  -0.282974       1/s ,    0.00000       Hz
Eigenvalue no      64:  -0.333329       1/s ,    0.00000       Hz
Eigenvalue no      65:  -0.333333       1/s ,    0.00000       Hz
Eigenvalue no      66: -0.188537E-01 1/s ,    0.00000       Hz
Eigenvalue no      67:  -0.171659       1/s ,    0.00000       Hz
Eigenvalue no      68:  -0.135826       1/s ,    0.00000       Hz
Eigenvalue no      69:  -0.141785       1/s ,    0.00000       Hz
Eigenvalue no      70:  -0.142467       1/s ,    0.00000       Hz
Eigenvalue no      71:  -0.142452       1/s ,    0.00000       Hz
Eigenvalue no      72:   -1.00000       1/s ,    0.00000       Hz
Eigenvalue no      73:   -1.00000       1/s ,    0.00000       Hz
Eigenvalue no      74:   -1.00000       1/s ,    0.00000       Hz
Eigenvalue no      75:   -1.00000       1/s ,    0.00000       Hz
Eigenvalue no      76:   -1.00000       1/s ,    0.00000       Hz
Eigenvalue no      77:   -1.00000       1/s ,    0.00000       Hz
```

12 Complete list of eigenvalues PSS4B, case 3:

```
Eigenvalue no       1: -0.200000       1/s ,    0.00000       Hz
Eigenvalue no       2: -1.00000        1/s ,    0.00000       Hz
Eigenvalue no       3: -1.00000        1/s ,    0.00000       Hz
Eigenvalue no       4: -1.00000        1/s ,    0.00000       Hz
Eigenvalue no       5: -1.00000        1/s ,    0.00000       Hz
Eigenvalue no       6: -1.00000        1/s ,    0.00000       Hz
Eigenvalue no       7: -1.00000        1/s ,    0.00000       Hz
Eigenvalue no       8: -1340.26        1/s ,    0.00000       Hz
Eigenvalue no       9: -715.271        1/s ,    0.00000       Hz
Eigenvalue no      10: -94.3768        1/s ,    0.00000       Hz
Eigenvalue no      11: -95.5040        1/s ,    0.00000       Hz
Eigenvalue no      12: -97.3307        1/s ,    0.00000       Hz
Eigenvalue no      13: -97.2766        1/s ,    0.00000       Hz
Eigenvalue no      14: -79.3839        1/s ,    0.00000       Hz
Eigenvalue no      15: -65.6081        1/s ,    0.00000       Hz
Eigenvalue no      16: -52.1650        1/s ,    0.00000       Hz
Eigenvalue no      17: -2.80981        1/s ,    4.74457       Hz
Eigenvalue no      18: -2.80981        1/s ,   -4.74457       Hz
Eigenvalue no      19: -45.4991        1/s ,    0.177821      Hz
Eigenvalue no      20: -45.4991        1/s ,   -0.177821      Hz
Eigenvalue no      21: -41.5386        1/s ,    0.00000       Hz
Eigenvalue no      22: -41.7051        1/s ,    0.00000       Hz
Eigenvalue no      23: -37.0444        1/s ,    0.00000       Hz
Eigenvalue no      24: -37.8509        1/s ,    0.00000       Hz
Eigenvalue no      25: -19.2500        1/s ,    3.36660       Hz
Eigenvalue no      26: -19.2500        1/s ,   -3.36660       Hz
Eigenvalue no      27: -20.2703        1/s ,    2.48166       Hz
Eigenvalue no      28: -20.2703        1/s ,   -2.48166       Hz
Eigenvalue no      29: -27.9387        1/s ,    0.00000       Hz
Eigenvalue no      30: -27.3447        1/s ,    0.00000       Hz
Eigenvalue no      31: -21.6794        1/s ,    0.00000       Hz
Eigenvalue no      32: -15.6040        1/s ,    0.00000       Hz
Eigenvalue no      33: -16.0550        1/s ,    0.00000       Hz
Eigenvalue no      34: -10.4188        1/s ,    0.00000       Hz
Eigenvalue no      35: -10.3571        1/s ,    0.00000       Hz
Eigenvalue no      36: -10.0831        1/s ,    0.00000       Hz
Eigenvalue no      37: -10.0732        1/s ,    0.00000       Hz
Eigenvalue no      38: -0.815939       1/s ,    1.15005       Hz
Eigenvalue no      39: -0.815939       1/s ,   -1.15005       Hz
Eigenvalue no      40: -0.725635       1/s ,    1.12299       Hz
Eigenvalue no      41: -0.725635       1/s ,   -1.12299       Hz
Eigenvalue no      42: -0.957974E-01   1/s ,    0.619892      Hz
Eigenvalue no      43: -0.957974E-01   1/s ,   -0.619892      Hz
Eigenvalue no      44: -6.44465        1/s ,    0.00000       Hz
Eigenvalue no      45: -6.10372        1/s ,    0.463091E-01  Hz
Eigenvalue no      46: -6.10372        1/s ,   -0.463091E-01  Hz
Eigenvalue no      47: -5.62263        1/s ,    0.00000       Hz
Eigenvalue no      48: -5.47443        1/s ,    0.00000       Hz
Eigenvalue no      49: -1.11105        1/s ,    0.426365      Hz
Eigenvalue no      50: -1.11105        1/s ,   -0.426365      Hz
Eigenvalue no      51: -3.41806        1/s ,    0.00000       Hz
Eigenvalue no      52: -1.73096        1/s ,    0.195718      Hz
Eigenvalue no      53: -1.73096        1/s ,   -0.195718      Hz
Eigenvalue no      54: -2.56432        1/s ,    0.00000       Hz
Eigenvalue no      55: -2.73490        1/s ,    0.00000       Hz
Eigenvalue no      56: -2.89193        1/s ,    0.00000       Hz
Eigenvalue no      57: -2.86100        1/s ,    0.00000       Hz
Eigenvalue no      58: -1.24654        1/s ,    0.870476E-01  Hz
Eigenvalue no      59: -1.24654        1/s ,   -0.870476E-01  Hz
Eigenvalue no      60: -1.30657        1/s ,    0.00000       Hz
```

```
Eigenvalue no        61:  -1.03847       1/s ,     0.00000      Hz
Eigenvalue no        62:  -0.918116      1/s ,     0.00000      Hz
Eigenvalue no        63:  -0.370737      1/s ,     0.00000      Hz
Eigenvalue no        64:  -0.188542E-01  1/s ,     0.00000      Hz
Eigenvalue no        65:  -0.267961      1/s ,     0.00000      Hz
Eigenvalue no        66:  -0.171346      1/s ,     0.00000      Hz
Eigenvalue no        67:  -0.333333      1/s ,     0.00000      Hz
Eigenvalue no        68:  -0.135763      1/s ,     0.00000      Hz
Eigenvalue no        69:  -0.141785      1/s ,     0.00000      Hz
Eigenvalue no        70:  -0.142467      1/s ,     0.00000      Hz
Eigenvalue no        71:  -0.142452      1/s ,     0.00000      Hz
Eigenvalue no        72:  -1.00000       1/s ,     0.00000      Hz
Eigenvalue no        73:  -1.00000       1/s ,     0.00000      Hz
Eigenvalue no        74:  -1.00000       1/s ,     0.00000      Hz
Eigenvalue no        75:  -1.00000       1/s ,     0.00000      Hz
Eigenvalue no        76:  -1.00000       1/s ,     0.00000      Hz
Eigenvalue no        77:  -1.00000       1/s ,     0.00000      Hz
```

13   Complete list of eigenvalues PSS4B, case 4:

```
Eigenvalue no         1:  -0.200000      1/s ,     0.00000      Hz
Eigenvalue no         2:  -1.00000       1/s ,     0.00000      Hz
Eigenvalue no         3:  -1.00000       1/s ,     0.00000      Hz
Eigenvalue no         4:  -1.00000       1/s ,     0.00000      Hz
Eigenvalue no         5:  -1.00000       1/s ,     0.00000      Hz
Eigenvalue no         6:  -1.00000       1/s ,     0.00000      Hz
Eigenvalue no         7:  -1.00000       1/s ,     0.00000      Hz
Eigenvalue no         8:  -1.00000       1/s ,     0.00000      Hz
Eigenvalue no         9:  -1.00000       1/s ,     0.00000      Hz
Eigenvalue no        10:  -1340.41       1/s ,     0.00000      Hz
Eigenvalue no        11:  -714.784       1/s ,     0.00000      Hz
Eigenvalue no        12:  -94.3739       1/s ,     0.00000      Hz
Eigenvalue no        13:  -95.4978       1/s ,     0.00000      Hz
Eigenvalue no        14:  -97.3306       1/s ,     0.00000      Hz
Eigenvalue no        15:  -97.2767       1/s ,     0.00000      Hz
Eigenvalue no        16:  -79.9673       1/s ,     0.00000      Hz
Eigenvalue no        17:  -61.5976       1/s ,     0.00000      Hz
Eigenvalue no        18:  -52.1621       1/s ,     0.00000      Hz
Eigenvalue no        19:  -47.0516       1/s ,     0.00000      Hz
Eigenvalue no        20:  -41.5355       1/s ,     0.00000      Hz
Eigenvalue no        21:  -41.7051       1/s ,     0.00000      Hz
Eigenvalue no        22:  -37.8560       1/s ,     0.00000      Hz
Eigenvalue no        23:  -37.0157       1/s ,     0.00000      Hz
Eigenvalue no        24:  -19.1271       1/s ,     3.35018      Hz
Eigenvalue no        25:  -19.1271       1/s ,    -3.35018      Hz
Eigenvalue no        26:  -32.5235       1/s ,     0.00000      Hz
Eigenvalue no        27:  -20.1600       1/s ,     2.43248      Hz
Eigenvalue no        28:  -20.1600       1/s ,    -2.43248      Hz
Eigenvalue no        29:  -27.8712       1/s ,     0.00000      Hz
Eigenvalue no        30:  -27.2898       1/s ,     0.00000      Hz
Eigenvalue no        31:  -21.4864       1/s ,     0.00000      Hz
Eigenvalue no        32:  -4.91338       1/s ,     2.13954      Hz
Eigenvalue no        33:  -4.91338       1/s ,    -2.13954      Hz
Eigenvalue no        34:  -16.0720       1/s ,     0.00000      Hz
Eigenvalue no        35:  -15.6140       1/s ,     0.00000      Hz
Eigenvalue no        36:  -10.4181       1/s ,     0.00000      Hz
Eigenvalue no        37:  -10.3567       1/s ,     0.00000      Hz
Eigenvalue no        38:  -10.0833       1/s ,     0.00000      Hz
Eigenvalue no        39:  -10.0731       1/s ,     0.00000      Hz
Eigenvalue no        40:  -0.815832      1/s ,     1.15002      Hz
Eigenvalue no        41:  -0.815832      1/s ,    -1.15002      Hz
```

```
Eigenvalue no        42: -0.720399      1/s ,    1.12304       Hz
Eigenvalue no        43: -0.720399      1/s ,   -1.12304       Hz
Eigenvalue no        44: -0.572951E-01  1/s ,    0.617751      Hz
Eigenvalue no        45: -0.572951E-01  1/s ,   -0.617751      Hz
Eigenvalue no        46:  -6.45405      1/s ,    0.00000       Hz
Eigenvalue no        47:  -6.10203      1/s ,    0.453244E-01  Hz
Eigenvalue no        48:  -6.10203      1/s ,   -0.453244E-01  Hz
Eigenvalue no        49:  -5.62186      1/s ,    0.00000       Hz
Eigenvalue no        50:  -5.47435      1/s ,    0.00000       Hz
Eigenvalue no        51:  -2.64331      1/s ,    0.404813      Hz
Eigenvalue no        52:  -2.64331      1/s ,   -0.404813      Hz
Eigenvalue no        53:  -2.78048      1/s ,    0.00000       Hz
Eigenvalue no        54:  -2.88930      1/s ,    0.00000       Hz
Eigenvalue no        55:  -2.86087      1/s ,    0.00000       Hz
Eigenvalue no        56:  -2.40773      1/s ,    0.274516E-01  Hz
Eigenvalue no        57:  -2.40773      1/s ,   -0.274516E-01  Hz
Eigenvalue no        58:  -1.51055      1/s ,    0.00000       Hz
Eigenvalue no        59:  -1.26401      1/s ,    0.986326E-01  Hz
Eigenvalue no        60:  -1.26401      1/s ,   -0.986326E-01  Hz
Eigenvalue no        61:  -1.04236      1/s ,    0.00000       Hz
Eigenvalue no        62: -0.912034      1/s ,    0.00000       Hz
Eigenvalue no        63: -0.337315      1/s ,    0.00000       Hz
Eigenvalue no        64: -0.281751      1/s ,    0.00000       Hz
Eigenvalue no        65: -0.188543E-01  1/s ,    0.00000       Hz
Eigenvalue no        66: -0.333333      1/s ,    0.00000       Hz
Eigenvalue no        67: -0.171296      1/s ,    0.00000       Hz
Eigenvalue no        68: -0.135766      1/s ,    0.00000       Hz
Eigenvalue no        69: -0.141785      1/s ,    0.00000       Hz
Eigenvalue no        70: -0.142452      1/s ,    0.00000       Hz
Eigenvalue no        71: -0.142467      1/s ,    0.00000       Hz
Eigenvalue no        72:  -1.00000      1/s ,    0.00000       Hz
Eigenvalue no        73:  -1.00000      1/s ,    0.00000       Hz
Eigenvalue no        74:  -1.00000      1/s ,    0.00000       Hz
Eigenvalue no        75:  -1.00000      1/s ,    0.00000       Hz
Eigenvalue no        76:  -1.00000      1/s ,    0.00000       Hz
Eigenvalue no        77:  -1.00000      1/s ,    0.00000       Hz
```

14 Complete list of eigenvalues PSS4B, case 5:

```
Eigenvalue no         1: -0.200000      1/s ,    0.00000       Hz
Eigenvalue no         2:  -1.00000      1/s ,    0.00000       Hz
Eigenvalue no         3:  -1.00000      1/s ,    0.00000       Hz
Eigenvalue no         4:  -1.00000      1/s ,    0.00000       Hz
Eigenvalue no         5:  -1.00000      1/s ,    0.00000       Hz
Eigenvalue no         6:  -1.00000      1/s ,    0.00000       Hz
Eigenvalue no         7:  -1.00000      1/s ,    0.00000       Hz
Eigenvalue no         8:  -1.00000      1/s ,    0.00000       Hz
Eigenvalue no         9:  -1.00000      1/s ,    0.00000       Hz
Eigenvalue no        10:  -1340.23      1/s ,    0.00000       Hz
Eigenvalue no        11:  -715.423      1/s ,    0.00000       Hz
Eigenvalue no        12:  -94.3736      1/s ,    0.00000       Hz
Eigenvalue no        13:  -95.4972      1/s ,    0.00000       Hz
Eigenvalue no        14:  -97.3306      1/s ,    0.00000       Hz
Eigenvalue no        15:  -97.2767      1/s ,    0.00000       Hz
Eigenvalue no        16:  -79.8561      1/s ,    0.00000       Hz
Eigenvalue no        17:  -64.5081      1/s ,    0.00000       Hz
Eigenvalue no        18:  -51.5748      1/s ,    0.00000       Hz
Eigenvalue no        19:  -47.5737      1/s ,    0.00000       Hz
Eigenvalue no        20:  -41.7051      1/s ,    0.00000       Hz
Eigenvalue no        21:  -41.5362      1/s ,    0.00000       Hz
Eigenvalue no        22:  -37.8539      1/s ,    0.00000       Hz
Eigenvalue no        23:  -37.0291      1/s ,    0.00000       Hz
```

```
Eigenvalue no     24:    -19.2459      1/s ,    3.34729       Hz
Eigenvalue no     25:    -19.2459      1/s ,   -3.34729       Hz
Eigenvalue no     26:    -6.69575      1/s ,    3.55422       Hz
Eigenvalue no     27:    -6.69575      1/s ,   -3.55422       Hz
Eigenvalue no     28:    -20.3652      1/s ,    2.45400       Hz
Eigenvalue no     29:    -20.3652      1/s ,   -2.45400       Hz
Eigenvalue no     30:    -30.2458      1/s ,    0.00000       Hz
Eigenvalue no     31:    -27.8644      1/s ,    0.00000       Hz
Eigenvalue no     32:    -27.2913      1/s ,    0.00000       Hz
Eigenvalue no     33:    -21.3703      1/s ,    0.00000       Hz
Eigenvalue no     34:    -16.0608      1/s ,    0.00000       Hz
Eigenvalue no     35:    -15.6074      1/s ,    0.00000       Hz
Eigenvalue no     36:    -10.4187      1/s ,    0.00000       Hz
Eigenvalue no     37:    -10.3570      1/s ,    0.00000       Hz
Eigenvalue no     38:    -10.0831      1/s ,    0.00000       Hz
Eigenvalue no     39:    -10.0732      1/s ,    0.00000       Hz
Eigenvalue no     40: -0.815925       1/s ,    1.15004       Hz
Eigenvalue no     41: -0.815925       1/s ,   -1.15004       Hz
Eigenvalue no     42: -0.724453       1/s ,    1.12296       Hz
Eigenvalue no     43: -0.724453       1/s ,   -1.12296       Hz
Eigenvalue no     44:    -6.46283      1/s ,    0.00000       Hz
Eigenvalue no     45:    -6.10461      1/s ,   0.454980E-01  Hz
Eigenvalue no     46:    -6.10461      1/s ,  -0.454980E-01  Hz
Eigenvalue no     47:    -5.62213      1/s ,    0.00000       Hz
Eigenvalue no     48:    -5.47438      1/s ,    0.00000       Hz
Eigenvalue no     49: -0.867562E-01   1/s ,   0.618383       Hz
Eigenvalue no     50: -0.867562E-01   1/s ,  -0.618383       Hz
Eigenvalue no     51:    -1.13669      1/s ,   0.409687       Hz
Eigenvalue no     52:    -1.13669      1/s ,  -0.409687       Hz
Eigenvalue no     53:    -2.74969      1/s ,    0.00000       Hz
Eigenvalue no     54:    -2.89124      1/s ,    0.00000       Hz
Eigenvalue no     55:    -2.86097      1/s ,    0.00000       Hz
Eigenvalue no     56:    -2.37737      1/s ,   0.312728E-01  Hz
Eigenvalue no     57:    -2.37737      1/s ,  -0.312728E-01  Hz
Eigenvalue no     58:    -1.51012      1/s ,    0.00000       Hz
Eigenvalue no     59:    -1.19050      1/s ,   0.984668E-01  Hz
Eigenvalue no     60:    -1.19050      1/s ,  -0.984668E-01  Hz
Eigenvalue no     61:    -1.04602      1/s ,    0.00000       Hz
Eigenvalue no     62: -0.883359       1/s ,    0.00000       Hz
Eigenvalue no     63: -0.343789       1/s ,    0.00000       Hz
Eigenvalue no     64: -0.188542E-01   1/s ,    0.00000       Hz
Eigenvalue no     65: -0.278317       1/s ,    0.00000       Hz
Eigenvalue no     66: -0.333333       1/s ,    0.00000       Hz
Eigenvalue no     67: -0.171370       1/s ,    0.00000       Hz
Eigenvalue no     68: -0.135776       1/s ,    0.00000       Hz
Eigenvalue no     69: -0.141785       1/s ,    0.00000       Hz
Eigenvalue no     70: -0.142452       1/s ,    0.00000       Hz
Eigenvalue no     71: -0.142467       1/s ,    0.00000       Hz
Eigenvalue no     72:    -1.00000      1/s ,    0.00000       Hz
Eigenvalue no     73:    -1.00000      1/s ,    0.00000       Hz
Eigenvalue no     74:    -1.00000      1/s ,    0.00000       Hz
Eigenvalue no     75:    -1.00000      1/s ,    0.00000       Hz
Eigenvalue no     76:    -1.00000      1/s ,    0.00000       Hz
Eigenvalue no     77:    -1.00000      1/s ,    0.00000       Hz
```